Thermo-physical properties of insulating refractory materials

Diana Vitiello

Ph.D. Thesis

Université de Limoges

UNIVERSITY OF LIMOGES

ED 609 - Sciences et Ingénierie des Matériaux, Mécanique, Énergétique (SIMME)

Institut de Recherche sur les Céramiques (IRCER)

A thesis submitted to University of Limoges
in partial fulfillment of the requirements of the degree of

DOCTOR OF PHILOSOPHY

Matériaux Céramiques et Traitements de Surface

Presented and defensed by

Diana VITIELLO

On April 29, 2021

Thermo-physical properties of insulating refractory materials

Thesis supervisors: David Stanley SMITH
Nicolas TESSIER-DOYEN and Benoit NAIT-ALI

JURY :

Jacques POIRIER	Professeur Emérite, CEMHTI, Université d'Orléans	Rapporteur
Agnès DELMAS	Maître de Conférences (HDR), INSA Lyon	Rapporteur
Thorsten TONNESEN	Professeur Associé, GHI - RWTH Aachen University	Examinateur
Sylvie FOUCAUD	Professeur, FST, Université de Limoges	Examinateur
David Stanley SMITH	Professeur, ENSIL - ENSCI, Université de Limoges	Examinateur
Nicolas TESSIER-DOYEN	Maître de Conférences, IUT, Université de Limoges	Examinateur
Benoit NAIT-ALI	Maître de Conférences, ENSIL - ENSCI, Université de Limoges	Invité
Marc HUGER	Professeur, ENSIL - ENSCI, Université de Limoges	Invité
Lionel REBOUILLAT	Pyrotek	Invité
Ulrich MARSCHALL	RHI-Magnesita	Invité
Sido SINNEMA	Tata Steel	Invité

Acknowledgements

This work was supported by the funding scheme of the European Commission, Marie Skłodowska-Curie Actions Innovative Training Networks in the frame of the H2020 European project ATHOR - Advanced THermomechanical multiscale mOdelling of Refractory linings [grant number 764987]. I would like to thank all the people who contributed to the realization of this amazing project. It gave me the opportunity to work in an international team with precious friends and colleagues. It has been an incredible journey, which has unfortunately arrived at the end.

This work was carried out at the Ceramics Research Institute (IRCER) of the University of Limoges (France) during Ph.D. studies. Three years of unforgettable moments. Thanks to my supervisors, office mates, friends, colleagues, technicians, professors, all the people working in the laboratory. They all contributed to create a stimulating work environment. Without their help and support, all the achievements would not have been possible.

Part of this work was developed during three secondments: two months and half at the Institute of Mineral Engineering (GHI) at RWTH Aachen University (Germany); two months at the Institute for Sustainability and Innovation in Structural Engineering (ISISE) at the Department of Civil Engineering in Coimbra (Portugal) and two weeks at RHI-Magnesita Technology Center in Leoben (Austria). A great thanks to my secondment mentors and technicians for the big help, both during and after the secondments. Despite equipment problems, limited time and a pandemic situation, I achieved really interesting results, sometimes unexpected.

The work was made on refractory materials produced by Pyrotek and RHI-Magnesita, and on materials received through TataSteel. This was my first experience to work in direct contact with companies. I found very incredible people. Thank you so much for answering to all my questions. The discussions with you were really useful. I learnt a lot about refractories and steel production.

Rights

Table of Contents

Symbols

ω	Frequency
Λ	Wavelength
k	Wave vector
G	Reciprocal lattice vector
v	Velocity
a	Interatomic distance
U	Internal energy
V	Volume
f	Spring constant
ε	Emissivity
σ	Stefan-Boltzmann's constant
k_B	Boltzmann's constant
l	Mean free path
θ_D	Debye temperature
N	Degree of freedom
λ	Thermal conductivity
α	Thermal diffusivity, coefficient of thermal expansion
C_v, C_p	Specific heat capacity
T	Temperature
ρ	Density
φ, q	Heat flow
ϕ	Heat flux density
R	Resistance, resistivity
d, δ	Thickness
P	Heat source/sink term, porosity, pressure
L	Length
h	Heat transfer coefficient, Plank's constant
S, A	Surface area
r	Radius, distance
P_0	Power output
t	Time
M, m	Mass

W	Water content
v_p	Pore volume fraction
n	Number of grain boundaries per unit length, refractive index
n (ω)	Number of phonons
g(ω)dω	Phonon density of states
B	Bulk modulus
γ	Grüneisen parameter

List of figures

List of tables

Introduction

This thesis is part of a European project dedicated to "Advanced THermomechanical multiscale mOdelling of Refractory linings" (ATHOR), in the framework of the European Union's Horizon 2020 Research and Innovation program, grant agreement number 764987. The project, started in October 2017, is a collaboration between 7 academic poles and 8 industrial partners (**Figure 1**) with the purpose of training 15 early stage researchers in multi-disciplinary engineering fields for a better understanding of thermomechanical behaviour of refractory linings used in the iron and steel industries [1]. The entire project is focused on steel ladle applications, the vessels to transport and hold the hot liquid steel in which all the secondary metallurgical operations take place. This part represents the biggest user of refractory items in a steel plant.

Figure 1: *ATHOR members (academic poles and industrial partners) and their locations* [1].

Nowadays, 60% of the refractory materials' market is devoted to the iron and steel making industry, while the remaining 40% concerns industries such as power generation, cement, glass, non-ferrous metal, petrochemical and chemical [2][3]. The first use of these materials dates back to the Iron Age, where the furnaces adopted for producing iron by reducing the iron ore with extreme heat were protected by unshaped fireclay, carbon-added composite materials and silica rocks [4]. However, it was only during the industrial revolution that refractory technology took great strides. These refractories created the necessary conditions for melting metals and glass on an industrial scale, as well as for the manufacture of coke, cement, chemicals, and ceramics.

To better understand the relationship between the steel and the refractory industry, let us describe in more detail steel production. To produce steel, two ways can be followed (**Figure**

2): i) blast furnace + basic oxygen furnace (BOF) or ii) electric arc furnace (EAF).

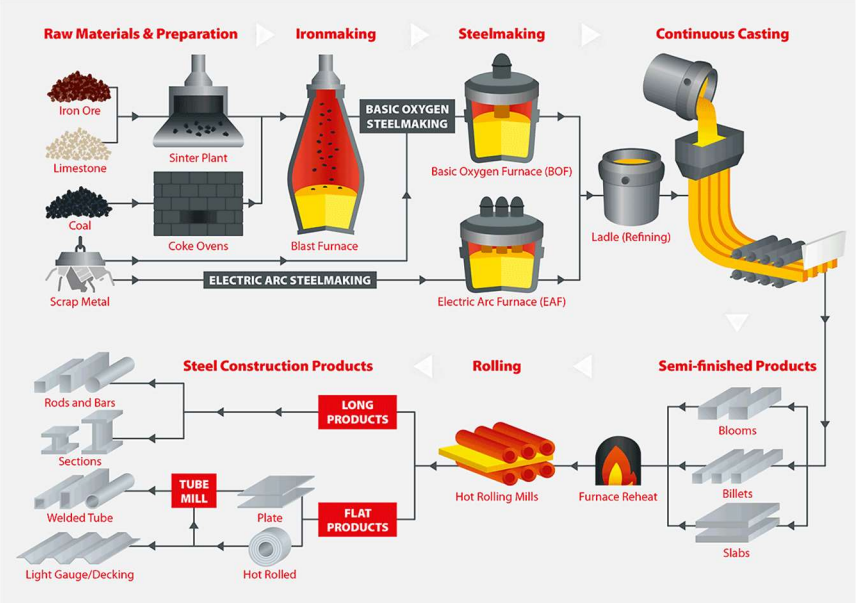

Figure 2: *Schematic diagram of steel production* [5].

The blast furnace is a metallurgical furnace to produce the pig iron, an intermediate product in steel production. This iron contains around 4 - 5% of carbon. The external shell of the furnace is protected by a refractory lining, which determines the duration of one non-stop campaign. One of the most used refractories are alumina-based materials with different percentages of Al_2O_3 depending in which zone they are used, and to which wear mechanisms they need to resist. For instance, at the top of the blast furnace (stack and belly), the bricks can contain 40 - 45% wt. of alumina to resist against the corrosion caused by the dust laden gases and to the abrasion due to the descent of the solid constituents. In the lower part (bosh and tuyeres), the bricks can contain 60 - 65% wt. of Al_2O_3 in order to support the higher temperatures [3]. Furthermore, to increase the life of the refractory lining, a water cooling system is also installed.

The process for producing the pig iron consists of introducing the solid raw materials (iron ore, limestone and coke) from the top part of the blast furnace, while the pre-heated air (above 1000 - 1100 °C) is blown through the tuyere pipes from a lower zone, which is the hottest part of the entire furnace (1900 - 2000 °C) [3]. At these temperatures, the hot air reacts with the coke to produce CO by an exothermic reaction. The hot gas travels upwards and reduces the iron and other oxides from the iron ore. Furthermore at temperatures above 840 °C, $CaCO_3$ dissociates into CaO, which will react with various acidic impurities present in the iron (notably silica) to produce the slag [3]. The hot metal is then tapped from the bottom part into a torpedo ladle and transferred into the BOF for producing the steel. During the transport, the pig iron is pre-treated to reduce the amount of sulphur, which makes the metal very brittle.

In the basic oxygen furnace, the steel shell is protected by two linings of refractories: a safety lining (SL) and a working lining (WL). The materials in the WL are chosen in order to resist against the abrasion caused by the introduction of the scrap and against the corrosion caused by the hot pig iron. The scrap has a double function: on one hand, it is a source of iron;

on the other hand, it helps to control the temperature inside the bath (many exothermic reactions happen during this step). Pure oxygen at supersonic speed mixed with powder CaO is then blown inside the furnace through a vertical lance for 15 - 20 min [3]. The O_2 reduces the amount of carbon by producing CO and CO_2, and it reacts with silica and phosphorous to form the respective oxides. These oxides then react with CaO to form the ladle slag. All this process takes around 60 min and no external heat is necessary due to the heat generated by the exothermic reactions [3]. At the end of the process, the BOF vessel is tilted towards the slagging side and the steel is poured through a tap hole into a steel ladle.

This first route produces low carbon steel. At the end of the 19th century, a second processing route was developed based on the electric arc furnace to produce stainless steel and other iron-based alloys. Furthermore, this process enables large-scale recycling of steel scrap. The scrap is melted by an electric arc generated by graphite electrodes. In the case of the alternating current furnace, 3 electrodes are attached to a removable refractory roof. On the contrary, in the case of the direct current furnace, only one is attached to the roof. Once the steel is ready, the furnace is inclined to pour the metal into a steel ladle. The shell of the EAF is protected by a permanent lining (PL) and a working lining (WL), directly in contact with the hot liquid steel. The choice of the refractories used in the WL is extremely important and depends on the design of the furnace and on the operating conditions.

After either processing route, the following step is the secondary steelmaking, which takes place in the steel ladle. The purposes of this step are: i) to reduce the concentration of gases, such as oxygen, nitrogen and hydrogen, in the metal; ii) to reduce the concentration of sulphur and phosphorus; iii) to reduce the amount of non-metallic inclusions; iv) to add elements for adjusting the composition depending on which kind of steel or alloy is produced [3]. All these operations require highly intensive energy in order to maintain the liquid steel at the right temperature (above the casting temperature). Therefore, the design of the steel ladle lining plays an important role. Nowadays, the majority of these vessels are composed of three layers of refractory materials to protect the external steel shell from the hot liquid steel: working lining, safety/permanent lining and insulating lining (**Figure 3**).

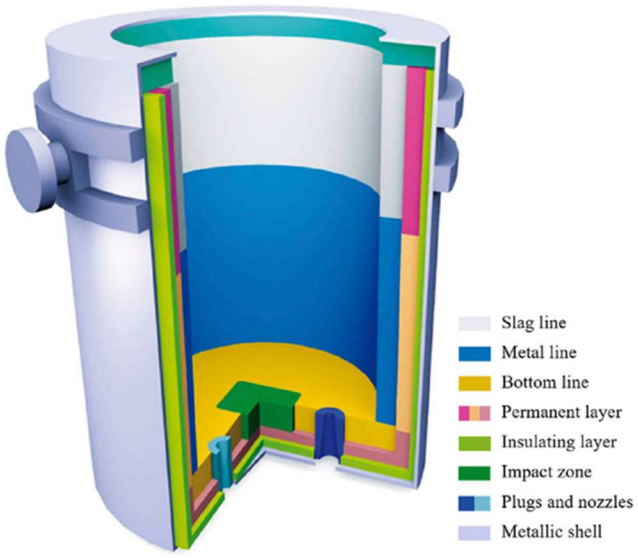

Figure 3: *Typical steel ladle lining configuration. © Calderys* [6]

The working lining is the innermost layer. It is divided into three zones, characterized by three different refractory materials. In the top part of the ladle, there is the slag zone, which means that the bricks are in contact with the slag. This is a very corrosive and aggressive environment due to both the liquid and the high temperatures (around 1650 °C). Therefore, the refractories need to have: i) a good thermal shock resistance and ii) a good corrosion resistance to resist against the attack of the slag. Magnesia-carbon bricks are an example. Carbon has a low thermal expansion and a high thermal conductivity, which both contribute to increase the thermal shock resistance. Furthermore, it has low wettability which is useful to resist against the slag corrosion. The disadvantage is that it is easily oxidized. In the middle zone, there is the metal line in contact with the hot liquid steel [7]. In this part, the temperatures are still high, but the environment is less aggressive than the slag zone. Typically in this zone the refractory bricks are alumina-spinel materials, which are characterized by good chemical and mechanical properties [8]. Finally, in the bottom part, the materials need to resist against the impact caused by the introduction of the hot liquid steel and against the thermal shock. One solution is the use of alumina-magnesia-carbon bricks. The main advantage of these materials is the formation of the spinel phase ($MgAl_2O_4$) in-situ, which involves expansion that helps to close joints [9].

The safety lining, also called the permanent lining, is the protective layer in case of damage of the working lining. Therefore, it should have: i) good thermal shock resistance and ii) good corrosion resistance both against the hot liquid steel and the slag. It is usually constituted of bricks or castables with high alumina content. This layer is extremely important, since the working lining needs to be replaced often, generally every 80 - 120 heats [10].

Finally, the last layer before the steel shell is the insulating lining. The purposes of this layer are: i) to reduce heat losses through the lining, to maintain the liquid steel at the right temperature and to save energy consumption, ii) to reduce environmental impact and iii) to keep the lining in a stable compressed condition to prevent joints opening and breakouts of hot liquid steel. Some typical refractory materials are: insulating fireclay bricks and insulating boards. These kinds of refractories are usually highly porous materials with very low thermal conductivity values ($\lambda < 1\ W \cdot m^{-1} \cdot K^{-1}$), but at the same time they have sufficient compressive strength [11].

This thesis is focused on the study of thermal properties mainly for the materials used in the insulating lining. As mentioned above, these materials are used to reduce heat losses through the lining and thus, the analysis of the specific heat, thermal conductivity (λ) and thermal expansion is of great importance. However, thermal properties are key physical properties for the performance of all refractory materials involved in high temperature processes. This is because when a material is subjected to a change of temperature (either during a heating or cooling process), the energy exchanged is controlled by thermal conductivity and heat capacity. Furthermore, such properties depend on the temperature itself and can evolve with the state of the microstructure. In other words, it means that the behaviour at room temperature and in service conditions is different. This knowledge is important for improving the performance of the material itself and to avoid serious working accidents [11]. Therefore, some studies were also made on the refractories used for the working lining.

Figure 4 summarizes the main topics investigated in the current work.

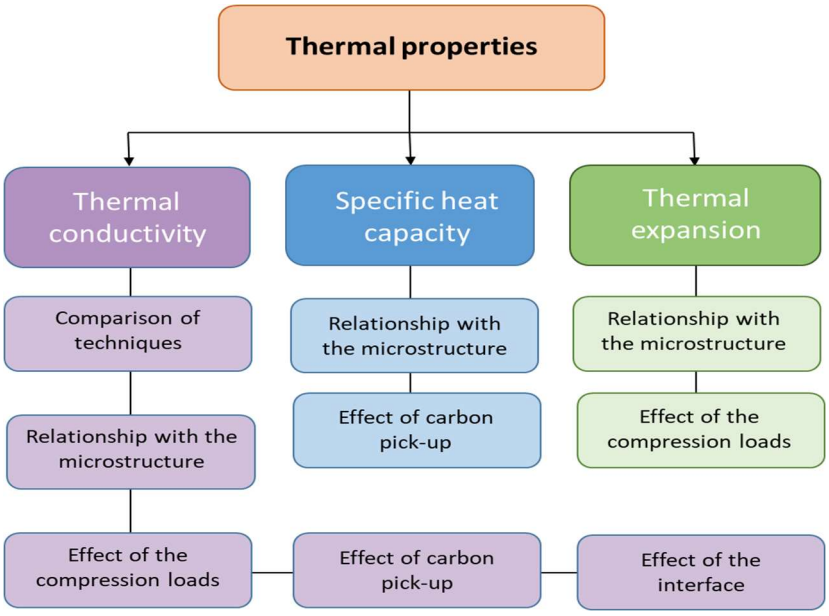

Figure 4: *Schematic diagram of the main topics investigated in the current work.*

The thesis has been organized in the following way:

Chapter 1 starts by briefly describing refractory materials and their use in industries working with very high temperature processes, such as steel, iron, glass and concrete manufacturing. It introduces the basics of the theory of lattice vibrations and phonons. This theory is used to describe the three main thermal properties: specific heat capacity, thermal conductivity and thermal expansion. Finally, it shows the close relationship between these properties and the microstructure. All this knowledge is fundamental for interpreting the results presented in the following chapters.

Chapter 2 presents the three kinds of refractory materials investigated during the current work: Insulating Boards, Insulating Fireclay Bricks and Alumina Spinel Bricks. It describes the five techniques, which have been compared, for the evaluation of the thermal conductivity values: the heat flow meter, the Dr. Klasse technique, the hot wire method, the hot disk method and the laser flash method. For each of them, the attention is focused on the advantages and disadvantages of each method linked to the material studied. The purpose is to try to give some insight for choosing the best technique to obtain the type of information sought.

Chapter 3 examines in detail the relationship between the thermal properties and the microstructure. The analysis is made on Alumina Spinel Bricks compared with alumina-based model materials. The purpose is to investigate the effects of porosity, grain boundaries, grain sizes, phase mixtures and presence of cement on the thermal conductivity values. The analysis shows how, by taking into account these factors, the λ of the alumina grains can be deduced from the experimental results and compared to single-crystal sapphire.

Chapter 4 is dedicated to the study of some real cases of industrial problems related to thermal properties: i) the interface thermal resistance; ii) the influence of compression load and iii) the influence of carbon pick-up in the insulating lining.

Chapter 1 :

Thermal properties of refractory materials

This thesis is devoted to the thermal properties of refractory materials. The intrinsic behaviour of the solid phase can be described using the theory of lattice vibrations and phonons. The present chapter will introduce the basics of this theory and then examine how the intrinsic thermal properties are modulated by the microstructure. It will start with the basic requirements of refractory materials.

1.1. Refractory materials: introduction

The International Organization for Standardization (ISO) defines refractory materials as "non-metallic materials or products (but not excluding those containing a proportion of metal) whose chemical and physical properties allow them to be used in a high temperature environment" [12]. Some of them can even withstand temperatures higher than 1400 °C without degrading or softening. Their main functions consist of: i) providing thermal insulation, ii) acting as a physical barrier between the hot medium such as molten steel and the wall of the vessel, iii) protecting against corrosion and erosion, iv) avoiding infiltration of the liquid through the lining. For these reasons, they are fundamental for all the industries working with very high temperature processes. Steel, iron, glass and concrete manufacturing are just a few examples.

Refractories can be classified in different ways (**Figure 1-1**) based on: chemical composition, method of manufacture, refractoriness ("the ability of maintaining a desired degree of chemical and physical integrity at high temperatures and in the environment and service conditions" [13]) and thermal conductivity.

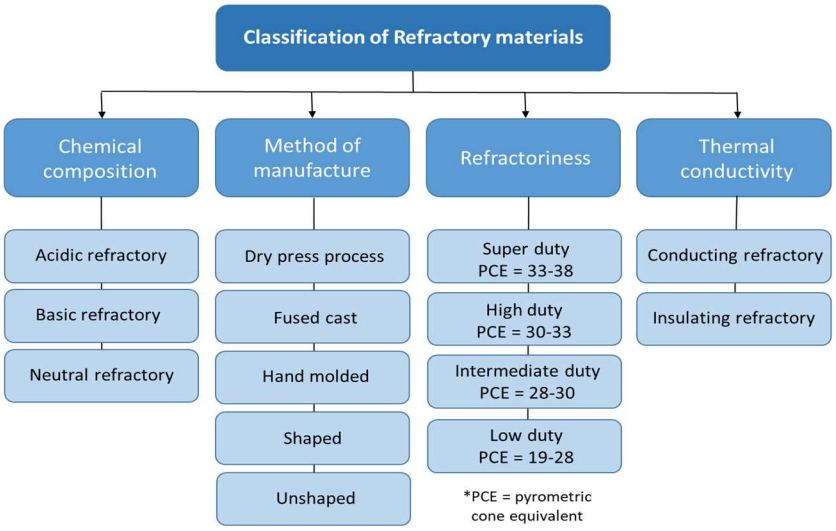

Figure 1-1: *Schematic of the different ways to classify a refractory material.*

Depending on their application, each refractory is designed and manufactured with a specific set of properties. For instance, the properties required for the working lining in steel ladles are different from those required for the electric arc furnace (EAF). In the first case, the refractories should be resistant to the steel and slag contacts and have a good thermal shock resistance parameter due to the high operating temperatures. In contrast for the EAF, they should have both mechanical strength to resist the impact of the scrap and high refractoriness to withstand the "hot spots" created by the required working arc [14]. Properties also vary between different sectors. In the petrochemical industry, for instance, the operating temperatures are lower than those achieved in the steel-making processes but in this case, the major requirement is a good abrasion resistance to resist against the action of the flow of high-velocity particles [14].

Refractory properties can be divided into three main categories: general physical, thermal and chemical. Physical characteristics, like density, porosity and strength, are the first parameters to consider for choosing a refractory material for an intended application. A porous material cannot be used for applications in which corrosion resistance is one of the major requirements. In contrast, it is suitable for insulation because it is generally characterized by a very low thermal conductivity value. Thermal properties (thermal conductivity, specific heat capacity and thermal expansion) are essential for improving the performance of refractory materials at high temperatures, and to avoid serious working accidents. They are temperature dependent and can evolve with the state of the microstructure. This means that the behaviour at room temperature and in service conditions is not necessarily the same [11]. Chemical properties depend on the chemical composition of the grains, on the kind of bond between the grains and on the ability to resist the action of liquids, such as molten steel and slag.

1.2. Thermal properties: lattice vibration theory

When a material is subjected to a change of temperature (either during a heating or cooling process), many of its properties change. The effect is linked to a transfer of energy in terms of heat, which causes a redistribution of the internal energy of the system [15]. In terms of thermal properties, the response of the material to input or output of heat energy can involve heat conduction, a change of temperature and a change in dimensions [16].

Thermal conductivity, specific heat capacity and the thermal expansion coefficient are fundamental characteristics for the performance of refractory materials. To describe these properties, it is crucial to introduce the concept of lattice vibrations.

For a crystalline material, the lattice can be described as an ordered structure of atoms, which vibrate around ideal equilibrium positions. These positions are maintained due to the forces exerted by neighbouring atoms. Because of the connections between the atoms, the displacement of one of them from their equilibrium position leads to the stimulation of vibrational waves [17][18]. This collective movement of atoms can be expressed in terms of elastic waves. Normal modes are characterized by a well-defined frequency ω, a wave vector k, which indicates the direction of propagation, and a specific wavelength Λ. These normal modes are very important because the overall vibrational motion of the lattice is given by the superposition of many normal modes.

Two types of vibrational waves in a crystal can be identified:

- Longitudinal (L): the atoms move in the propagation direction of the wave.
- Transverse (T): the atoms move perpendicularly to the propagation direction of the wave.

Each normal mode can be considered like a harmonic oscillator in which only some energy values are allowed. The first one to introduce this concept of "quantized energy" was Einstein [19]. The minimum amount of vibrational energy is called a "phonon" in analogy with the "photon", the minimum quantum of energy in the electromagnetic field. For each energy level, the eigenvalues are given by **Equ. 1-1**:

$$\varepsilon = \left(n + \frac{1}{2}\right)\hbar\omega \qquad \textit{Equ. 1-1}$$

where n is a positive integer and $\hbar = \frac{h}{2\pi}$ (h is Planck's constant).

The analysis for a three-dimensional crystal lattice is quite complicated, but it can be solved by making some simplifications. First of all, let us make the assumption that the amplitude of oscillation of the lattice vibrations is quite small (called the harmonic approximation). Then, let us consider the simplest possible system: an infinite one-dimensional linear chain with one kind of atom. The forces between the atoms can be described by elastic springs. In this case, the dispersion relation between neighbouring atoms is given by **Equ. 1-2**:

$$\omega = 2\sqrt{\frac{f}{M}}\left|\sin\left(\frac{ka}{2}\right)\right| \qquad \textit{Equ. 1-2}$$

where f is the spring constant, M the mass of the atom and a the interatomic distance [20]. The obtained curve is shown in **Figure 1-2.**

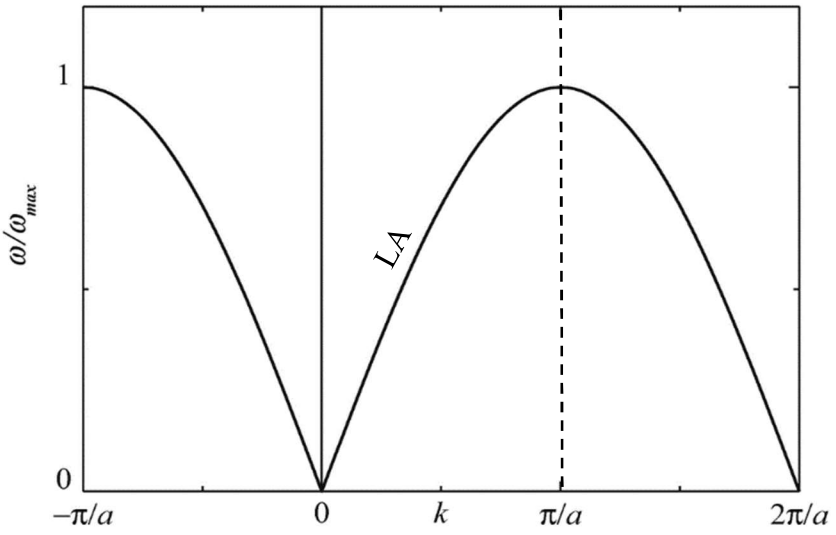

Figure 1-2: *Dispersion curve of acoustic phonons for an infinite one-dimensional linear chain with one kind of atom* [20]. *The normalized frequency ω is expressed as a function of the wave vector k within the first Brillouin zone (-π/a < k < π/a).*

An important aspect is the periodicity of the curve. The first period, in the range $-\frac{\pi}{a} < k < \frac{\pi}{a}$, is called the first Brillouin zone. For k→0, **Equ. 1-2** becomes:

$$\omega = 2\sqrt{\frac{f}{M}}\frac{ka}{2} = \upsilon_o k \qquad \textit{Equ. 1-3}$$

where υ_o is the sound velocity in the crystal. For this reason, these curves are called the acoustic branches (A). For k→ $\pm\frac{\pi}{a}$, the group velocity (the velocity of a wave packet) [20] goes to zero (the dispersion curve becomes flat) and the neighbouring atoms start to vibrate in opposition. As a consequence, the wave becomes a standing wave (also called stationary wave).

Let us consider now the case of two different atoms with respectively mass M_1 and M_2. In this case, the dispersion relation has two possible solutions (**Equ. 1-4**):

$$\omega^2 = f\left(\frac{1}{M_1}+\frac{1}{M_2}\right) \pm f\sqrt{\left(\frac{1}{M_1}+\frac{1}{M_2}\right)^2 - \frac{4}{M_1 M_2}\sin^2\left(\frac{ka}{2}\right)} \qquad \textit{Equ. 1-4}$$

For k→0, one branch goes to zero as in the previous case (acoustic branch) and one goes to high frequencies. This second branch is responsible for the characteristic optical behaviour of a crystal, and for this reason, it is called the optical branch (O). It is evident from **Figure 1-3** that optical branches show a much weaker dispersion of frequencies in the Brillouin zone than the acoustic branches.

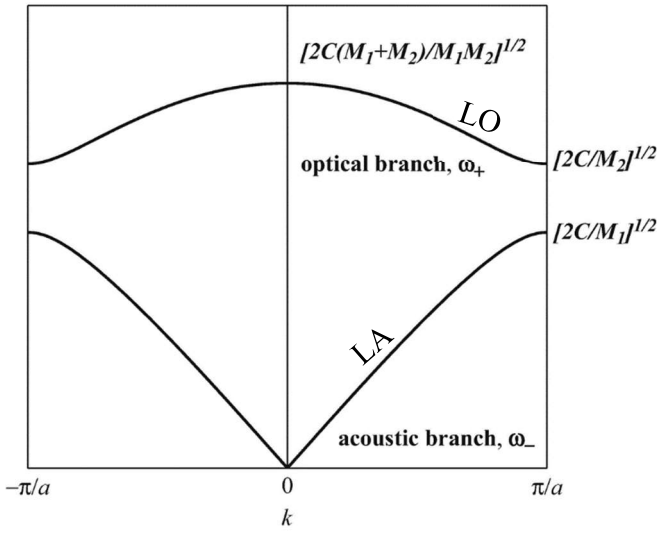

Figure 1-3: *Dispersion curve of phonons for an infinite one-dimensional linear chain with two kinds of atoms in the first Brillouin zone* [20]. *Two branches can be observed: one optical (high frequency) and one acoustic (low frequency).*

For k→ $\pm\frac{\pi}{a}$, the two branches tend to two finite values of frequency, which depend on the mass of the two atoms. If M_1 is close to M_2, the gap between the acoustic and optical branches is small. In the extreme case of $M_1 = M_2$, the optical branch disappears since it is similar to the previous case described (linear chain with one kind of atom).

All these considerations can be then applied to a three-dimensional lattice. Generally, for N-atoms, there are three acoustic branches (one longitudinal and two transverses) and 3(N-1) optical branches (N-1 longitudinal and 2(N-1) transverses) [17][20].

As mentioned at the beginning of the paragraph, the theory about phonons and lattice vibrations is essential to interpret the solid-state properties: specific heat capacity, thermal conductivity and thermal expansion. Let us discuss them in more detail.

1.2.1. Specific heat capacity

The specific heat capacity at constant volume (C_v) is defined by **Equ. 1-5**:

$$C_V(T) = \left(\frac{\partial U}{\partial T}\right)_V \qquad \textit{Equ. 1-5}$$

This physical property represents the amount of heat energy necessary to increase the temperature of a substance by one degree Celsius. U is the internal energy and it is generally the sum of two contributions: thermal energy due to all lattice vibrations (U_{vib}) and thermal energy due to free electrons (U_{elec}) [17][18]. In ceramic materials, $U_{vib} >> U_{elec}$ because the number of free electrons is very small. Therefore, it is possible to make the approximation that $U \approx U_{vib}$ and it is given by **Equ. 1-6**:

$$U(T) = \int_0^{\omega_D} \mathrm{g}(\omega) d\omega \left[\frac{1}{e^{\frac{\hbar\omega}{k_B T}} - 1}\right] \hbar\omega \qquad \textit{Equ. 1-6}$$

where T is the absolute temperature, k_B the Boltzmann's constant, g(ω)dω the phonon density of states, which can be defined so that g(ω) is the total number of modes with frequencies between ω and ω+dω. The term in the brackets is the number of phonons which occupy the mode ω, obtained by Bose-Einstein statistics (**Equ. 1-7**):

$$n\,(\omega) = \frac{1}{e^{\frac{\hbar\omega}{k_B T}} - 1} \qquad \textit{Equ. 1-7}$$

The phonon density of states is obtained using the Debye approximations: i) the crystal behaves as a continuous medium, ii) the speed of the elastic waves is constant, iii) beyond the Debye frequency (ω_D) the vibrational modes are not occupied and thus, the phonon density is equal to zero [17][20]. The Debye model is then obtained by combining **Equ. 1-5** and **Equ. 1-6** to give:

$$C_V(T) = 9k_B N \left(\frac{T}{\theta_D}\right)^3 \int_0^{\theta_D/T} \frac{x^4 e^x}{(e^x - 1)^2} dx \qquad \textit{Equ. 1-8}$$

where $\theta_D = \frac{\hbar\omega_D}{k_B}$ is the Debye temperature, $x = \frac{\hbar\omega}{k_B T}$ and N the number of degrees of freedom in the system, equivalent to the number of atoms.

The equation shows that the values of specific heat capacity are temperature dependent

up to a limiting value. In particular, for high temperatures ($T > \theta_D$), $k_B T >> \hbar\omega$ so **Equ. 1-8** becomes [20]:

$$C_V(T) = 3Nk_B \qquad \textit{Equ. 1-9}$$

This means that at high temperatures, the specific heat capacity is constant. This result was first obtained by Dulong and Petit using a classical model [21]. However, the Dulong-Petit law is not able to explain why at low and intermediate temperatures, the specific heat deviates from the constant value (**Figure 1-4**). This discrepancy is linked to the classical theory in which the atoms vibrate individually. Einstein [19] was able to solve this problem introducing the concept of "quantized energy". Nevertheless, the Einstein model starts to fail at very low temperatures ($T \rightarrow 0$) due to the approximation that all the modes have the same frequency.

At low temperatures, only the acoustic branches contribute to the specific heat capacity. For $T \rightarrow 0$, the specific heat approaches to zero. In the Einstein model, this approach is exponential, while experimentally it is found to follow a T^3 behaviour. Debye solved the problem by introducing the concept of vibrational waves: the atoms move collectively (**Equ. 1-8**) [18]. The frequency of these collective vibrations depends on wavelengths, described by the Debye approximation: $\omega = v_0 k$. An example of the specific heat capacity curve calculated according to the Debye model is shown in **Figure 1-4**.

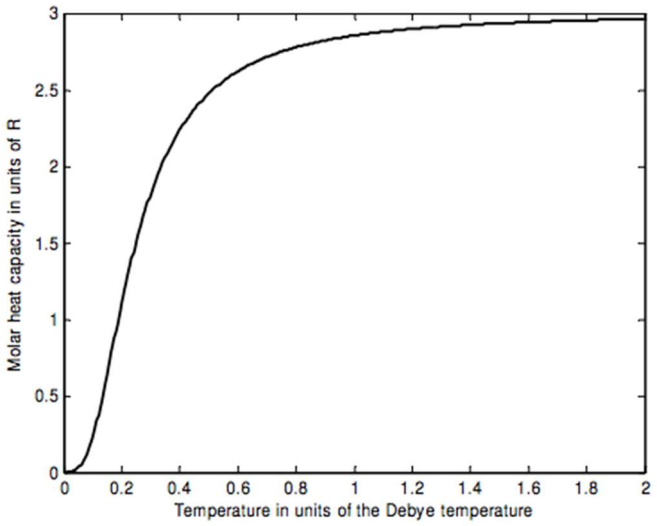

Figure 1-4: *Specific heat capacity curve according to Debye model* [17].

It is important to remember that the theory described until now is based on the harmonic approximation (**paragraph 1.2**), that is to consider the amplitude of oscillation of the lattice vibrations as small. This approximation can explain a wide range of material properties as in the case of the specific heat. However, some important properties, such as thermal conductivity and thermal expansion, can be described only by taking into account anharmonic effects.

1.2.2. Thermal conductivity: single-crystal

When a system is subjected to a gradient of temperature, a transfer of thermal energy (heat) occurs. These are three major heat transfer mechanisms:

- Conduction
- Convection
- Radiation

Heat conduction is caused by microscopic interactions between particles and it takes place in all the phases (solid, liquid, gas). When an object is heated, the particles start to vibrate faster (with higher frequency) and to push or hit their neighbours. The heat energy is thus passed to the neighbours, which also start to vibrate faster and to push other atoms. A sort of domino mechanism is established until the object reaches the thermal equilibrium.

Heat convection occurs between a surface and a fluid (gas or liquid) and leads to a flow of matter in the fluid. The process can be natural due to a difference in temperature (hot fluids are less dense than cold fluids) or forced by a fan or similar mechanical tools.

Thermal radiation is the transfer of energy associated with electromagnetic waves and it becomes significant at high temperatures. It can occur in any transparent medium (solid or fluid) and in the vacuum.

Even if the three mechanisms have different characteristics, they often occur simultaneously in the same system.

The thermal conductivity (λ) can be defined as the ability of the material to propagate heat. In ceramic materials, it is determined by elastic collisions and scattering of phonons. In analogy with the kinetic theory of gases, Debye [22] expressed this property as:

$$\lambda = \frac{1}{3}\int_0^{\omega_D} C_V(\omega)v(\omega)l(\omega)d\omega \qquad \textit{Equ. 1-10}$$

where υ is the elastic wave velocity and l the mean free path of lattice vibrations. As shown in **Equ. 1-8**, the specific heat capacity is temperature dependent affecting the thermal conductivity.

However, the temperature dependence of λ is also linked to the mean free path l. To understand how, it is important to take a look at the phonon-phonon scattering mechanism, which was first described by Peierls in 1929 [17][23]. He showed that two conservation laws had to be satisfied: the conservation of energy (**Equ. 1-11**) and the conservation of the crystal momentum (**Equ. 1-12**).

$$\hbar\omega_1 + \hbar\omega_2 = \hbar\omega_3 \qquad \textit{Equ. 1-11}$$

$$\overrightarrow{k_1} + \overrightarrow{k_2} = \overrightarrow{k_3} + \vec{G} \qquad \textit{Equ. 1-12}$$

where G is a reciprocal lattice vector. At low temperatures, the two equations are satisfied by $\vec{G} = 0$. The total momentum before and after collisions is unchanged and thus, these scattering events do not contribute to the thermal resistivity. These processes are called normal (or N-processes). Furthermore, as shown in **Figure 1-5**, k_3 is smaller than $2\pi/a$. Scattering processes in general concern: phonon-phonon interactions, phonon-defect interactions or phonon scattering with the external boundaries of a single-crystal [17]. At low temperatures, dominated

by N-processes, the sample dimensions limit the mean free path: the thermal conductivity is then controlled by the specific heat capacity and is proportional to T^3 (**Equ. 1-8**).

At high temperatures, the average number of phonons is higher in each mode $\vec{k}$ (**Equ. 1-7**) and consequently the probability of phonon-phonon interactions is higher. A significant number of interactions occur with $\overrightarrow{k_3'}$ outside of the first Brillouin zone. The resultant elastic wave can be described in the first Brillouin zone by adding a reciprocal lattice vector $\vec{G} \neq 0$, but it ($\overrightarrow{k_3}$) now points in the reverse direction to the heat flow. These processes are called Umklapp (or U-processes) and provide thermal resistance unlike N-processes. These two processes are summarized in **Figure 1-5**. The collisions between phonons have as a consequence to reduce the mean free path. Since l is inversely proportional to the number of phonons, it is proportional to 1/T. Furthermore, at high temperatures, the specific heat is constant (**Equ. 1-9**), so the thermal conductivity is controlled by the mean free path [17][23].

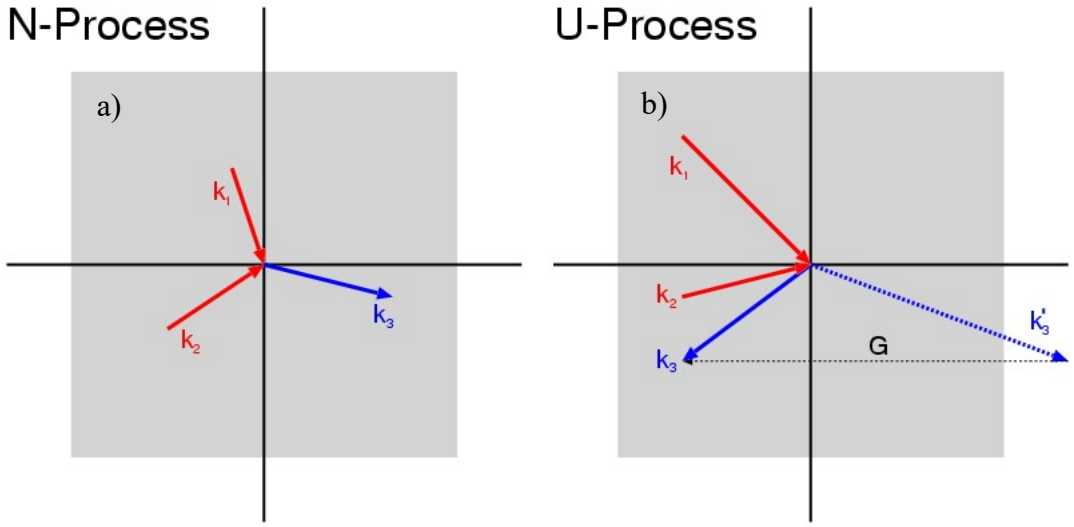

Figure 1-5: *Summary of the scattering mechanisms between the phonons: a) normal process, b) Umklapp process. In grey is highlighted the first Brillouin zone (-π/a < k < π/a)* [24].

It is important to remember that the majority of ceramic materials are polycrystalline materials and this has to be taken into account in the calculation of the thermal conductivity. The phonons can interact not only with other phonons but also with the defects, grains, pores… and this can affect the mean free path. All these imperfections act as scattering sites and, therefore, they reduce the mean free path and consequently the thermal conductivity.

1.2.2.1. Effect of grain boundaries and grain sizes

Physically, grain boundaries should influence the heat conduction in two ways. On one hand, they mark a local change in the crystallite orientation, which leads to a change in the velocity of the vibrational waves in the direction of the heat flow. On the other hand, they are disordered regions, which cause a local change in the phonon mean free path [25]. The first aspect is important for all the materials that show an anisotropic behaviour. Klemens [22][26] studied the influence of the grain boundaries in terms of mean free path, and deduced that when several scattering mechanisms are present, the total mean free path (l_{tot}) is given by **Equ. 1-13**,

known as Matthiessen's rule [27]:

$$\frac{1}{l_{tot}} = \frac{1}{l_{ph}} + \frac{1}{l_{imp}} \qquad \textit{Equ. 1-13}$$

where l_{ph} is linked to the phonon-phonon interactions and l_{imp} to phonon-imperfection interactions. The term "imperfection" is a general word to include all the mechanisms, which can affect the mean free path like impurities, dislocations, grain boundaries etc… At low temperatures, l_{tot} is of the order of magnitude of the dimensions of the crystal and it has little influence on the thermal conductivity (**paragraph 1.2.2**) unless there is a strong presence of defects.

Generally, the mean free path due to small imperfections (point defects) is assumed to be constant with the temperature [22][28]. Thus, the total thermal resistivity, which is the inverse of the thermal conductivity, is given by **Equ. 1-14**:

$$R = \frac{1}{\lambda_{poly}} = aT + b \qquad \textit{Equ. 1-14}$$

where a is determined by the lattice conductivity, which is the conductivity due to the U-processes, and b depends on the concentration and type of imperfections. It is evident from **Equ. 1-14** that the effect of scattering due to the presence of imperfections is greater for materials with higher lattice conductivity. Furthermore, since the conductivity decreases with the increase of temperature, the effect is higher at lowest temperatures.

Another approach to describe the influence of grain boundaries on heat conduction is to consider them as Kapitza resistances at the interfaces (**Figure 1-6a**) [29][30].

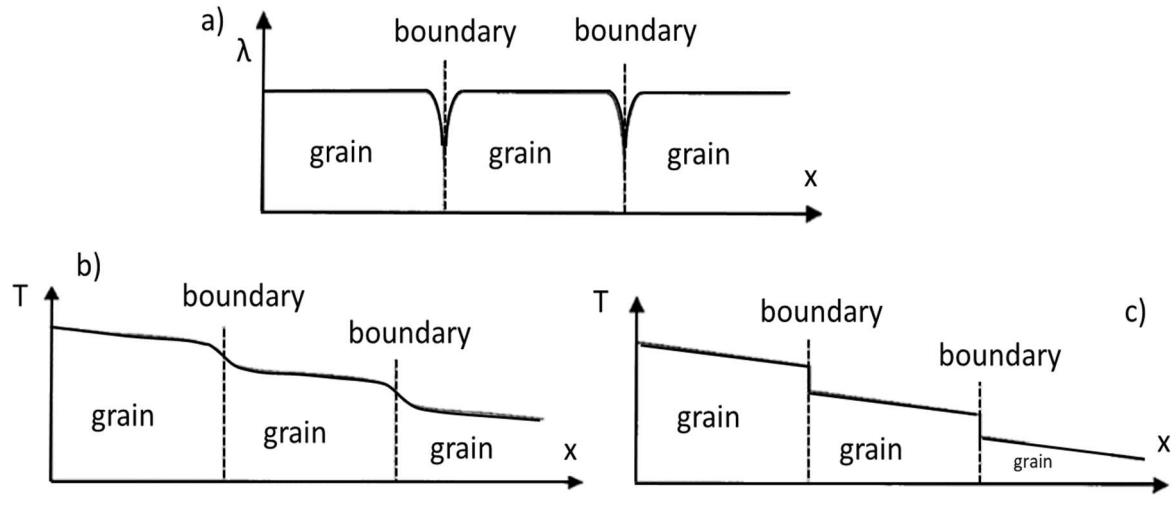

Figure 1-6: *a) change of the thermal conductivity due to the presence of grain boundaries; b) change of the temperature profile due to the presence of the grain boundaries; c) simplification of the temperature profile for calculating the thermal resistance (series model)* [25][30].

Local disorder leads to a decrease of the mean free path and consequently of the thermal conductivity. If a phonon is in the centre of a large grain, the scattering probability is controlled

only by phonon-phonon interactions. This value increases with the increase of the temperature and of the concentration of phonons. On the other hand, if a phonon is close to the grain boundary, the scattering probability increases due to the presence of the boundary itself (phonon-grain boundary interactions). When a thermal gradient is applied to a polycrystalline ceramic, the temperature drops at the grain-grain interface due to the presence of a thermal resistance (**Figure 1-6b**). The drop is simplified as a temperature discontinuity at the interface (**Figure 1-6c**).

On this basis, the thermal conductivity of a polycrystalline material (λ_{poly}) can be written as:

$$\frac{1}{\lambda_{poly}} = \frac{1}{\lambda_{grain}} + nR_{int} \qquad \textit{Equ. 1-15}$$

where λ_{grain} is the thermal conductivity of the single-crystal, n the number of grain boundaries per unit length and R_{int} the average grain boundary thermal resistance. Grandjean has provided experimental evidence for tin oxide that R_{int} is invariant with temperature between room temperature and 500 °C [31].

The Kapitza approach of resistors in series seems to be an alternative model to the approach adopted by Klemens. However, recent work from the Limoges group on alumina ceramics [30] attempts to combine both approaches by suggesting the presence of a second mechanism. They proposed that not only the grain boundaries interrupting the heat flow path act as Kapitza resistances, but also the grain size has an influence on the grain thermal conductivity (λ_{grain}). Small grain sizes reduce λ_{poly} and this effect seems to be emphasized for grains with dimensions less than 0.3 μm. Small grain sizes means higher number of grain boundaries (n). Since the last term of **Equ. 1-15** is greater for materials with small grain sizes, the thermal resistivity is higher and consequently the thermal conductivity is smaller. However, the grain size has an effect also on λ_{grain}. When the grains are small (< 0.3 μm), the hypothesis of an ideal infinite lattice is no longer valid and this cuts off all the low frequency long wavelength phonons, which cannot contribute to the thermal conductivity of the crystallite. This is, in essential, Klemens approach. The second term of **Equ. 1-15** becomes greater and again the thermal conductivity is reduced.

1.2.2.2. Effect of pores

The influence of the porosity can be studied by considering a mixture of two phases, in which the pores correspond to one of the phases. With the increase of the pore volume fraction, the effective thermal conductivity of the material decreases due to the low thermal conductivity of the gas.

In the case of porous materials, heat conduction is not the only mechanism to consider. In fact, also convection and radiation can transfer heat through the porous material. However, convection is not taken into account because for pore sizes less than 5 mm it is negligible [32]. Radiation is discussed in the next section (**paragraph 1.2.2.3**).

Heat conduction takes place in the solid and in the gas. The thermal conductivity of an

ideal gas (λ_g) is describing by a relation based on the kinetic theory of gases [33]:

$$\lambda_g = \frac{1}{3} C_V l_g v \qquad \textit{Equ. 1-16}$$

where C_V is the specific heat of the gas, l_g the mean free path of the gas and v the velocity of the molecules. It is evident that **Equ. 1-16** is similar to **Equ. 1-10**. However, there is an important difference. In the case of solids, collisions between phonons cause a decrease of the mean free path and consequently of the thermal conductivity. In the case of gases, molecular collisions are fundamental for heat conduction. The gases exchange part of their momentum during the collision and this leads to the propagation of the heat. With the increase of the temperature, the root mean square speed of the molecules increases and consequently so does the thermal conductivity. The kinetic theory of gases predicts that λ_g is proportional to $T^{1/2}$ [33] and this result is confirmed experimentally (**Figure 1-7**).

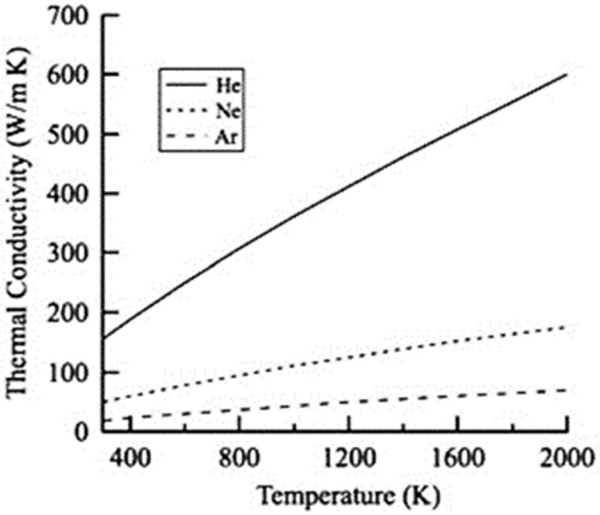

Figure 1-7: *Example of thermal conductivity curves as a function of temperature for three kinds of gases: helium (He), argon (Ar) and neon (Ne)* [34].

The thermal conductivity of gases also varies with the pressure [35]:

$$\lambda_g = \frac{\lambda_{atm}}{1 + C\left(\frac{T}{P\delta}\right)} \qquad \textit{Equ. 1-17}$$

where λ_{atm} is the thermal conductivity at atmospheric pressure, δ the thickness of the gas layer, C a constant depending on the type of gas. The thickness of the gas layer is linked to the mean free path by the Knudsen number (K_n) [35]:

$$K_n = \frac{l_g}{\delta} \qquad \textit{Equ. 1-18}$$

This parameter is important for small pores [35]. When the pore is small, the collision between two molecules of gas is less significant than the collision between the molecule of gas and the wall of the pore (Knudsen effect). Therefore, if $K_n >> 1$, the Knudsen effect is the most significant scattering mechanism [35][36].

To summarize, temperature, pressure and size of the pores are important parameters controlling the conductivity of the pore phase. However for the effective thermal conductivity of the porous material, the most important aspects to consider are shape, orientation and pore volume fraction (v_p). Taking into account these factors, several models can be used for the prediction of the effective thermal conductivity (λ_{eff}). In particular, three ranges depending on the pore volume fraction can be identified.

For $v_p < 0.15$, most relations give close results. The simplest one is Loeb's relation [32][37]:

$$\lambda_{eff} = \lambda_s(1 - v_p) \qquad \textit{Equ. 1-19}$$

where λ_s is the thermal conductivity of the solid phase. Loeb considered the solid and the pore phases as thermal resistors in parallel without interaction between each other (**Figure 1-8**). Furthermore, he made the assumption that the thermal conductivity of the pore phase (λ_p) is equal to 0 $W \cdot m^{-1} \cdot K^{-1}$ because it is much smaller than λ_s.

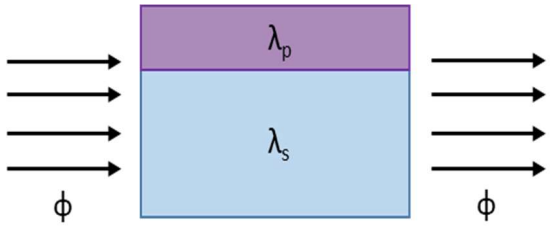

Figure 1-8: *Schematic of Loeb model (Φ = heat flow).*

However, if the pores are dispersed uniformly in the solid in the form of closed spherical pores with different diameters (**Figure 1-9**), the Maxwell-Eucken's relation [38] or the equivalent Hashin-Shtrikman upper bound [39] are more suitable:

$$\lambda_{eff} = \lambda_s \frac{\lambda_p + 2\lambda_s + 2v_p(\lambda_p - \lambda_s)}{\lambda_p + 2\lambda_s - v_p(\lambda_p - \lambda_s)} \qquad \textit{Equ. 1-20}$$

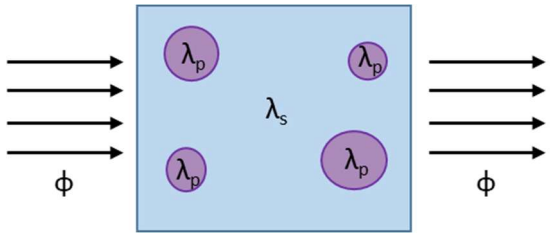

Figure 1-9: *Schematic of Maxwell-Eucken model (Φ = heat flow).*

For $v_p < 0.15$, the Landauer's relation predicts similar results. However, for $0.15 < v_p < 0.65$, this relation also describes successfully the influence of open porosity on thermal conductivity (**Figure 1-10**) [40][41]:

$$\lambda_{eff} = \frac{1}{4}[\lambda_P(3v_P - 1) + \lambda_s(2 - 3v_P)] + \{[\lambda_P(3v_P - 1) + \lambda_s(2 - 3v_P)]^2 + 8\lambda_P\lambda_s\}^{\frac{1}{2}} \qquad \textit{Equ. 1-21}$$

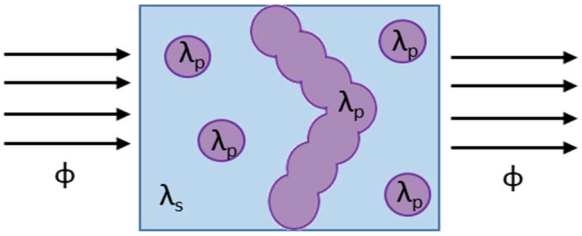

Figure 1-10: *Schematic of Landauer model (Φ = heat flow).*

Finally, for $v_p > 0.65$, it is important to underline that the presence of a continuous solid phase is necessary in order to guarantee the minimum mechanical strength in the material. In this range, **Equ. 1-21** is no longer valid because the relation assumes discontinuity of the solid phase around 0.7. A better alternative is Russell's relation [42], which is a parallel/series method with cubic pores dispersed in the matrix (**Figure 1-11**):

$$\lambda_{eff} = \frac{\lambda_s\left[\lambda_s + v_p^{\frac{2}{3}}(\lambda_p - \lambda_s)\right]}{\lambda_s + (\lambda_p - \lambda_s)\left(v_p^{\frac{2}{3}} - v_p\right)} \qquad \textit{Equ. 1-22}$$

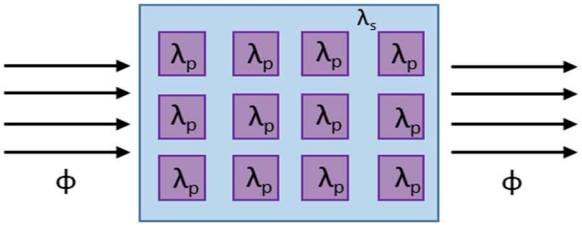

Figure 1-11: *Schematic of Russell model (Φ = heat flow).*

Figure 1-12 shows a summary of the different thermal conductivity vs pore volume fraction dependent relations in the three zones of study.

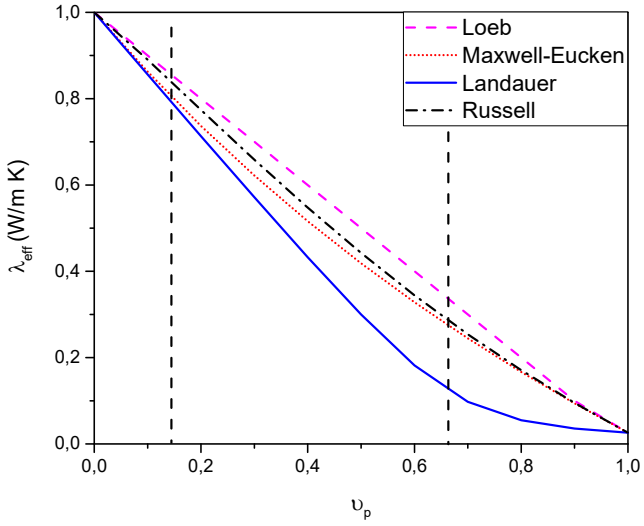

Figure 1-12: *Predicted values of effective thermal conductivity as a function of the pore volume fraction using different relations. The dotted vertical lines indicate the three zones of study.*

Equ. 1-19, **Equ. 1-20**, **Equ. 1-21** and **Equ. 1-22** can be also used for studying the influence of a second phase. In this case, the term λ_p is replaced with the λ_s of the second phase.

As mentioned at the beginning of the section, in the case of porous materials another mechanism to take into account is heat transfer due to radiation. Let us discuss it in more detail.

1.2.2.3. Effect of the radiation mechanism

The radiation mechanism is the transmission of heat in the form of electromagnetic waves. It can take place both in the solid and in the pores. The electromagnetic waves are constituted by photons, which scatter with mechanisms that are somewhat similar to those of the phonons. Thus, the total thermal conductivity of the material is given by the sum of phonon and photon conduction.

The thermal conductivity of the solid phase due to the radiation mechanism is given by **Equ. 1-23:**

$$\lambda_s(rad) = \frac{16}{3}\sigma n^2 T^3 l_{rad} \qquad \textit{Equ. 1-23}$$

where n is the refractive index, σ the Stefan-Boltzmann's constant, l_{rad} the mean free path of the photons [43]. From **Equ. 1-23** it is evident that the contribution of this mechanism becomes important at high temperatures ($\propto T^3$). Another important parameter to consider is the mean free path. In a perfectly transparent medium, $l_{rad} \rightarrow \infty$ which means that the more transparent the material, the higher is λ_s(rad). For opaque materials, $l_{rad} \rightarrow 0$ and this mechanism is negligible. Furthermore, the mean free path is determined by two processes: absorption linked to the type of material (l_a) and scattering due to interactions with the microstructure (l_{sc}). For a polycrystalline material, l_{sc} is limited by scattering with interfaces (solid-solid interface or solid-pore interface) [43]. **Figure 1-13** shows the difference between a single-crystal and a polycrystalline material in terms of thermal conductivity where the radiation contribution is revealed at high temperatures by the increasing discrepancy between the curves. In other words, radiation heat transfer has been strongly attenuated in the polycrystalline ceramic.

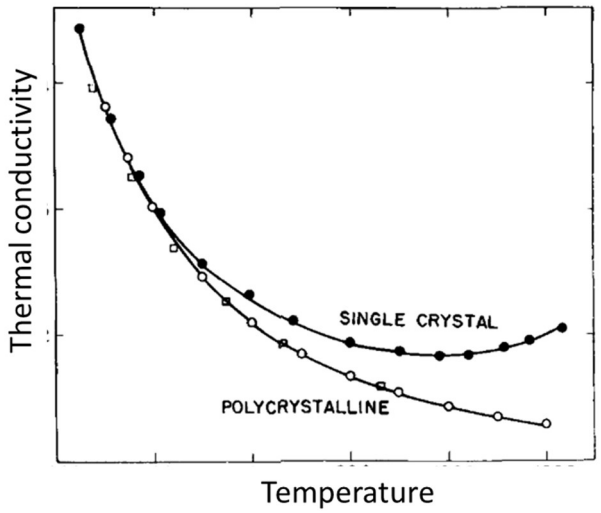

Figure 1-13: *Temperature variation of phonon and photon conductivity for crystals and glasses* [22][43].

If the pore volume fraction is high, heat transfer by radiation through the pores becomes significant, especially at high temperatures. The thermal conductivity of the pore phase is also the sum of two contributions: the thermal conductivity of the gas (**Equ. 1-17**) [35] and the thermal conductivity due to radiation (**Equ. 1-24**) [32].

$$\lambda_p(rad) = 4\gamma d\varepsilon\sigma T^3 \qquad \textit{Equ. 1-24}$$

where ε is the emissivity of the surface, d the dimensions of the pores and γ a geometrical factor. This factor is equal to 1 for laminar and cylindrical pores with axes parallel to the heat flow; 2/3 for spherical pores; π/4 for cylindrical pores with axes perpendicular to the heat flow [32].

1.2.3. Thermal expansion

Another property related to anharmonic effects in lattice vibrations is the thermal expansion. This property is the tendency of a material to change its volume or its dimensions due to a change of temperature (**Figure 1-14**).

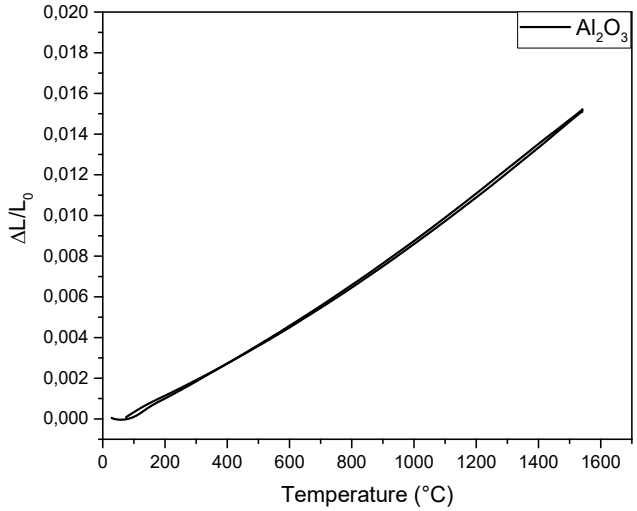

Figure 1-14: *Dilatometry measurement on standard alumina subjected to a thermal cycle. The graph shows the change in length normalized with the initial length (L_0) as a function of temperature. The coefficient of linear expansion is given by the slope of the linear fit.*

Generally, materials increase their volume with the increase of temperature. These changes are normally small, but nevertheless of great importance. Indeed, internal stresses resulting from dimensional variations can occur during large and/or rapid temperature changes, liable to promote a catastrophic failure in the extreme case. That is why some industrial developments are highly focused on refractories exhibiting low values of thermal expansion coefficient. Refractory materials are usually a mixture of two or more solid phases. If these phases have different thermal expansion coefficients (α), the induced mismatch will cause the formation of micro-cracks within the microstructure. This diffuse damage can be beneficial for resistance to thermal shock because it favours the reduction of the overall thermal expansion, though it can sometimes lead to rupture.

The coefficient of linear expansion (α_L) is given by **Equ. 1-25**:

$$\alpha_L = \frac{1}{L_0}\left(\frac{\partial L}{\partial T}\right)_P \qquad \textit{Equ. 1-25}$$

where L_0 is the initial length. The coefficient of linear expansion represents the change of the material in one dimension (length) due to a change of temperature (**Figure 1-14**). The expansion means that the interatomic distance between two atoms increases with the increase of temperature and this can be easily understood considering atomic vibrations [20]. With the increase of the temperature, the atoms start to vibrate with higher amplitude, which causes an increase of the distance between atoms due to asymmetry of the interatomic pair potential. This increase will appear as on overall increase of the length (or more in general of the volume).

For isotropic materials:

$$\alpha_L = \frac{1}{3}\alpha_V = \frac{1}{3V}\left(\frac{\partial V}{\partial T}\right)_P \qquad \textit{Equ. 1-26}$$

where α_V is the volumetric coefficient of thermal expansion. **Equ. 1-26** can be also written as:

$$\alpha_L = \frac{1}{3B}\left(\frac{\partial P}{\partial T}\right)_V \qquad \textit{Equ. 1-27}$$

where B is the bulk modulus, which describes how resistant to compression is a material [17][44].

In the case of cubic crystal structures [17], **Equ. 1-27** is often expressed as:

$$\alpha_L = \frac{\gamma C_V}{3B} \qquad \textit{Equ. 1-28}$$

which means that the thermal expansion has a similar temperature dependence as the specific heat capacity. In particular: i) at low temperatures, α_L approaches zero as T^3; ii) at high temperatures, it tends to a constant.

γ is the Grüneisen parameter. This parameter measures the anharmonic effects on the crystal and can be either calculated using theoretical models (**Equ. 1-29**) or derived from thermal expansion measurements [45]:

$$\gamma = -\left(\frac{\partial lnT}{\partial lnV}\right)_S \qquad \textit{Equ. 1-29}$$

where V is the volume, T the temperature and S the entropy of the system.

1.3. Conclusion

Refractory materials are ceramic materials used in processes that involve high temperatures, such as steel making. Some of them, like alumina spinel or magnesia carbon refractories, can even resist temperatures higher than 1400 °C. Thermal properties are fundamental physical properties for the performance of these kinds of materials because they determine the response time to steady-state behaviour, heat losses from the process and stresses

due to dimensional changes of parts in the system. These properties are temperature dependent and can evolve with the state of the microstructure. In other words, the behaviour at room temperature and in service conditions is not necessarily the same. The knowledge of the evolution of thermal properties as a function of temperature can help to avoid serious accidents.

In this chapter, the theory of lattice vibrations and phonons was used to describe three of the main thermal properties:

- Specific heat capacity
- Thermal conductivity
- Thermal expansion

The specific heat capacity represents the amount of heat energy necessary to increase the temperature of a substance by one degree Celsius. This property is related to the internal energy, whose major contribution for ceramic materials is given by lattice vibrations. The specific heat capacity increases from "zero" at T = 0 K following a T^3 behaviour at low temperatures. Above the Debye temperature (θ_D), it tends towards an asymptotic constant value.

The temperature dependence of the specific heat capacity also affects the thermal conductivity. This property represents the ability of the material to propagate heat, both in the solid and pore phases. For a polycrystalline material, the thermal conductivity of the solid phase is the sum of two contributions: a) heat conduction due to lattice vibrations, b) radiation due to the presence of a transparent medium. This second contribution is usually negligible. Furthermore, the thermal conductivity of a ceramic or a refractory is strongly modulated by the microstructure. The presence of pores, grain boundaries, impurities etc. inhibits heat transfer through the material and consequently reduces the thermal conductivity.

Finally, the thermal expansion is the ability of the material to change its dimensions due to a change of temperature. This change is linked to the atomic vibrations and asymmetry in the interatomic pair potential: with the increase of the temperature, the atoms vibrate with higher amplitude and as a consequence, the interatomic distance between two atoms increases.

Chapter 2 :

Comparison of techniques for thermal conductivity measurements

Several techniques can be used for the determination of the thermal conductivity of refractory materials but this can lead to variations in the obtained values. For this reason, the discussion about which is the best technique is still open in the refractory field. The present chapter will be dedicated to the comparison of five different techniques: the laser flash method, the hot disk method, the hot wire method, the heat flow meter and the Dr. Klasse technique. The analysis will go into detail in order to explain the differences between each technique for three characteristic industrial refractory materials, Insulating Boards, Insulating Fireclay Bricks and Alumina Spinel Bricks, with thermal conductivity spanning from 0.2 to 6.5 $W \cdot m^{-1} \cdot K^{-1}$ at room temperature.

2.1. Materials

Insulating Boards (IB) and Insulating Fireclay Bricks (IFB), characterized by low thermal conductivity values, are used in the insulation layer of steel ladles (**Figure 2-1**).

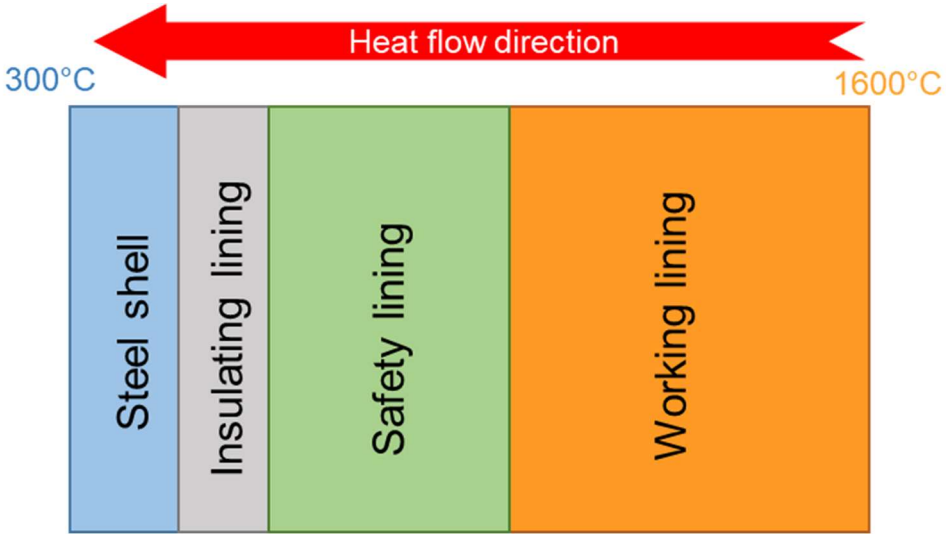

Figure 2-1: *Schematic representation of a steel ladle lining.*

This layer is the interlayer between the external steel shell and the safety lining. Its purposes are: i) to reduce heat losses through the lining, ii) to maintain the liquid steel at the right temperature to ensure the final product quality, iii) to save energy consumption and reduce environmental impact, iv) to keep the lining in a stable compressed condition to prevent joints opening and breakouts of hot liquid steel.

The more thermally conducting Alumina Spinel Bricks (ASB) are used in the working

lining (**Figure 2-1**) because of their good thermal shock and corrosion resistance. The working lining is the lining in contact with the hot liquid steel and the slag. It is subjected to brutal thermal cycles due to the operations of filling/emptying of the ladles and to a highly corrosive environment.

2.1.1. Insulating Boards

Insulating Boards (IB) are composed of: 25 - 55% wt. vermiculite and 5 - 25% wt. forsterite. These boards provide excellent strength and dimensional stability up to 1000 °C. For this thesis, three types of IB were studied (**Table 2-1**):

Table 2-1: *Summary of the three types of Insulating Boards studied (A = surface area; d = thickness). The values are obtained from data sheets and verified experimentally.*

Materials	***Porosity***	***Density***	***Dimensions***
Low Density Insulating Boards (IB-LD)	55 - 65%	1.0 g/cm^3 ± 7%	A: 410x101 mm^2 d: 12.7 and 16 mm
Medium Density Insulating Boards (IB-MD)	45 - 55%	1.2 g/cm^3 ± 7%	
High Density Insulating Boards (IB-HD)	35 - 45%	1.5 g/cm^3 ± 7%	

The vermiculite $(Mg,Fe^{2+},Fe^{3+})_3[(Al,Si)_4O_{10}](OH)_2 \cdot 4H_2O$ is a natural clay material that is formed via hydrothermal alteration of biotite and phlogopite. It is constituted of layers of two silica tetrahedral sheets attached to a central magnesia octahedral sheet. The substitution of Si^{4+} ions by Al^{3+} ions in the tetrahedral and octahedral sheets leads to the generation of a negative charge. This charge limits the expansion properties of the clay and determines a well compact structure [46]. Furthermore, the layer structure (**Figure 2-2**) gives an anisotropic behaviour to the refractory material, which should be taken into account in the evaluation of thermal properties.

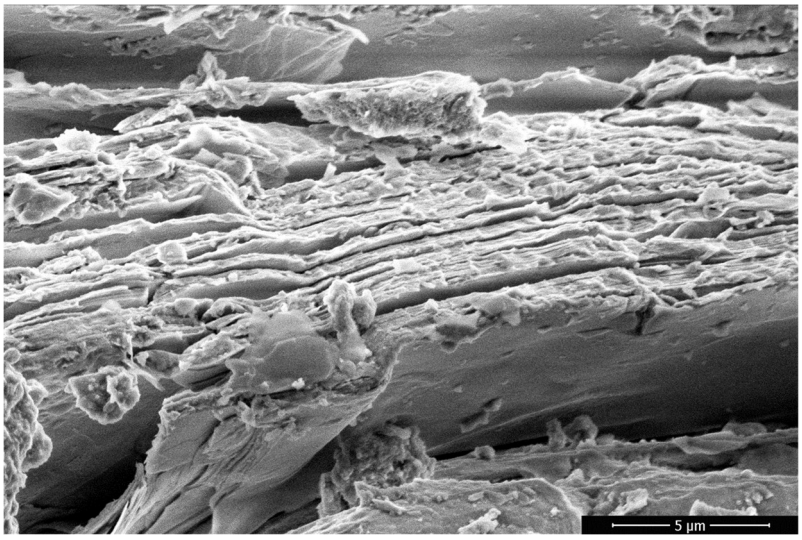

Figure 2-2: *SEM micrograph of an Insulating Board. It is possible to distinguish the layer structure of the vermiculite. The image was taken with an environmental microscope (FEI Quanta 450 FEG).*

An important aspect of the vermiculite is its ability to expand, when heated to 300 - 400

°C, because this process transforms the material into a very efficient thermal insulator with a density of 60 - 150 kg/m^3. Many hypotheses were made to explain why and how the vermiculite expands. At the moment, the most acceptable theory involves the removal of the interlayer water and the formation of intermediate phases [46].

Forsterite (Mg_2SiO_4) is a naturally occurring mineral, which is a magnesia rich end-member of the olivine solid solution series. It has a low thermal expansion and excellent insulation properties also at high temperatures [47]. The advantage of adding this material to vermiculite is the improvement of thermo-mechanical properties at high temperatures [48].

2.1.2. Insulating Fireclay Bricks

Insulating Fireclay Bricks (IFB) are composed of: 60 - 70% wt. alumina and 25 - 35% wt. silica. They are typically used in the temperature range of 1300 - 1600 °C.

Table 2-2: *Description of Insulating Fireclay Bricks. The values are obtained from data sheets and verified experimentally.*

Materials	*Porosity*	*Density*	*Dimensions*
Insulating Fireclay Bricks (IFB)	70 - 75%	0.9 g/cm^3 ± 7%	230x114x32 mm^3

The advantages of using alumina-silica refractories can be explained with the Al_2O_3-SiO_2 phase equilibrium diagram (**Figure 2-3**).

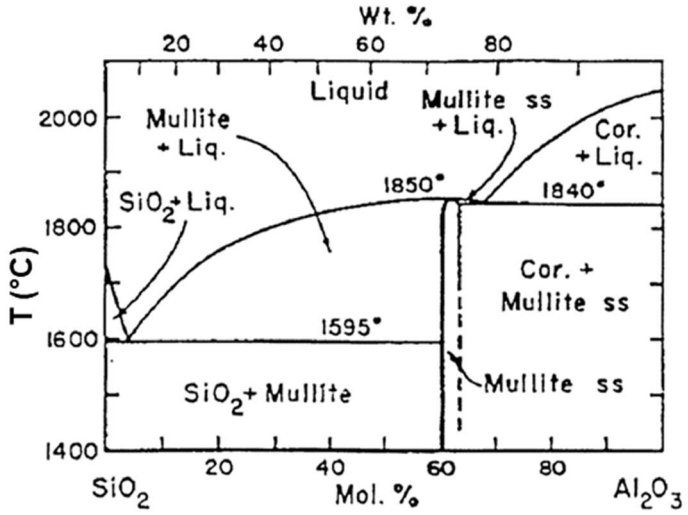

Figure 2-3: *Al_2O_3-SiO_2 phase equilibrium diagram* [14].

One of the compounds is mullite ($3Al_2O_3 \cdot 2SiO_2$) which exhibits a very high melting point. With the increase of the amount of this compound, the refractoriness of the material increases. In fact, above 75% wt. of Al_2O_3 the solidus is 1840 °C, which means that the material exhibits a solid phase up to this temperature. At the same time, the glass content decreases, which improves the mechanical strength. The amount of glass phase is linked to the presence of oxides in the raw materials, such as sodium oxide (Na_2O), potassium oxide (K_2O), calcium oxide (CaO), iron oxide (Fe_2O_3) and titanium dioxide (TiO_2) [14].

An example of the microstructure of Insulating Fireclay Bricks is shown in **Figure 2-4**. The picture shows alumina grains with a porous structure and alumina-silica phases, which are denser and randomly oriented.

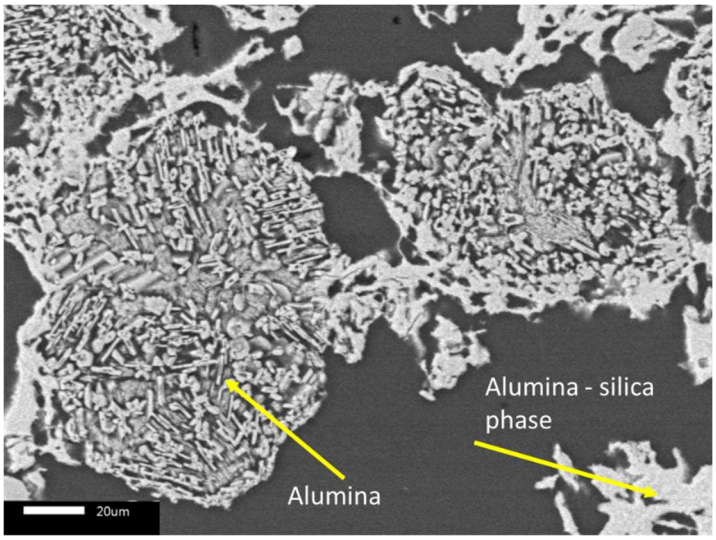

Figure 2-4: *SEM micrograph of an Insulating Fireclay Brick. The picture was taken with a scanning electron microscope (JEOL IT 300 LV) in backscattered mode. The darkest phase corresponds to the embedding resin required for the specimen preparation.*

The refractoriness is not the only interesting aspect of these materials. Insulating Fireclay Bricks are also characterized by a low thermal conductivity value and by a reversible thermal expansion which guarantee thermal insulation and dimensional stability [14].

2.1.3. Alumina Spinel Bricks

Alumina Spinel Bricks (ASB) are composed of: 94% wt. alumina and 5% wt. magnesia. Then, the two oxides react to form the spinel phase ($MgAl_2O_4$).

Table 2-3: *Description of Alumina Spinel Bricks. The values are obtained from data sheets and verified experimentally.*

Materials	***Porosity***	***Density***	***Dimensions***
Alumina Spinel Bricks (ASB)	15 - 20%	2.6 g/cm^3 ± 7%	160-140x140x100 mm^3

These refractory materials are characterized by good chemical and mechanical properties. In particular, they have high refractoriness (the melting temperature of spinel is around 2135 °C) and high resistance to chemical attacks, which make them suitable for the working lining in steel ladles [14]. However, the properties change depending on the raw materials and on the process of manufacture.

Let us consider the crystal structure. In alumina-rich spinel, Al^{3+} ions replace Mg^{2+} ions on tetrahedral sites with the formation of vacant cation sites (the radius of Al^{3+} is much smaller than that of Mg^{2+}). This leads to a wide range of properties depending on the cation that occupies the vacancy. For instance, if the vacancy is occupied by Fe^{2+} or Mn^{2+}, the refractory

exhibits higher slag penetration resistance [14]. **Figure 2-5** shows an example of their microstructure: alumina grains of different sizes with a fine spinel matrix [49].

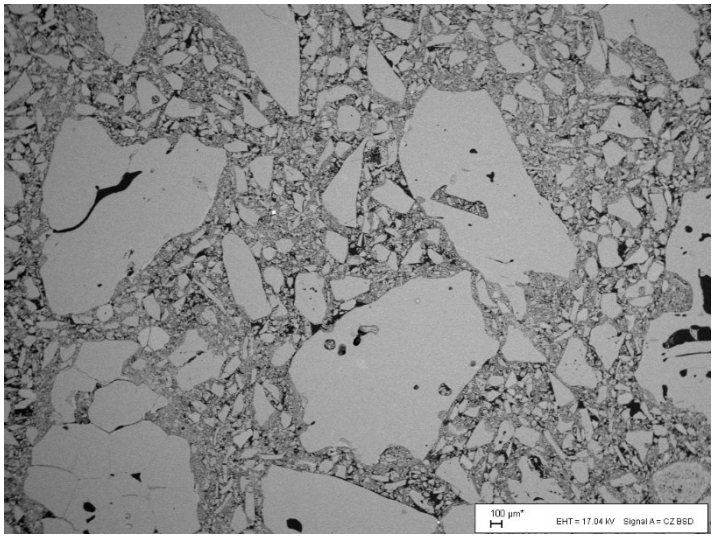

Figure 2-5: *SEM micrograph of an Alumina Spinel Brick. The image was taken at the Montanuniversität Leoben (Austria) by S. Samadi* [49].

2.2. Thermal conductivity measurement methods

All the available techniques of thermal conductivity evaluation can be divided into two categories: steady-state and transient methods [16]. In steady-state methods, such as the heat flow meter and the Dr. Klasse technique, the sample has a constant temperature at each point and the thermal conductivity is obtained by measuring the one-dimensional heat flux and the temperature gradient between two opposite surfaces. This kind of approach is frequently used but it requires long times in order to achieve the equilibrium temperature distribution inside the material. Furthermore, the time to reach equilibrium is longer for insulating refractory materials with lower thermal conductivity values. Transient methods, such as the laser flash, the hot disk and the hot wire methods, are faster. One of the advantages of having a short measurement time consists in reducing heat losses, which can affect the final results. Another advantage of the transient methods is that in some cases, it is even possible to measure different thermal properties with one experiment [11][16].

For each refractory material **(paragraph 2.1**), five different techniques were compared: the heat flow meter, the Dr. Klasse technique, the hot wire method, the hot disk method and the laser flash method. Let us analyse them in more detail.

2.2.1. Heat flow meter

The heat flow meter (HFM) is a steady-state method [16][50]. It can be applied to a wide range of insulating materials ($\lambda < 1$ $W \cdot m^{-1} \cdot K^{-1}$) at ambient conditions, but, as for all the steady-state methods, needs a long measurement time.

The procedure consists of placing a sample between two thin parallel copper plates equipped with thermocouples and heat flow sensors. Furthermore, in the top plate an electrical

resistance is embedded, which acts as a heat source. The power dissipation is chosen in order to impose a temperature difference ΔT of approximately 4 °C between the upper and lower face of the sample. For each measurement, it takes between 40 and 60 min to attain equilibrium conditions inside the material (similar and quite stable values of incoming and outgoing heat flows). To improve the thermal contact between the sample and the two plates, a weight is placed on top of the upper plate [51]. A simplified schematic of the measurement is shown in **Figure 2-6a**:

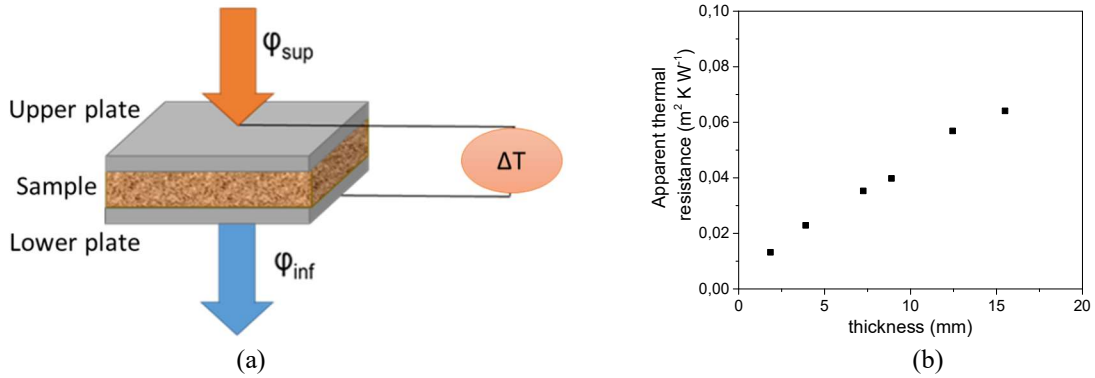

Figure 2-6: *a) Schematic diagram of the heat flow meter; b) the experimental results (**appendix A1**) are plotted as a function of the thickness (d).*

The apparent thermal resistance (R_{app}) is evaluated using **Equ. 2-1**:

$$R_{app} = \frac{\Delta T}{(\varphi_{sup} + \varphi_{inf})/2} \qquad \textit{Equ. 2-1}$$

where φ_{sup} is the heat flow supplied to the sample through the upper plate and φ_{inf} the heat flow coming out of the sample detected by the lower plate. The apparent thermal resistance is the sum of two contributions: the thermal resistance of the sample R_{th} and the contact resistance R_c between the sample and the two plates (**Equ. 2-2**).

$$R_{app} = R_{th} + R_c = \frac{d}{\lambda} + R_c \qquad \textit{Equ. 2-2}$$

where d is the thickness of the sample and λ the thermal conductivity. Measurements on samples with different thicknesses allow the last term (R_c) to be eliminated. Though R_c may depend on surface roughness, it can be assumed that the contact resistance does not vary between samples. Plotting the experimental data as a function of the thickness should then yield a linear relation (**Figure 2-6b**). The thermal conductivity is given by the inverse of the slope and the contact resistance is obtained by the intercept with the y-axis.

In terms of precision, the main factor that affects this value is the thickness for two main reasons. The first reason is that the samples are assumed to have two perfectly parallel faces, but a difference of ± 2% can be estimated. The second concerns the increase of the thickness, such that the lateral heat losses become significant. If they are not taken into account in the calculation, the overall thermal conductivity increases by up to 8% for the data in **Figure 2-6b**. While, if they are taken into account the accuracy is ± 1%. Thus, the uncertainty of this method

at room temperature is taken to be ± 3% [50] [52].

To better understand the influence of the lateral heat losses, let us consider an analogy with an electrical circuit. These losses act as a parallel thermal resistance, which reduces the overall thermal resistance of the system and consequently, it increases the apparent value of measured thermal conductivity.

To introduce the effect of heat losses, a correction was made by introducing heat losses through a heat sink term (P) in the one-dimensional steady-state heat equation [53]:

$$\frac{d^2T}{dz^2} + \frac{P}{\lambda} = 0 \qquad \textit{Equ. 2-3}$$

where λ is the thermal conductivity calculated considering samples with d < 6 mm. This value is chosen using the approximation that for small thicknesses, the lateral heat losses are negligible. P is the heat source/sink term ($W \cdot m^{-3}$) used to take into account the lateral heat losses due to convection heat transfer (**Equ. 2-4**) and it is attributed with a negative value:

$$P = \frac{hS(T_{air} - T(z))}{V} = \frac{4h(T_{air} - T(z))}{L} \qquad \textit{Equ. 2-4}$$

where h is the heat transfer coefficient. For natural convection in air a value of 15 $W \cdot K^{-1} \cdot m^{-2}$ can be used. S is the lateral surface area, V the volume, L the length of the sample, T_{air} the temperature of the air and T(z) the temperature of the material. Combining **Equ. 2-3** and **Equ. 2-4**, a differential equation is obtained, with a general solution given in **Equ. 2-5**:

$$T(z) = C_1 e^{Az} + C_2 e^{-Az} + T_{air} \qquad \textit{Equ. 2-5}$$

where $A = 2\sqrt{\frac{h}{L\lambda}}$. To evaluate the two constants C_1 and C_2, another equation is needed; Fourier's law in one-dimension:

$$\varphi(z) = -\lambda \frac{dT}{dz} = -\lambda A C_1 e^{Az} + \lambda A C_2 e^{-Az} \qquad \textit{Equ. 2-6}$$

with two boundary conditions: z = 0 (φ_{sup}) and z = d (φ_{inf}). **Equ. 2-5** and **Equ. 2-6** are used to re-calculate the incoming and outgoing heat flows through the sample, as well as the upper and lower temperatures. All these new values are then introduced in **Equ. 2-1** to calculate the new apparent thermal resistance (R_{app}*). This procedure was used in particular to investigate interface thermal resistance between samples, which requires the use of an assembly with a large thickness.

2.2.1.1. Sample preparation and set-up

From the original board/brick, between four and six square slabs with typical dimensions of 30x30 mm^2 were cut using a DeWalt circular saw with a diamond disk of 250 mm. Each slab had a different thickness (from 2 mm to 15 mm). To obtain the desired thickness, a precision automatic Presi Mecatome T210 micro-chainsaw was used. The SiC cutting disk was set at a rotation speed of 1500 rpm and the moving platform speed at 0.01 mm/s. These

parameters were chosen in order to have two flat parallel surfaces. All the steps were made without the presence of water as lubricant. The heat flow meter measurements were then performed using the equipment provided by CAPTEC, France, in ambient conditions.

2.2.2. Dr. Klasse technique

The Dr. Klasse technique (DKT) is a steady-state method developed at the RHI Technology Center in Leoben (Austria) to measure the thermal conductivity of different kinds of refractory materials [54], normally with $\lambda > 1$ $W \cdot m^{-1} \cdot K^{-1}$.

The apparatus is composed of a cylindrical kiln with a disk shaped electrical heating plate at the bottom. On this plate, an aluminium nitride (AlN) slab is placed in order to guarantee a homogeneous distribution of the heat. The sample is then placed directly on this slab. Finally, a reference material (same dimensions as the investigated specimen but with a known thermal conductivity value) is placed on the top of the sample. All around the pile, an insulating refractory material is inserted to minimize radial heat losses [54]. A schematic diagram of the equipment is shown in **Figure 2-7**.

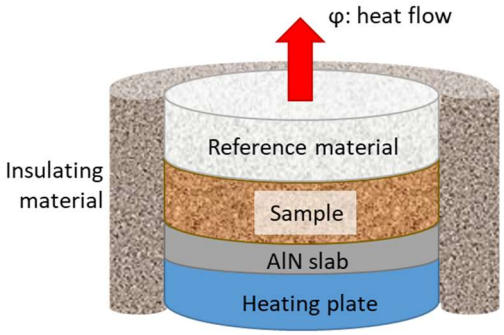

Figure 2-7: *Schematic diagram of the Dr. Klasse technique.*

The measurements are carried out at fixed temperatures starting from 200 °C. To be sure that the temperature of the furnace and that of the specimen are similar, the samples are left 2 h at the chosen temperature before making the measurements. Normally, a complete experiment takes two days.

The heat flow (φ) is calculated using Fourier's law applied to the reference material. The flow is then assumed to be the same in the investigated material (**Equ. 2-7**):

$$\varphi = -\lambda_{ref} S_{ref} \frac{\Delta T_{ref}}{d_{ref}} = -\lambda S \frac{\Delta T}{d} \qquad \textit{Equ. 2-7}$$

where λ_{ref} and λ are respectively the thermal conductivity of the reference material and the thermal conductivity of the investigated sample, ΔT_{ref} the temperature difference between the upper and lower faces of the reference material, ΔT the temperature difference between the upper and lower faces of the investigated material, S_{ref} the cross-sectional surface area of the reference material, S the cross-sectional surface area of the investigated material, d the thickness of the investigated material and d_{ref} the thickness of the reference material. Consequently, the thermal conductivity of the investigated sample is calculated using **Equ. 2-8**

[55]:

$$\lambda(T) = \lambda_{ref} \frac{\Delta T_{ref}}{\Delta T} \frac{d}{d_{ref}} \qquad \textit{Equ. 2-8}$$

The uncertainty of this method is taken to be ± 5%. This value is affected by two main factors: i) the thermal conductivity of the reference material, ii) the behaviour of the material investigated. In the first case, the results are more precise when $\lambda_{ref} \cong \lambda$. In the second case, if the hot side of the sample starts to warp, this means that the specimen partially loses the contact with the plates above and below it, which causes some errors in the results.

2.2.2.1. Sample preparation and set-up

The measurements were carried out on disk samples of typical dimensions: 100 mm in diameter and 25 mm in thickness. These dimensions are the same both for the refractory material under investigation and for the reference material. Furthermore, on the analysed samples two grooves are cut for the thermocouples. The sample preparation was made by RHI-Magnesita following refractory brick manufacture on the production line. The measurements were carried out in an air atmosphere using the equipment developed by the company.

2.2.3. Hot wire method

The hot wire method (HWM) is considered as an accurate method for determining the thermal conductivity of refractory materials with $\lambda < 15$ W·m^{-1}·K^{-1} [56].

For this method, four variations are known. The configuration chosen for this thesis is the hot wire parallel technique. For each measurement, three samples are needed (**Figure 2-8a**) [57]. A platinum wire and a thermocouple are placed between the bottom and the central samples in two parallel ground grooves at a known distance (15 mm). A reference thermocouple is positioned between the central and the top samples in a perpendicular direction compared to the wire. Furthermore, to ensure the same atmosphere all around the samples, the bottom sample is placed on two supports (also to avoid direct contact with the furnace).

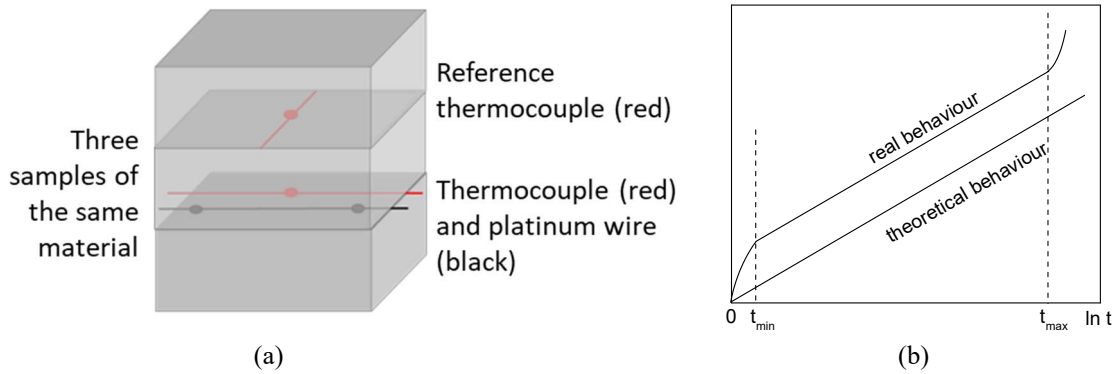

Figure 2-8: *a) Schematic diagram of the hot wire method, b) the graph shows the difference between the theoretical and the real temperature-time curves.*

The measurements are carried out at a fixed temperature, which means that initially

inside the samples there is a uniform temperature. The wire is connected to an electrical power supply. When a constant electrical current is applied, a constant amount of heat flux is generated all along the wire and this causes a transient temperature field, which for a given position is logarithmically dependant on time (**Figure 2-8b**). The wire is assumed to be ideal, infinitely thin and long and surrounded by an infinite medium [16][58]. The non-linearity at the beginning of the temperature-time response (from t = 0 to t_{min}) is due to the contact resistance between the samples and the wire, while the non-linearity at the end ($t > t_{max}$) is due to the finite dimensions of the samples.

The thermal conductivity for the parallel configuration is calculated using **Equ. 2-9**:

$$\lambda(T) = -\frac{q}{4\pi T(t)} E_i\left(\frac{-r^2}{4\alpha t}\right) \qquad \textit{Equ. 2-9}$$

where q is the heat flow, α the thermal diffusivity, r the distance between the wire and the thermocouple, T(t) the temperature rise compared to the initial temperature and t the time to reach that temperature [56][59]. E_i is a function given by **Equ. 2-10**:

$$-E_i(-x) = \int_x^{\infty} \frac{e^{-t}}{t} dt \qquad \textit{Equ. 2-10}$$

where $x = \frac{r^2}{4\alpha t}$.

The uncertainty of this method is taken to be ± 6% for small power levels and ± 1% for high power levels. These are related to: i) nonzero heat capacity of the wire, ii) thermal radiation, iii) outer boundary conditions (axial and radial heat losses), iv) non-constant power dissipation in the Pt wire, v) finite integration time of the voltmeter, vi) temperature drift of the sample surroundings and vii) radius of the wire [60]. Furthermore, in the case of an anisotropic material, the result represents an average value over the different heat flow directions through the sample.

2.2.3.1. Sample preparation and set-up

For this kind of measurement, it was not necessary to cut the samples, which were delivered with the suitable dimensions (250x114x50 mm^3). On one sample (bottom sample), two parallel grooves were drawn: one along the central axis (r = 0) for the wire, and one at r = 15 mm for the thermocouple (**Figure 2-8a**). The grooves were only a few millimetres deep. Once the wire and the thermocouple were placed inside the grooves, a bit of material powder was used to cover them. A similar operation was made on another sample (central sample). In this case, only one perpendicular line was drawn for the reference thermocouple (**Figure 2-8a**). The measurements were performed at the Institute of Mineral Engineering (GHI) of RWTH Aachen University using a Netzsch TCT 426 in an air atmosphere.

2.2.4. Hot disk method

The hot disk method is also known as the transient plane source (TPS) technique or

Gustafson probe from its precursor [61]. The main advantages of this method are: i) wide thermal conductivity range (from 0.005 $W \cdot m^{-1} \cdot K^{-1}$ to 500 $W \cdot m^{-1} \cdot K^{-1}$), ii) short measurement time (from 10 s to 10 min), iii) application to liquids, gels and solids, iv) easy sample preparation (only flat surfaces in contact with the probe are required), v) different sensor sizes to accommodate different sample types, vi) non-destructive, vii) high accuracy, viii) simultaneous measurements of thermal conductivity and thermal diffusivity [11][62].

The principle consists of putting a TPS probe between two halves of the sample material (**Figure 2-9a**). This probe is a double nickel spiral supported by two thin sheets of an insulating material (kapton, mica or teflon) for protection and electrical insulation. It has a double function: on one hand, it works as heat source for increasing the temperature of the sample; on the other hand, as a ‘‘resistance thermometer’’ for recording the time-dependent temperature increase (**Figure 2-9b**).

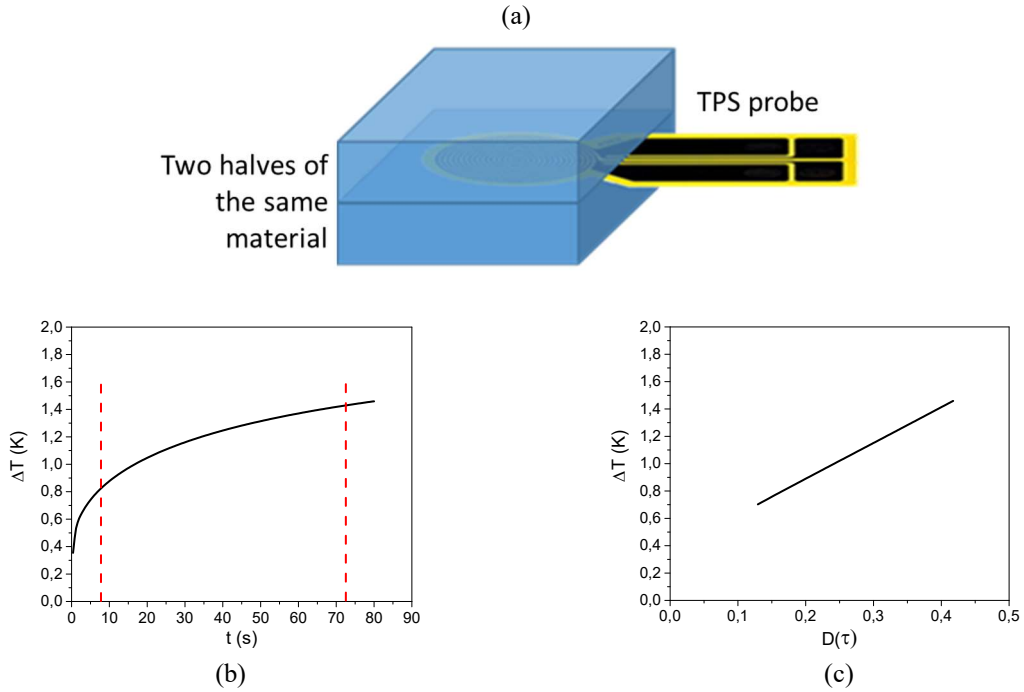

Figure 2-9: *a) Schematic diagram of the hot disk method; b) the graph shows the increase of the temperature as a function of time (**appendix A2**); c) linear relationship between the temperature increase and the dimensionless specific time function D(τ) (**appendix A2**). The red lines underline the two limit values: t_{min} and t_{max}.*

The theory is fairly similar to the hot wire method. It assumes that the probe is placed in a medium of infinite dimensions [61][62]. To adapt the model to the reality, two parameters must be chosen: the radius (r) of the probe and the measurement time (t). In the first case, the probe should cover only the central part of the samples in order to have enough material between the probe and the borders. In the second case, the time t should be chosen to guarantee a thermal penetration depth which is smaller than the real dimensions of the samples in all directions. For this reason, during the analysis of the thermal conductivity, a t_{max} is chosen in order to take into account the finite dimensions of the samples. Furthermore, the model also assumes a perfect contact between the probe and the samples. Taking into account the probe-sample contact thermal resistance, some of the initial points recorded (from t = 0 to t_{min}) are

removed from the calculation. A third parameter to choose is the heating power. This value is chosen in order to have a temperature increase less than 2 K [63].

The temperature increase is the sum of two contributions (**Equ. 2-11**): i) the temperature increase of the sample surface facing the TPS sensor (ΔT_s) and ii) the temperature increase which stems from the insulating layers of the nickel spiral, as well as from the contact resistance between the sample and the probe (ΔT_i) [64]:

$$\Delta T = \Delta T_s + \Delta T_i \qquad \textit{Equ. 2-11}$$

In the case of isotropic materials, the evaluation starts with an iteration procedure, which gives as final step the thermal diffusivity (α). The iteration establishes a linear relationship between the temperature increase and the dimensionless specific time function D(τ) (**Figure 2-9c**). The slope is ΔT_s, while the intercept with the y-axis is ΔT_i. The function D(τ) depends on the geometrical parameters of the nickel spiral and also τ given by **Equ. 2-12**:

$$\tau = \sqrt{\frac{\alpha t}{r^2}} \qquad \textit{Equ. 2-12}$$

where α is the thermal diffusivity, t the measurement time and r the radius of the probe. The thermal conductivity is calculated using **Equ. 2-13**:

$$\Delta T_s(\tau) = P_0 \left(\pi^{\frac{2}{3}} r \lambda\right)^{-1} D(\tau) \qquad \textit{Equ. 2-13}$$

where P_0 is the power output, r the radius of the probe, $\tau = \left(\frac{t}{\theta}\right)^{\frac{1}{2}}$ and $\theta = \frac{r^2}{\alpha}$ [64]. Then, the specific heat per unit volume ($\rho \cdot C_p$) is calculated using **Equ. 2-14**:

$$\lambda = \alpha \rho C_p \qquad \textit{Equ. 2-14}$$

For anisotropic materials, the procedure is quite similar. However in this case, it is important to firstly determine the specific heat per unit volume, which is necessary to calculate the thermal properties in the two directions. If the value inserted is wrong, the ratio between radial and axial results would be false [63]. The iteration procedure gives as results the radial thermal diffusivity (α_{rad}). The radial thermal conductivity (λ_{rad}) is then calculated using **Equ. 2-14**. The axial thermal conductivity (λ_{ax}) can be calculated using **Equ. 2-15** [64] and the axial thermal diffusivity (α_{ax}) using **Equ. 2-14**:

$$\Delta T_s(\tau_{rad}) = P_0 \left[\pi^{\frac{2}{3}} r (\lambda_{rad} \lambda_{ax})^{\frac{1}{2}}\right]^{-1} D(\tau_{rad}) \qquad \textit{Equ. 2-15}$$

The uncertainty of this method is estimated to be around 2 - 5% for the thermal conductivity and 5 - 10% for the thermal diffusivity [64]. These values depend on the accuracy of the output power, on the radius of the TPS probe and on the time. Furthermore, in the case of anisotropic materials, the values in the two directions strongly depend on the accuracy of the specific heat per unit volume.

2.2.4.1. Sample preparation and set-up

For each refractory material, six cubic samples were prepared with 70x70 mm^2 of surface area. Depending on the availability, thicknesses between 25 - 35 mm were cut. The preparation was made using a DeWalt circular saw with a diamond disk of 250 mm in dry conditions. The cubic shape was chosen for convenience of handling. Careful attention was paid to preparing two flat surfaces for contact with the probe. The measurements were performed both at the Department of Civil Engineering in Coimbra (FCTUC) using a TPS 2500 S and at the Ceramics Research Institute in Limoges (IRCER) using a TPS 1500. Two kapton sensors were used at room temperature: r = 14.61 mm and r = 6.403 mm. A mica sensor was used for measurements up to 400 °C: r = 14.61 mm. The measurements were carried out in an air atmosphere.

2.2.5. Laser flash method

Laser flash analysis (LFA) is often used for the determination of thermal properties of a wide range of materials. Developed by Parker et al. in 1961 [65][66], this transient method measures directly the thermal diffusivity of a solid with typical values between 0.1 and 1000 mm^2/s. Experimentally it can operate in the temperature range from 75 to 2800 K [65][67]. Some of the advantages of this technique are: i) simple specimen geometry (cylindrical/square shape), ii) small specimens, iii) rapidity of measurements (a few seconds for room temperature analysis), iv) ease of handling [65].

The principle consists of sending a short duration light energy pulse to impact on the front face of a sample placed at a certain temperature, which is measured by a thermocouple placed near the specimen. The temperature inside and outside the samples is assumed to be the same. An infrared detector records the temperature increment on the back face as a function of time (**Figure 2-10a**). The advantage is that there is no contact resistance between the sample and the heat source.

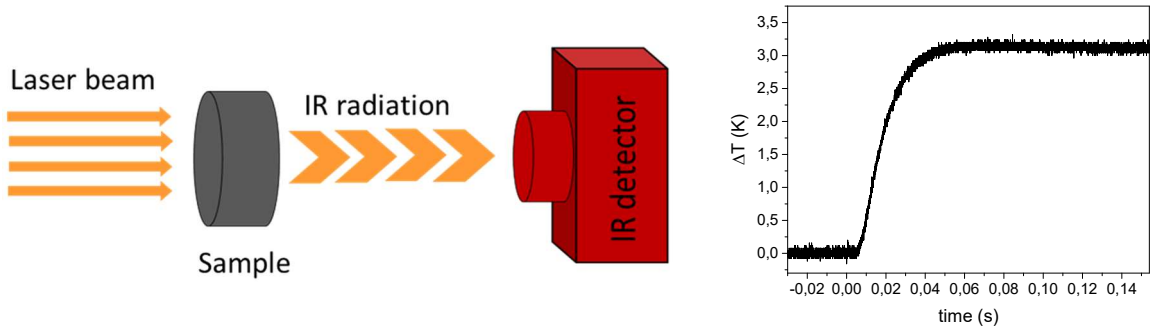

(a) (b)

Figure 2-10: *a) Schematic diagram of the laser flash method, b) evolution of the temperature on the opposite face as a function of time* ***(appendix A3)****.*

The evaluation of the thermal diffusivity (α) from the temperature – time behaviour can be performed with different models. In the case of negligible heat losses, it is possible to use Parker's equation [65]:

$$\alpha = 0.139\frac{d^2}{t_{1/2}} \qquad \textit{Equ. 2-16}$$

where d is the thickness of the sample and $t_{1/2}$ the time necessary for the opposite face to reach half of the maximum temperature. However, the hypothesis of negligible heat losses is not always applicable, especially at high temperatures. For this reason, many other models were developed for taking into account this effect, such as those of Cape-Lehman [68] and Degiovanni [69]. Furthermore, in the case of semi-transparent materials, another aspect to consider is the direct transmission between the two faces due to radiation effects (e.g. Mehling's model [70]). For these reasons, the analysis of thermal diffusivity in this work was made using the Mehling's model for all the investigated temperatures.

Once the thermal diffusivity is evaluated, the thermal conductivity (λ) can then be calculated using **Equ. 2-14** [67]. For more complex formulations, C_p can be estimated from data for simple components using the rule of mixtures (**Equ. 2-17**) [71]:

$$C_p = \sum_i m_i C_{pi} \qquad \textit{Equ. 2-17}$$

where m_i is the percentage in mass of each compound and C_{pi} the specific heat of each of them [72]. The percentage can be evaluated using inductively coupled plasma mass spectrometry (ICP-MS) or with X-ray fluorescence (XRF) analysis. Furthermore, the values of C_{pi} are temperature dependent, so **Equ. 2-17** should be applied to each temperature.

The uncertainty of this method is taken to be ± 5% at room temperature [65]. The main factors that influence the thermal conductivity results are: i) density (± 2%), because the faces might be not perfectly parallel; ii) C_p (± 3%), this is affected by the technique used to estimate the chemical composition since it is evaluated with the rule of mixtures; iii) precise knowledge of sample thickness (± 0.5%). At high temperatures, the uncertainty value can increase up to 10 - 15% depending on the material and on the quality of the T-t curve, which can present noise due to the hot environment and radiation effects.

2.2.5.1. Sample preparation and set-up

The measurements were carried out on small discs. Starting from a brick of refractory material, a carrot of 10 mm in diameter was machined. The carrot was subsequently divided in different pieces of around 2 mm thick using a precision automatic Presi Mecatome T210 micro-chainsaw. The operating parameters were set: SiC cutting disk with a rotation speed of 1500 rpm and a moving platform speed of 0.01 mm/s.

The samples were coated with a layer of graphite on both faces to improve the capability of the sample to absorb the applied energy, especially in the case of transparent materials [65]. The purposes of this layer are: i) to increase the heat absorbed on the front face; ii) to increase the radiation emitted by the back face; iii) to keep the absorption constant even if the sample changes colour; iv) to prevent the laser from passing directly through the sample to the detector. The graphite was applied using a spray, three times per face to ensure the presence of the layer also at high temperatures, with a final thickness of a few microns.

Albers et al. [73] demonstrated the importance of having this layer on both sides. They saw that in the case of black samples, the graphite layer has no influence. On the other hand, for a white material, it strongly influences the thermal diffusivity. In particular, if the graphite is applied only on the front face, the values of α are quite close to those obtained without the coating. This means that the radiative contributions hit the detector when the heat is not entirely redistributed inside the material, which causes a decrease of $t_{1/2}$ and consequently an increase of the apparent value for thermal diffusivity (**Figure 2-11a**) [73][74]. If the coating is applied on both sides, any errors are negligible. Furthermore, if the coating on the front face is imperfect or damaged, a pronounced peak appears in the initial instant because the laser radiation transmits directly to the back face (**Figure 2-11b**) [74].

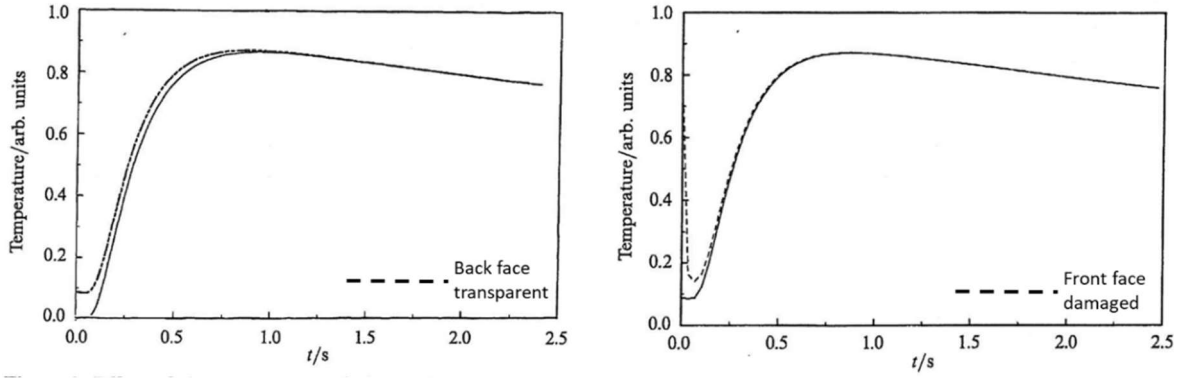

Figure 2-11: *a) Effect of transparency of the back face, b) effect of damage of the graphite layer on the front face* [74].

After graphite coating, the sample was placed on a sample holder made of alumina and covered by a cap of silicon carbide. Measurements were made using a Netzsch LFA 427 apparatus in an argon atmosphere at the Ceramics Research Institute in Limoges (IRCER). The apparatus is based on a vertical setup: the laser system is placed at the bottom and connected to the sample holder by an optical fibre, while the InSb detector is placed on the top and cooled by liquid nitrogen.

2.3. Comparison of the experimental results

Ideally the different measurement methods would yield the same value of thermal conductivity. However in fact the different techniques do not probe the material in the same heat flow direction, assess the thermal conductivity over the same sample volume or in identical experimental conditions. Consequently the chosen method to characterize the refractory material provides information which, though related, does not always compare directly to that given by another technique.

As mentioned in the **paragraph 2.1.1**, Insulating Boards (IB) are anisotropic materials, so at least two heat flow directions should be investigated. The “cross-plane” direction corresponds to the heat flow crossing the large faces of these boards (i.e. heat flow parallel to the pressing direction forming the boards). The “in-plane” direction corresponds to the heat flow parallel to plane of the boards (i.e. heat flow perpendicular to the pressing direction). On

the other hand, Insulating Fireclay Bricks (IFB) and Alumina Spinel Bricks (ASB) are considered macroscopically isotropic. This hypothesis was verified experimentally by measuring samples in different directions with the laser flash method. The obtained results were similar (± 10%). The anisotropic behaviour of Insulating Boards was studied using the laser flash method by cutting disk samples in two different directions. In contrast with the hot disk method, no change in sample configuration was necessary but an anisotropic analysis software module was used. For the Dr. Klasse technique and the heat flow meter, it was not possible to take into account this aspect because there was insufficient volume available for cutting samples in different directions. In the case of the hot wire method, the technique yields a value of λ corresponding to an average over the radial heat flow direction out of the "wire".

In the following sections, the results obtained with the five techniques previously described will be compared. Attention will be focused on aspects, such as reproducibility, heat losses, humidity variation, heterogeneity and anisotropy, to try to explain any differences in results.

2.3.1. Reproducibility of the results

For each refractory material, room temperature measurements were made using the laser flash method, the hot disk method and the heat flow meter. In the case of the laser flash method, two samples of each material were characterized with an average of three measurements per specimen. In the case of the hot disk method, three pairs of samples were studied and for each couple, four measurements were made. Finally, in the case of the heat flow meter, between five and six samples with different thicknesses were measured twice.

Room temperature measurements were not made with the Dr. Klasse technique and the hot wire method because the time to achieve the equilibrium temperature distribution inside the material was too long. Furthermore, if the material is insulating, this time is even longer. Therefore, the accuracy of the values at temperatures < 200°C was considered to be insufficient.

Table 2-4 shows the thermal conductivity results for the "cross-plane" direction for the three techniques at room temperature. This direction is of great importance since it corresponds to the heat flow direction through the lining in service.

Table 2-4: *Thermal conductivity values obtained with the heat flow meter (HFM), the hot disk method (TPS) and the laser flash method (LFA) at room temperature in the "cross-plane" direction. The table also shows the standard deviations (%) for each technique.*

Materials	***HFM*** λ ***(W·m^{-1}·K^{-1})***	***TPS*** λ ***(W·m^{-1}·K^{-1})***	***LFA*** λ ***(W·m^{-1}·K^{-1})***
IB-LD	0.26 ± 3%	0.29 ± 2.6%	0.19 ± 1%
IB-MD	0.36 ± 3%	0.35 ± 1.5%	0.22 ± 1.7%
IB-HD	0.36 ± 3%	0.43 ± 1%	0.27 ± 1.5%
IFB	0.45 ± 3%	0.38 ± 3.9%	0.36 ± 3.5%
ASB	-	5.3 ± 1%	6.5 ± 1.7%

Each set of results is reproducible. The standard deviations are around 3% for the heat flow meter (HFM), between 1% and 4% for the hot disk method (TPS) and between 1% and 3.5% for the laser flash method (LFA). This is of great importance especially for the LFA. Due to the small dimensions of the samples, this technique is not always "accepted" in the refractory field. However, in literature it is possible to find several statistical studies, which demonstrate the accuracy of this method. Fayette measured 10 samples of alumina refractory KR98AA and found a deviation of ± 10% [75]. Tonnesen et al. compared the laser flash and the hot wire methods for different refractory materials [57]. They found a reproducibility between 1.5% and 3.1% for the LFA. Lindemann and Neidhardt from Netzsch did the same for inhomogeneous refractories with an error bar of ± 10% [76]. It is also important to underline that the accuracy of the laser flash method is in part linked to the effect of the heterogeneity, which will be discussed in **paragraph 2.3.4**.

It is evident that the three methods give different results of thermal conductivity. **Table 2-4** shows a maximum discrepancy of around 38%. This value is sufficiently high to merit a more detailed investigation. However, it can be noted that the discrepancy is less for the isotropic material (IFB).

2.3.2. Role of the heat losses

Heat losses modify diffusivity values obtained by the laser flash (LFA) method using Parker's relation (**Equ. 2-16**), especially at high temperatures. However, the α values were corrected using Mehling's model [70], which has been built into the LFA software. In the case of conductivity values measured with the heat flow meter (HFM), the correction for heat losses was made using **Equ. 2-3** (**paragraph 2.2.1**). The corrected values for the HFM are shown in **Table 2-5**.

Table 2-5: *Heat flow meter (HFM) results before and after correction taking into account lateral heat losses.*

Materials	***HFM*** $\lambda\ (W \cdot m^{-1} \cdot K^{-1})$	
	Before	after
IB-LD	0.26 ± 3%	0.24 ± 3%
IB-MD	0.36 ± 3%	0.30 ± 3%
IB-HD	0.36 ± 3%	0.33 ± 3%
IFB	0.45 ± 3%	0.40 ± 3%

The corrected values (column called "after") are similar to that of λ determined for samples with small thickness (d < 6 mm). In other words, heat losses can be neglected by taking into account only the smallest samples with the heat flow meter.

Comparing **Table 2-4** and **Table 2-5**, it is possible to observe that in the case of Insulating Fireclay Bricks (IFB) the difference between the three methods is now within 10%. While in the case of Insulating Boards (IB), the difference between the heat flow meter and the other two methods is around 26%. Bourret et al. found similar discrepancy comparing the laser

flash method and the heat flow meter for geomaterial foams [51]. This means that some other aspects should be taken into account.

2.3.3. Effect of the humidity

Nait-Ali et al. studied the effect of humidity on porous zirconia materials [77]. Oummadi studied the drying behaviour of ceramic green bodies [78][79]. Both of them showed how the thermal conductivity increases with the increase of the water content. This can be explained by replacing the air in the pores with a thermal conductivity of 0.026 $W \cdot m^{-1} \cdot K^{-1}$ [80] at room temperature by water with a thermal conductivity equal to 0.6 $W \cdot m^{-1} \cdot K^{-1}$ [81] at room temperature.

This factor can help to explain why the laser flash method gives the lowest values of thermal conductivity. As mentioned in the **paragraph 2.2.5.1**, the measurements were made in an argon atmosphere. To be sure that inside the furnace there was Ar, the samples were firstly subjected to three cycles of vacuum followed by filling with argon. As a consequence, the samples were effectively dried before the measurements. On the other hand, the hot disk method and the heat flow meter were made in the air atmosphere of standard laboratory conditions, with a typical relative humidity of 40 - 50%. In fact, the nature of the Insulating Boards (IB) containing layered vermiculite grains makes these IB samples particularly sensitive to their thermal and hydric history.

To verify the influence of humidity and water content, the IB samples used for the hot disk method were left inside the oven at 200 °C for 24 h, cooled down 30 min in a desiccator and then measured again. This temperature was chosen in order to remove the physically adsorbed water and the water molecules residing in the particle spaces of the vermiculite. According to literature studies [82][83], this intercalated water forms layers not in immediate contact with the cation (Mg^{2+} in this work). This temperature was also confirmed by differential thermal analysis (DTA) results, which exhibit an endothermic peak between 20 °C and around 250 °C. Furthermore, the same temperature was used also in the case of Insulating Fireclay Bricks (IFB) to have comparable experimental conditions. The results are shown in **Table 2-6**.

Table 2-6: *Hot disk (TPS) results before and after drying.*

Materials	***TPS*** λ $(W \cdot m^{-1} \cdot K^{-1})$	
	before	After
IB-LD	0.29 ± 2.6%	0.23 ± 2.6%
IB-MD	0.35 ± 1.5%	0.28 ± 1.5%
IB-HD	0.43 ± 1%	0.34 ± 1%
IFB	0.38 ± 3.9%	0.38 ± 3.9%

Furthermore, for each refractory material, the water content (W) was calculating using **Equ. 2-18** [78]. The calculation is made on the dry basis.

$$W(\%) = \left(\frac{m_i - m_f}{m_f}\right) \cdot 100 \qquad \textit{Equ. 2-18}$$

where m_i is the mass of the sample before drying and m_f the mass of the sample after drying. The analysis gave 4 - 5% wt. of water content in the case of Insulating Boards (IB) and less than 0.05% wt. in the case of Insulating Fireclay Bricks (IFB).

Thermogravimetric analyses (TGA) were made on Insulating Fireclay Bricks. The results show no change in mass up to 1000 °C. This means that these kinds of refractories do not adsorb water despite they are highly porous (**Table 2-2**). The interpretation is consistent with **Table 2-6**, where the λ remains the same after drying (0.38 $W \cdot m^{-1} \cdot K^{-1}$). The situation is different in the case of Insulating Boards. By removing 4 - 5% wt. of water content, the hot disk values decreased by 26%. Therefore, drying is an important step to avoid overestimating the thermal conductivity.

To summarize, taking into account the lateral heat losses and the effect of the humidity, the heat flow meter, the hot disk method and the laser flash method give the following results (**Table 2-7**).

Table 2-7: *Thermal conductivity values obtained with the heat flow meter (HFM), the hot disk method (TPS) and the laser flash method (LFA) at room temperature in the "cross-plane" direction after considering the effects of heat losses and humidity. The HFM results have been adjusted to equivalent "dry" conditions.*

Materials	***HFM*** λ $(W \cdot m^{-1} \cdot K^{-1})$	***TPS*** λ $(W \cdot m^{-1} \cdot K^{-1})$	***LFA*** λ $(W \cdot m^{-1} \cdot K^{-1})$
IB-LD	0.18 ± 3%	0.23 ± 2.6%	0.19 ± 1%
IB-MD	0.22 ± 3%	0.28 ± 1.5%	0.22 ± 1.7%
IB-HD	0.26 ± 3%	0.34 ± 1%	0.27 ± 1.5%
IFB	0.40 ± 3%	0.38 ± 3.9%	0.36 ± 3.5%
ASB	-	5.3 ± 1%	6.5 ± 1.7%

In the case of the heat flow meter (HFM), the values were corrected mathematically to remove the effect of the humidity by considering equivalent "dry" conditions as shown for the hot disk measurements (26%) in **Table 2-6**. In the case of Alumina Spinel Bricks (ASB), the effect of the humidity was considered negligible due to the low porosity (**Table 2-3**) and it was verified experimentally with TG measurements, which do not show change in mass between room temperature and 200 °C.

Table 2-7 shows that the values obtained with the heat flow meter and the laser flash method are rather close. The maximum discrepancy is within 10%. These two techniques probe similar heat flow directions (linear in both cases). On the other hand, the hot disk method involves different experimental conditions, and the heat flow is spherically radial from the disc shape probe. This method gives the highest thermal conductivity values in the case of the anisotropic materials (IB) with a maximum discrepancy of around 26%.

In the case of the isotropic material (IFB), the three methods find a good agreement. The results are within 10%. However, in the case of Alumina Spinel Bricks (ASB), the discrepancy

is around 20% even if the material is isotropic. This value might be linked to the heterogeneous nature of the refractory. Therefore, let us examine in more detail the effects of the anisotropy and heterogeneity.

2.3.4. Role of the anisotropy and heterogeneity

An important parameter to consider if the material presents a heterogeneous microstructure is that of the sample dimensions. For instance, measurements on alumina spinel castables produced by I. Kieliba (RWTH - Aachen), with the biggest grain size of ~ 6 mm, showed very different values of thermal conductivity on different samples with the laser flash method (from 5 $W \cdot m^{-1} \cdot K^{-1}$ to 12 $W \cdot m^{-1} \cdot K^{-1}$). In fact, depending on the zone in which the sample is machined, there might be a different grain/matrix ratio, and this affects the results. Therefore, the evaluation made on a larger volume sample will give a more accurate average value [84].

The Insulating Fireclay Bricks (IFB) have a fine microstructure which, at the macroscale, is homogeneously distributed (**Figure 2-4**). This means that small mm sized samples can be representative of the entire brick. This interpretation is confirmed by the results shown in **Table 2-7**, where the three techniques give really close values (within 10%).

On the other hand, the Insulating Boards (IB) have microstructures with greater heterogeneity, mostly linked to the layer structure of the vermiculite and its orientation (**Figure 2-2)**. The difference between the hot disk and the other two methods, in this case, is within 26%. As mentioned, the effect of heterogeneity is in part related to the anisotropic conductivity of individual grains. Furthermore, orientation of these grains in brick forming leads to anisotropic thermal conductivity at the macroscopic scale. In fact, the difference between the three kinds of IB is linked to the casting pressure, which is higher in the case of High Density Insulating Boards. Maxwell-Eucken's relation (**Equ. 1-20**) was used for determining the thermal conductivity of the solid phase in the two directions for all the Insulating Boards. In the case of Low Density and Medium Density Insulating Boards, a λ_s of 0.6 $W \cdot m^{-1} \cdot K^{-1}$ was estimated in the "cross-plane" direction and ~ 1 $W \cdot m^{-1} \cdot K^{-1}$ in the "in-plane" direction. In the case of High Density Insulating Boards (IB-HD), λ_s changes from 0.6 $W \cdot m^{-1} \cdot K^{-1}$ in the "cross-plane" direction to 1.4 $W \cdot m^{-1} \cdot K^{-1}$ in the "in-plane" direction. This simple calculation highlights that IB-HD exhibits more anisotropy due to the higher portion of solid phase.

Two techniques were used to determine the anisotropic behaviour of the Insulating Boards: the laser flash and the hot disk methods. In the first case, the measurements were made on two different samples, which were cut with the faces in two different directions. In the second case, the measurements were made on the same pair of samples using an anisotropic software module. Both techniques give higher thermal conductivity values in the "in-plane" direction than the "cross-plane" direction. This is of great importance because the materials are used to reduce heat losses through the lining of the ladle, to reduce energy cost and environmental impact. Another advantage of having higher thermal conductivity values in the "in-plane" direction is that the heat is conducted more easily in the circumferential direction of the ladle, and this will help to keep the temperature constant inside the bath. The measurements also show that the difference between the two directions increases with the decrease of the

porosity both for the laser flash and the hot disk methods. This confirms the hypothesis that the anisotropic behaviour is related to the orientation of the layer structure of the vermiculite.

Let us now examine the results for the hot wire method. As mentioned in the **paragraph 2.2.3**, this technique gives an average value of λ. Therefore, the values obtained with the hot wire method are compared with those obtained with the laser flash method in the two directions (**Figure 2-12**). The graphs show similar temperature behaviours with the two techniques for the three refractory materials. Furthermore, the thermal conductivity values obtained with the hot wire method are in between the values obtained with the laser flash method in the two directions, which validates the hypothesis that this technique gives an average value. If these results are used as input parameters in the modelling studies, the calculation will overestimate the thickness of the insulation to apply, with economic consequences. **Figure 2-12** also confirms the increase of the effect of the anisotropy with the reduction of the porosity. IB-HD is characterized by the lower pore volume fraction (**Table 2-1**) and **Figure 2-12c** shows a higher difference between the values in the two directions than IB-LD (**Figure 2-12a**) and IB-MD (**Figure 2-12b**). The higher proportion of solid phase in the High Density Insulating Board emphasizes this characteristic compared to the homogenizing effect of the isotropic pores.

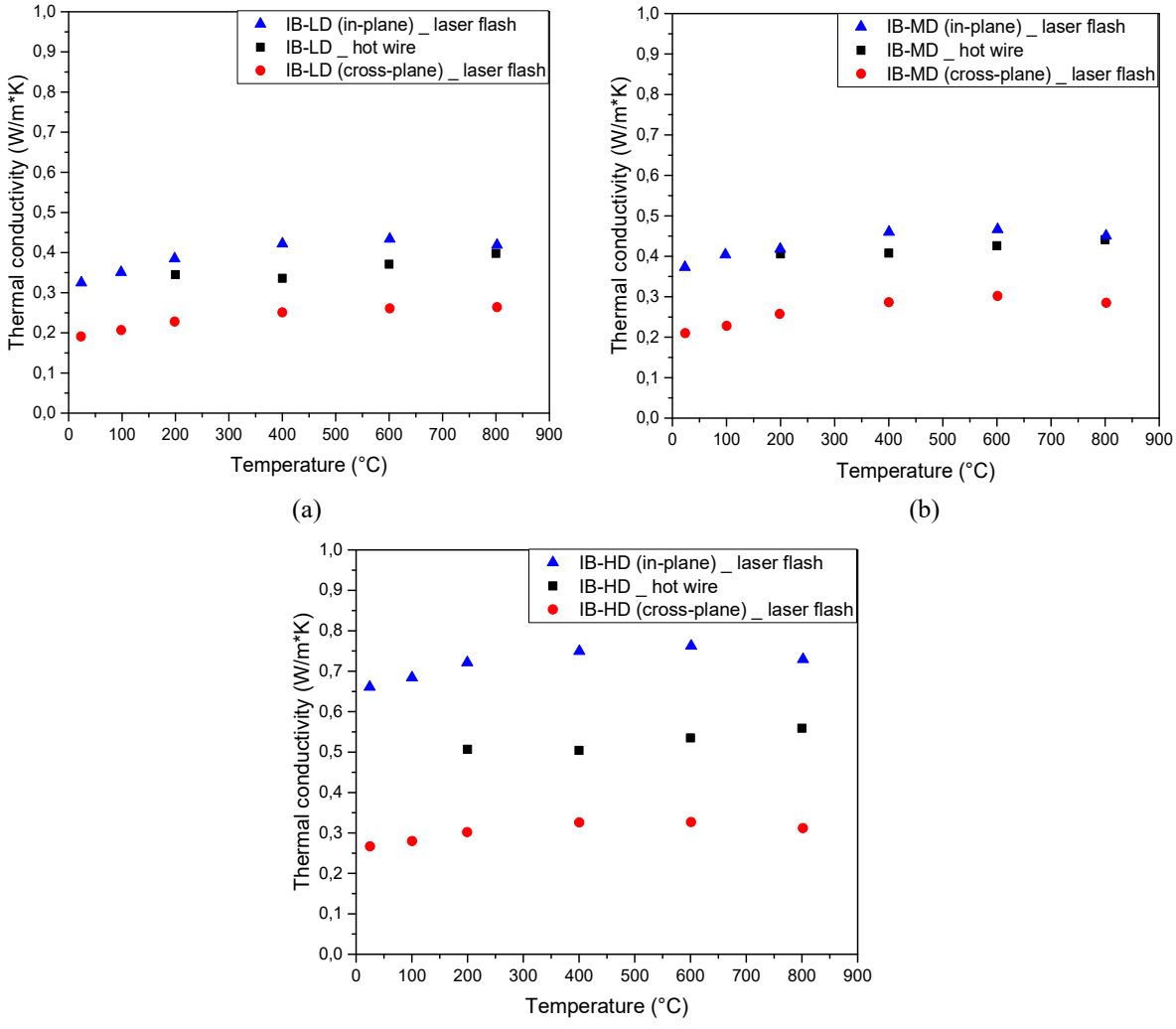

Figure 2-12: *Comparison between the hot wire and the laser flash methods on Insulating Boards (Low Density (a), Medium Density (b) and High Density (c)).*

2.3.5. Measurements at medium and high temperatures

Let us study in more detail the effect of the temperature. Three techniques were used for high temperature measurements: the Dr. Klasse technique, the hot wire method and the laser flash method. The laser flash measurements were made in an argon atmosphere up to 900 °C for the Insulating Boards (IB), up to 1200 °C for the Insulating Fireclay Bricks (IFB) and Alumina Spinel Bricks (ASB). For all the refractory materials, starting from 400 °C, the laser voltage was increased by 20 V each 100 °C to reduce the noise in the signal caused by the hot environment. Hot wire measurements were performed in the temperature range 200 - 800 °C for IB and 200 - 1200 °C for ASB, both in an air atmosphere. Finally, Dr. Klasse measurements were performed in the temperature range 200 - 800 °C for IB, 200 - 900 °C for IFB and 200 - 1000 °C for ASB, all in an air atmosphere.

Figure 2-13 shows the thermal conductivity values as a function of the temperature for all the refractory materials obtained with the laser flash method. All the measurements are taken in the "cross-plane" direction. For each material, two samples were characterized and at each temperature, three measurements of the sample were made.

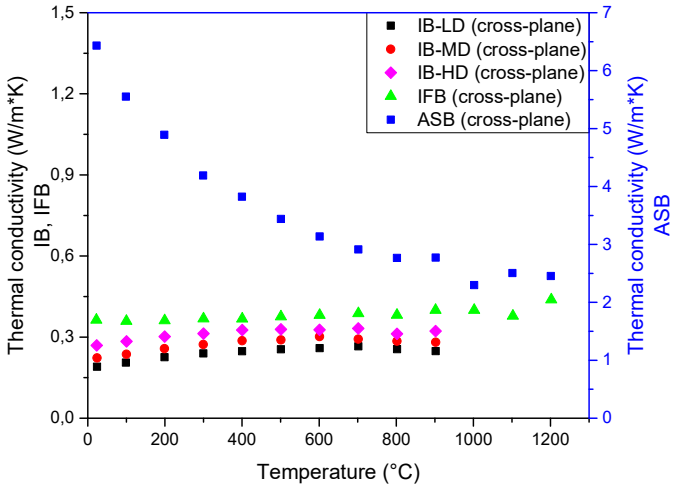

Figure 2-13: *Laser flash results for Low Density Insulating Boards (black), Medium Density Insulating Boards (red), High Density Insulating Boards (pink), Insulating Fireclay Bricks (green) and Alumina Spinel Bricks (blue).*

It is important to underline that the standard deviation of measurements increases at high temperatures due to the presence of a hot environment. The maximum value obtained for each material is: ± 9.6% IB-LD ("cross-plane") and ± 10% IB-LD ("in-plane"); ± 12% IB-MD ("cross-plane") and ± 10% IB-MD ("in-plane"); ± 5.5% IB-HD ("cross-plan") and ± 5% IB-HD ("in-plane"); ± 15% IFB and ± 21% ASB.

The graph shows three types of behaviour with temperature. In the case of Insulating Boards (IB), the thermal conductivity slightly increases with the increase of the temperature. This is similar to the behaviour of gases (**Figure 1-7**). For these materials, λ is strongly controlled by the thermal conductivity of the gas (λ_g), since they are highly porous (**Table 2-1**). To verify this hypothesis, a simple calculation was made. Maxwell-Eucken's relation (**Equ. 1-20**) was firstly used to evaluate the thermal conductivity of the solid phase at room

temperature (λ_s). This value was assumed to be constant in the temperature range 20 - 900 °C. Then, **Equ. 1-20** was used to evaluate the thermal conductivity of the refractory material in argon atmosphere. The obtained results show an increase of λ with temperature following the increase of λ_p, which is also a function of temperature. On the other hand, the increase of the thermal conductivity values can be also linked to the specific heat, but this effect seems to be less significant.

In the case of Insulating Fireclay Bricks (IFB), the thermal conductivity is quite constant up to 1000 °C. Above this temperature, there is a slight increase. This might be linked to the fact that in this range, the meta-kaolin partially melts and then recrystallizes into an Al/Si phase which leads to an increase in the thermal conductivity of the solid phase [14][85]. Or it might be attributed to radiation effects (**paragraph 1.2.2.3**).

Finally, in the case of Alumina Spinel Bricks (ASB), the thermal conductivity decreases with the increase of temperature and this is linked to the increase of phonon-phonon scattering (**paragraph 1.2.2**). Furthermore, in the range of 1000 - 1200 °C, it is possible to observe a shift of the thermal conductivity trend. Kieliba and the Aachen group related this phenomena to the ongoing process of α-Al_2O_3 precipitation from non-stoichiometric spinel grains at the alumina-spinel interfaces [86]. Let us now compare the three techniques (laser flash method, hot wire method and Dr. Klasse technique) in the case of Alumina Spinel Bricks (**Figure 2-14**).

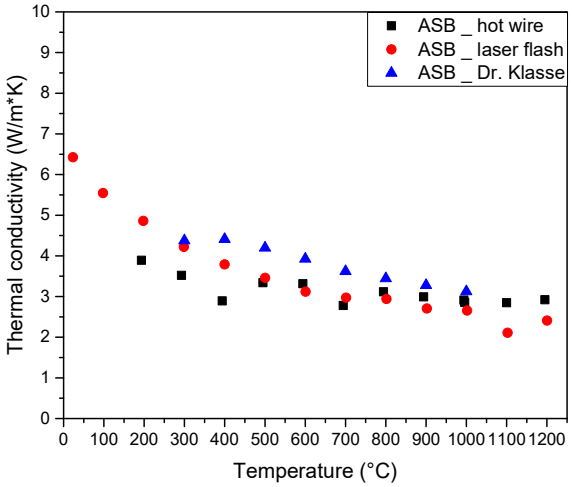

Figure 2-14: *Comparison between the hot wire and the laser flash methods and the Dr. Klasse technique on Alumina Spinel Bricks. The hot wire results were performed at the Institute of Mineral Engineering of RWTH Aachen University (Germany) by I. Kieliba, while the Dr. Klasse results at RHI-Magnesita (Leoben).*

Figure 2-14 shows that up to 500 °C, the hot wire method gives the lowest thermal conductivity values. Above this temperature, the results are similar to those obtained with the laser flash method. Similar behaviour was found by Lindemann and Neidhardt from Netzsch on magnesia-spinel bricks [76]. On the other hand, the Dr. Klasse technique (DKT) and the laser flash method show similar trends. It can be noted that the DKT gives the highest thermal conductivity values. To explain this difference, let us consider **Equ. 2-7**. The heat flow is calculated with the reference material and ideally it should be the same as the investigated material, but this is not the situation. If part of the heat passing through the investigated sample and the reference is lost due to lateral heat losses (even if this is reduced by the presence of an

insulating refractory), the apparent heat flow indicated by the reference material is higher. Thus, the apparent thermal resistance of the investigated sample (**Equ. 2-1**) is lower than the real value and consequently, the measured thermal conductivity value is higher.

Let us now make the same analysis for the insulating materials (**Figure 2-15**). The graphs show the comparison between the laser flash (LFA) and the hot wire (HWM) methods, and the Dr. Klasse technique (DKT). In the case of the Insulating Boards (IB), both directions are shown. **Figure 2-15a**, **b**, **c** show that the results obtained for the DKT (blue points) are similar to those obtained with the HWM (black points). However, this is only a coincidence. The Dr. Klasse technique measures the thermal conductivity in the "cross-plane" direction and thus, it should be compared with the laser flash in the same direction (red points). For all the four insulating refractories, it is possible to observe that the Dr. Klasse technique gives consistently higher thermal conductivity values than the laser flash method, as in the previous case. Furthermore, the % differences between the DKT and LFA curves are higher.

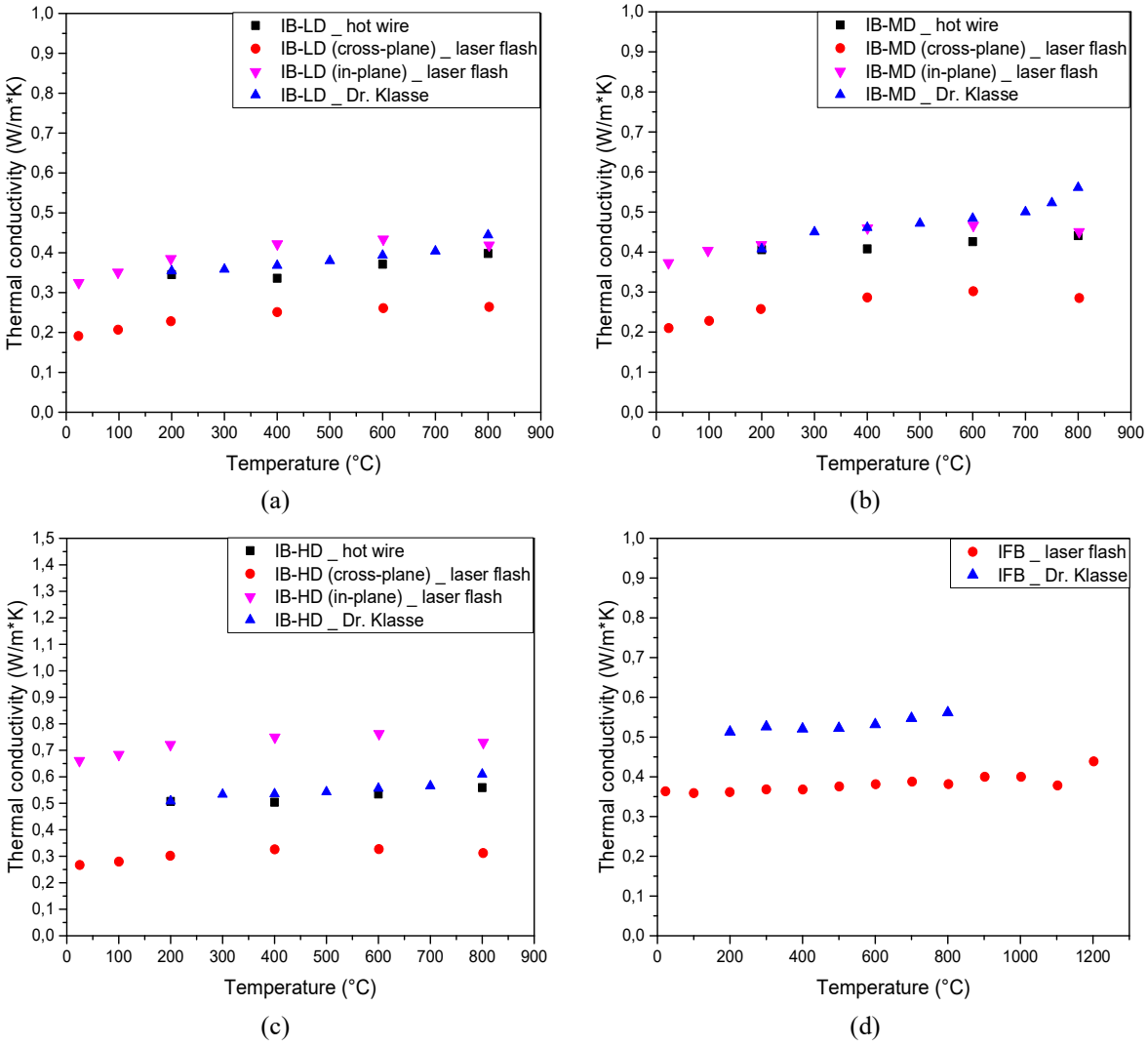

Figure 2-15: *Comparison between the laser flash method, the hot wire method and the Dr. Klasse technique on a) Low density Insulating Boards, b) Medium Density Insulating Boards, c) High Density Insulating Boards and d) Insulating Fireclay Bricks.*

The higher discrepancy between the two methods might be explained considering that

in the case of the Dr. Klasse technique, the heat losses from the reference material and the investigated sample are relatively higher than the previous case (ASB). This is linked to the thermal conductivity of the two specimens: λ_{ref} is 2.7 $W \cdot m^{-1} \cdot K^{-1}$ and λ of the investigated samples is < 1 $W \cdot m^{-1} \cdot K^{-1}$. Thus, the systematic error is increased. The thermal resistance of contacts between the investigated specimen and the reference in the set-up may also play a role. This last aspect merits further investigation.

2.4. Conclusion

The thermal conductivity of refractory materials is an input parameter, which is required for modelling of heat transfer through a steel ladle lining. Therefore, its estimation is of primary importance. Several methods can be used but each of them leads to some variations in the obtained values. Therefore, the chapter was dedicated to the comparison of five measurement methods: heat flow meter (HFM), Dr. Klasse technique (DKT), hot wire method (HWM), hot disk method (TPS) and laser flash method (LFA). For each technique, advantages and disadvantages were investigated on three kinds of refractory materials: Insulating Boards, Insulating Fireclay Bricks and Alumina Spinel Bricks. Furthermore, the analysis went into detail to explain the influence of parameters, which can affect the thermal conductivity results, and for each of them a percentage was estimated. The investigated factors were: i) heat losses, which can increase the λ values by 5 - 10%; ii) humidity, which can increase the λ values by 15 - 25% on highly porous materials; iii) anisotropy and heterogeneity, intrinsically linked, which can vary the λ values by 10 - 15%. Thus, if all these effects are taken into account, it is possible to find a good agreement between all techniques. According to the current work, the best technique for the investigated materials seems to be the hot disk method. This method has many advantages: i) it can estimate the thermal conductivity in two directions with one experiment, ii) the results are obtained in a short time, iii) the samples have sufficient volume to take into account the heterogeneity of the material. The following table summarizes the main advantages and disadvantages of each technique.

Method	*Measured parameter*	*Range**	*Uncertainty**	*Sample shape*	*Sample dimensions*	*Heat source*	*Anisotropy*	*Heat losses*	*Heterogeneity*
LFA	α	0.1-1000 $mm^2 s^{-1}$	± 5%	Square / Cylindrical	Φ: 10 mm d: 2 mm	Light energy	2 values - 2 samples	Model correction	-
TPS	λ α	0.005-500 $W m^{-1} K^{-1}$	2-5% 5-10%	Square / cylindrical	70x70x25-35 mm^3	Electrical resistance	2 values - 1 measurement	-	More precise average value
HWM	λ	< 15 $W m^{-1} K^{-1}$	1-6%	Square	250x114x50 mm^3	Electrical resistance	Average value	-	More precise average value
HFM	λ	< 1 $W m^{-1} K^{-1}$	± 3%	Square	30x30x1.5-16 mm^3	Electrical resistance	2 values - 2 samples**	Model correction	-
DKT	λ	> 1 $W m^{-1} K^{-1}$	± 5%	Cylindrical	Φ: 100 mm d: 25 mm	Electrical heating plate	2 values - 2 samples**	Insulating material around sample	More precise average value

*ASTM and ISO standards.

** It is possible to determine the anisotropic behaviour of a material, if sufficient volume of the material is available to cut samples in different directions.

Chapter 3 :

Influence of the microstructure on the thermal conductivity

To understand the thermal behaviour of a refractory material, as well as for any material, it is fundamental to analyse the relationship between the thermal properties and the microstructure. Low thermal conductivity values are essential for all the applications in which the reduction of heat losses is the main requirement. In contrast, high thermal conductivity values are suitable for those materials, whose function is to remove heat or that need to resist strong thermal shocks. The present chapter will go into detail in order to explain the effects of the porosity, grain boundaries, grain sizes and second phases on the thermal conductivity values of Alumina Spinel Bricks. Furthermore, the results will be compared with different alumina-based model materials including nuances with the presence of cement for a better interpretation of the behaviour of the refractory material.

3.1. Refractory materials: manufacturing

The microstructure can strongly influence the thermal, mechanical and other physical properties of a ceramic material. The **paragraphs 1.2.2.1** and **1.2.2.2** discuss how the presence of pores and small grains reduces the thermal conductivity. Therefore, the properties of a refractory material are controlled by the microstructure and are chosen depending on its functional application (**Figure 3-1**).

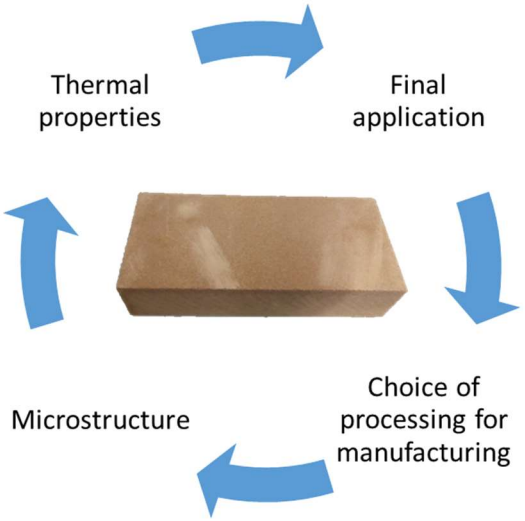

Figure 3-1: *Diagram of the four important steps for the realization of a refractory material.*

To obtain the desired microstructure, it is important to choose the right processing in manufacturing. This is a very delicate matter and is based on the know-how of each specialized industrial sector. It can be divided into three main steps (**Figure 3-2**).

Firstly, it is essential to choose suitable raw materials as a powder. Refractories are usually a mixture of two or more phases. Each of them has specific properties and will react in a specific way. Phase diagrams are precious allies for understanding which kind of compound will be formed at a certain temperature. The materials are then mixed to create a new material with the desired characteristics.

Secondly, the desired shape of the ceramic body is formed. During this step, the powders are compacted together to form the "green body" and create the initial adhesion between the particles (small contact area). One of the forming methods is pressing. Usually higher pressing force leads to reduced porosity up to a packing limit.

Finally, the green body is fired at high temperatures to obtain the final product. This is a fundamental step. The heat treatment creates the solid bridges between the particles and gives to the material the final properties, as well as the final dimensions. Normally, higher firing temperature and longer dwell time improve the densification, i.e. reduces the porosity. Therefore, depending on the need to have a dense or a porous material, the heat treatment will be chosen appropriately. Either it could be respectively the classic sintering temperature (about 200 °C - 300 °C below the melting point of the compound) or the minimum temperature, which guarantees a minimum mechanical strength.

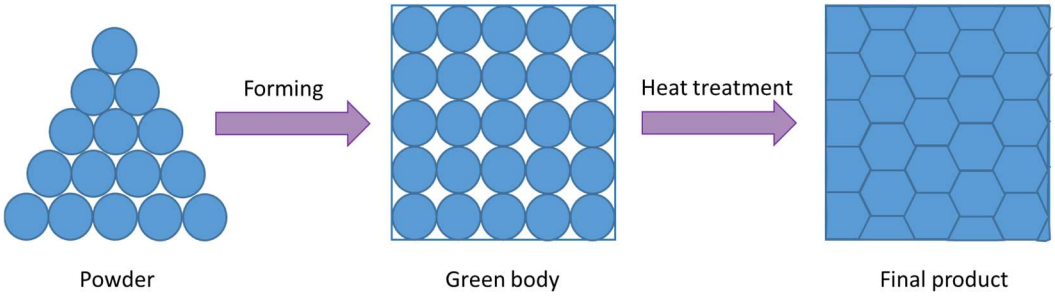

Figure 3-2: *Schematic of the process to form a refractory material.*

Let us say that the production of refractory materials is "a life of choices". Depending on the raw materials, pressing force, firing cycle (maximum temperature, dwell time, heating rate), are chosen, the final product will have a specific microstructure and set of properties. Furthermore, the choice is strongly influenced by the final application.

However, refractories are very complicated ceramic materials and it is not always easy to understand the relationship between the microstructure and the thermal properties. As already mentioned, they are a mixture of two or more solid phases with the presence of impurities, defects, pores… Furthermore, their microstructure can evolve with the temperature and, as a consequence, the properties can change in service conditions. Nowadays, it is not always possible to attribute a specific behaviour to a specific phase or to the presence of a particular impurity. Furthermore, the influence of the grain boundaries should be identified. In some refractories, grain boundaries are not well-defined due to the formation of another phase or to the precipitation of compounds. Therefore, in this work we have chosen to study these materials by comparison of their behavior with model materials with comparable composition and characteristics. The aim is to elucidate the contribution of each feature in the microstructure to

the overall thermal conductivity of the refractory material.

3.2. From model to industrial materials

Let us examine the case of a sample of Alumina Spinel Brick (**paragraph 2.1.3**). Its behaviour is compared with four alumina-based model materials: sapphire, dense alumina, alumina AKP-1450 and AKP-1300. **Table 3-1** summarizes the porosity, average grain size and sintering temperature of each material.

Table 3-1: *Summary of the porosity, average grain size and sintering temperature of five alumina-based materials.*

Materials	***Porosity (%)***	***Average grain size (µm)***	***Sintering temperature (°C)***
Sapphire	0	Single-crystal	-
Dense Alumina	3	< 0.40	1200
Alumina AKP-1450	20	0.45	1450
Alumina AKP-1300	38	0.30	1300
Alumina Spinel	19	-	-

The dense alumina was made by Honda at NITech (Japan) using the pulse electric current sintering (PECS). This innovative technique has the advantage to produce almost fully dense materials in shorter times and lower temperatures than a conventional electric furnace [87], keeping grain growth to a minimum. The dense alumina samples were sintered at 1200 °C for 5 min with a heating rate of 100 K/min and under a uniaxial pressure of 100 MPa. The alumina AKP-1300 and AKP-1450 samples were prepared by Puech at IRCER by uniaxial pressing of the dry powder (both AKP30) and then fired respectively at 1300 °C and 1450 °C for 6 min [30]. The alumina spinel bricks have grains of different sizes (**Figure 2-5**) that make the evaluation of the average grain size difficult.

3.2.1. Effect of the temperature

Figure 3-3 shows the thermal conductivity results as a function of the temperature of five alumina-based materials: four model materials and one refractory material. For each of them, two samples were analysed. The measurements were carried out up to 1000 °C (with a heating rate of 5 K/min) in an argon atmosphere using the laser flash method (**paragraph 2.2.5**). For each temperature, three measurements were made.

All the materials show that the thermal conductivity values decrease with the increase of the temperature. The increase of temperature leads to an increase of the density of phonons and consequently an increase of the phonon-phonon scattering mechanism. This reduces the mean free path of the phonons and consequently the thermal conductivity. Furthermore, the graph shows that the values of thermal conductivity are quite different from each other, despite they are all alumina-based materials. For instance, at room temperature, single-crystal sapphire exhibits a value of 37 $W \cdot m^{-1} \cdot K^{-1}$ whereas the Alumina Spinel Brick yields a value of 6.5

$W \cdot m^{-1} \cdot K^{-1}$.

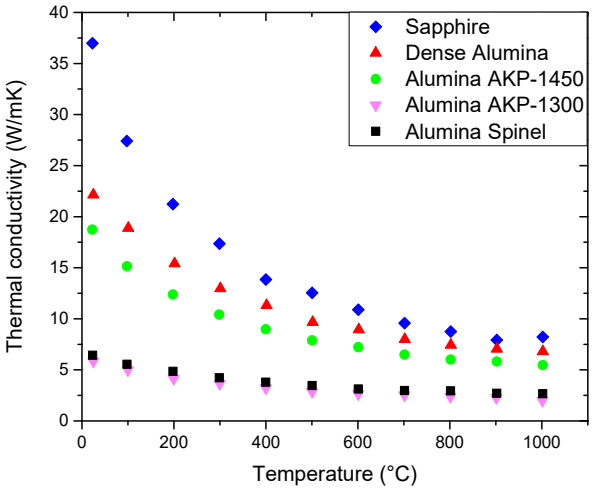

Figure 3-3: *Thermal conductivity results as a function of the temperature of five alumina-based materials.*

To explain this wide gap, it is essential to consider the influence of other parameters such as porosity, grain boundaries, grain sizes and the presence of a second phase. In the following sections, estimates of the grain conductivity will be made from the experimental values by correcting for the effects of the microstructure based on the analytical relations introduced in **Chapter 1**. The calculations predict a final value equal or at least closer to that of the single-crystal. Let us start by taking into account the effect of the porosity.

3.2.2. Effect of the porosity

For each material, the percentage of porosity (P) was calculated using **Equ. 3-1**:

$$P(\%) = \left(1 - \frac{\rho_{app}}{\rho_r}\right) \cdot 100 \qquad \textit{Equ. 3-1}$$

where ρ_{app} is the bulk density (mass/volume) and ρ_r the theoretical density (3.98 g/cm^3) or the true density measured using a helium pycnometer, in the case of the refractory material. The calculated values are summarized in **Table 3-1**.

Let us consider for a moment only the four model materials: sapphire (no porosity), dense alumina (3% of porosity), alumina AKP-1450 (20% of porosity) and alumina AKP-1300 (38% of porosity). With the increase of the pore volume fraction, the thermal conductivity decreases due to the low thermal conductivity of the gas (**Figure 3-3**). Therefore, it is tempting to think that a material with higher pore volume fraction exhibits a lower thermal conductivity, but this is correct only if the thermal conductivity of the solid phase (λ_s) is the same.

To support this statement, let us examine also the refractory material: alumina spinel with 19% of porosity. This material has an amount of porosity close to that of the alumina AKP-1450 (green points). Therefore, it is expected that also the thermal conductivity values are similar, which is not the case (**Figure 3-3**). The alumina spinel (black points) exhibits a thermal conductivity closer to that of the alumina AKP-1300 (magenta points), even if the porosity is

almost two times lower. These results suggest that the materials have different λ_s.

To verify this hypothesis, the effect of the pore phase was removed using Landauer's relation (**Equ. 1-21**). The thermal conductivity of the argon is 0.02 $W \cdot m^{-1} \cdot K^{-1}$ at room temperature and it slightly increases with temperature [34]. However, since it is much smaller than the thermal conductivity of the materials, the approximation of $\lambda_P = 0$ $W \cdot m^{-1} \cdot K^{-1}$ was used. To verify the error caused by this simplification, a couple of calculations were made using $\lambda_P =$ 0.02 $W \cdot m^{-1} \cdot K^{-1}$ with its increase in temperature. Values were modified by not more than 0.1%. **Equ. 1-21** is then simplified as:

$$\lambda_{eff} = \frac{1}{2}[\lambda_s(2 - 3\nu_P)] \qquad \textit{Equ. 3-2}$$

and re-expressed as:

$$\lambda_s = \frac{\lambda_{eff}}{(1 - 3/2\nu_P)} \qquad \textit{Equ. 3-3}$$

The results are shown in **Figure 3-4**.

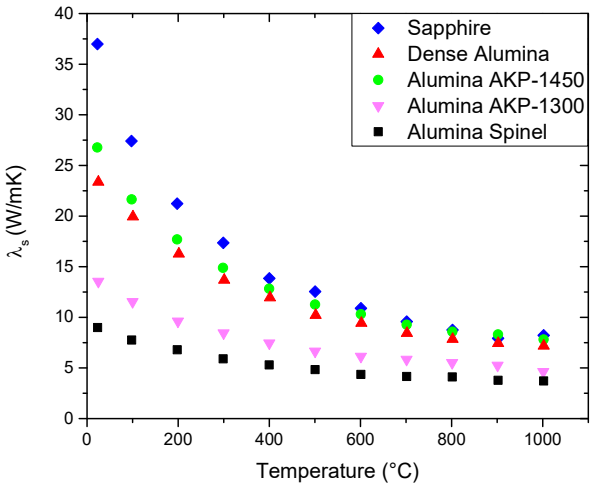

Figure 3-4: *Thermal conductivity of the solid phase as a function of the temperature.*

The hypothesis is confirmed. The graph shows that the thermal conductivity of the solid phases of the model and refractory materials are different from each other and they are still far from the one of the sapphire. For instance, the alumina AKP-1450 exhibits a λ_s = 27 $W \cdot m^{-1} \cdot K^{-1}$ and the alumina spinel a λ_s = 9 $W \cdot m^{-1} \cdot K^{-1}$, both a room temperature. This discrepancy underlines that other factors should be considered.

3.2.3. Effect of the grain boundaries

Another effect is linked to the presence of grain boundaries. The sapphire is a single-crystal and thus, it has only external boundaries, while all the other alumina-based materials are polycrystalline.

In the **paragraph 1.2.2.1**, it was shown that phonons can interact not only with other

phonons but also with "imperfections", such as grain boundaries. These are disordered regions, which act as scattering sites reducing the mean free path and consequently the thermal conductivity. Using the Kapitza approach of a temperature drop at an interface, the thermal conductivity of a polycrystalline material can be described by **Equ. 3-4**, which was already introduced in **Chapter 1** (**Equ. 1-15**):

$$\frac{1}{\lambda_{poly}} = \frac{1}{\lambda_{grain}} + nR_{int} \qquad \textit{Equ. 3-4}$$

where λ_{grain} is the thermal conductivity of the grains, n the number of grain boundaries per unit length and R_{int} the average grain boundary thermal resistance [30]. This equation underlines the presence of two mechanisms: i) effect of grain boundaries crossing the heat path given by the second term of the right hand side in **Equ. 3-4** and ii) effect of the grain size which can affect the first term of the right hand side in **Equ. 3-4**.

At each boundary in the heat path, an interface thermal resistance (R_{int}) is attributed. If the grains are small, the number (n) of grain boundaries increases and thus, the thermal resistivity of the polycrystalline material increases. This is the inverse of the thermal conductivity, which therefore decreases. Furthermore, if the grains are small, the hypothesis of an ideal infinite lattice is no longer valid and this cuts off all the low frequency long wavelength phonons, which cannot contribute to the thermal conductivity of the crystallite. Therefore, the thermal resistivity of the polycrystalline material increases and as a consequence, λ decreases [30].

These two effects related to grain size explain the differences in **Figure 3-4** between the alumina AKP-1300 and AKP-1450, as well as between sapphire and dense alumina. For very small grain sizes (< 0.3 μm), the effect is more pronounced. However, the finite grain size effect for λ_{grain} is less relevant to refractories with larger grain sizes.

If the thermal resistivity of a crystallite varies linearly with the temperature in a suitable range, this can be written as [30]:

$$\frac{1}{\lambda_{poly}} = aT + nR_{int} \qquad \textit{Equ. 3-5}$$

where a is a constant.

To go further in the analysis, let us separate the model materials (**Figure 3-5a**) from the refractory material (**Figure 3-5b**). The results are expressed in terms of thermal resistivity of the solid phases as a function of the temperature. A linear fit can be applied for all the investigated materials (**Equ. 3-5**).

Figure 3-5 shows that in the case of the dense alumina (red points) and alumina AKP-1450 (green points), the thermal resistivity values lie above and parallel to the single-crystal (blue points). In contrast, for the alumina AKP-1300 (magenta points) and the alumina spinel (black points), the thermal resistivity results are still above the single-crystal, but they are not parallel to its behaviour. The slope with temperature takes a higher value. This trend suggests that the amount of porosity, used for the correction made with Landauer, may not be completely

taken into account with precision.

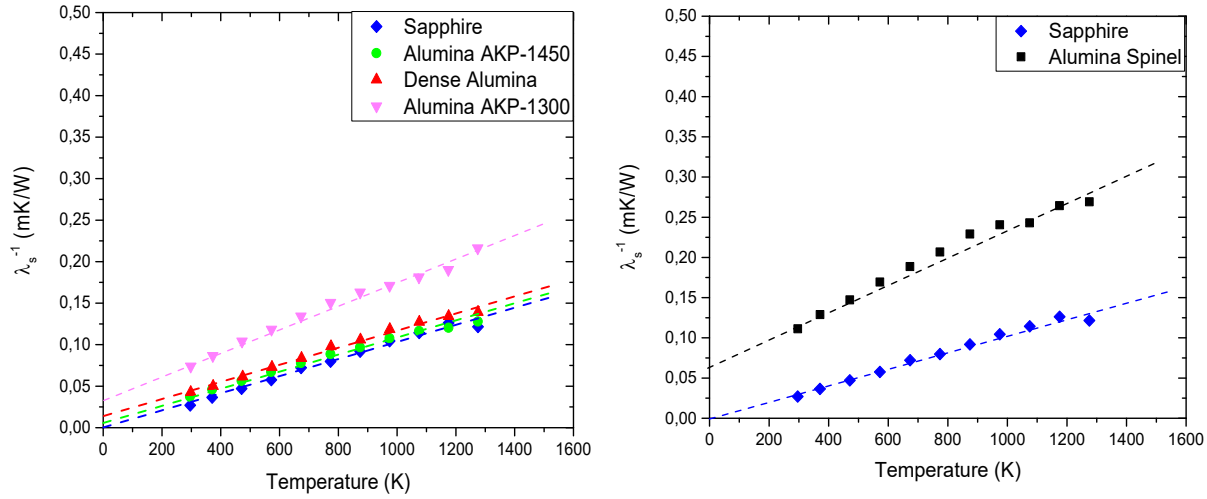

Figure 3-5: *Thermal resistivity values as a function of the temperature for the three model materials (a) and the refractory material (b).*

In the case of the refractory material, there is also the difficulty to evaluate the average grain size. The microstructure is characterized by grains of different sizes (**Figure 2-5**), with the biggest grain size of ~ 3 mm. Another aspect to consider is the presence of impurities that may increase the thermal resistance [88].

Despite these complications, calculations of the alumina grain conductivity were made by removing the grain boundary thermal resistance. For the alumina samples, the intercept with the y-axis (T = 0 K) gives a residual thermal resistance (λ_0^{-1}), which can be attributed to the total grain boundary thermal resistance:

$$\lambda_0^{-1} = nR_{int} \qquad \textit{Equ. 3-6}$$

which corresponds to the last term of **Equ. 3-5**. Subtracting λ_0^{-1} from the resistivity values (λ_s^{-1}), it is possible to evaluate the grain contribution (second term of **Equ. 3-4**):

$$\lambda_{grain}^{-1} = \lambda_s^{-1} - \lambda_0^{-1} = \lambda_s^{-1} - nR_{int} \qquad \textit{Equ. 3-7}$$

For polycrystalline alumina with grain size > 0.3 µm, if all the microstructural effects are accounted for, the grain conductivity should be the same as the sapphire. The results are expressed in terms of thermal conductivity vs temperature (**Figure 3-6**). The graph shows a good agreement between the model materials (**Figure 3-6a**). Only the alumina AKP-1300 exhibits a higher discrepancy. As mentioned above, this may be linked to an imperfect evaluation of pore volume fraction for this sample, but also to the effect of finite grain size. In fact, alumina AKP-1300 has the lowest grain size (**Table 3-1**). Applying the same analysis, the situation for the refractory material is a bit different (**Figure 3-6b)**. The two curves are still apart. However, it is important to underline that the thermal conductivity values of the alumina spinel grains and the sapphire are much closer than the beginning. The experimental value obtained for the refractory was 6.5 $W \cdot m^{-1} \cdot K^{-1}$ at room temperature. After the corrections for

the porosity and the grain boundary thermal resistance, the new value is 28 $W \cdot m^{-1} \cdot K^{-1}$. Therefore, the difference with the sapphire sample is within 25%.

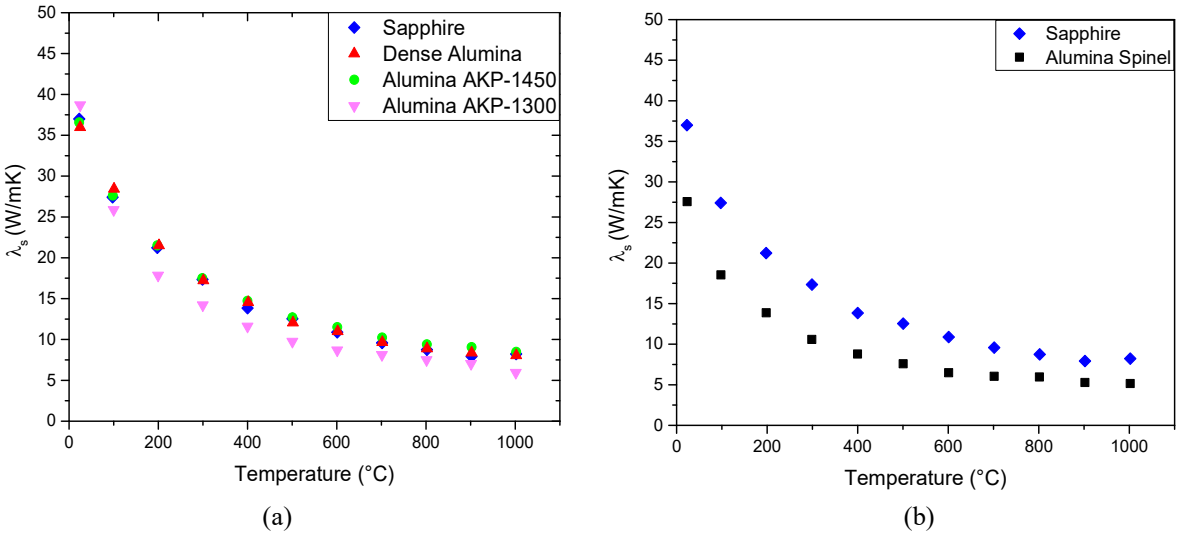

Figure 3-6: *Thermal conductivity as a function of the temperature after removing the microstructural effects (porosity and grain boundaries) in the case of model materials (a) and refractory material (b).*

Another aspect that can be considered in the case of the Alumina Spinel Bricks is the presence of a second phase. Let us make the assumption that the refractory material is composed only by two phases: alumina (the grains) and spinel (the matrix). XRD measurements show the presence of 20 - 25% wt. spinel phase and consequently of 75 - 80% wt. alumina. These values were calculated from the XRD patterns using the Rietveld method [89].

3.2.4. Phase mixtures

Let us determine firstly the thermal conductivity of the spinel phase in a specially prepared model material (**Figure 3-7**).

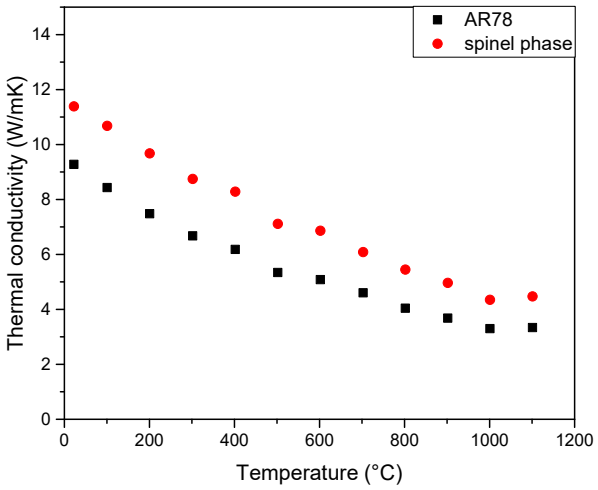

Figure 3-7: *Thermal conductivity as a function of the temperature of alumina-rich spinel AR78. The graph also shows the thermal conductivity values of the spinel phase (red points) obtained after removing the effects of the porosity, grain boundaries and presence of a second phase.*

For this purpose, samples of alumina-rich spinel AR78 (78% wt. of Al_2O_3) were made by I. Kieliba (RWTH - Aachen) by uniaxial pressing of the dry powder and then sintering at 1600 °C for 6 h, with typical dimensions of 10 mm in diameter and 2 mm thick. The measurements were carried out with the laser flash method up to 1000 °C in an argon atmosphere (**Figure 3-7**). Two samples were characterized and for each temperature, three measurements were repeated.

The AR78 is one of the raw materials used for the fabrication of the Alumina Spinel Bricks. The graph shows a decrease of the thermal conductivity values with the increase of the temperature linked to the increase of the phonon-phonon scattering. For this material, the previously adopted analysis was made.

Equ. 3-1 was used to evaluate the amount of porosity in the AR78 specimens. A value of 20% was estimated. Then, **Equ. 3-3** was used to correct the experimental results and evaluate the thermal conductivity of the solid phase. This yielded a value of 13.3 $W \cdot m^{-1} \cdot K^{-1}$ at room temperature. Finally, the chemical composition was used to evaluate the amount of spinel (v_1 = 0.88% vol.) and corundum (v_2 = 0.12% vol.) in the sample. Therefore, the λ_s values were corrected from the influence of a second phase using **Equ. 1-21**. Landauer's relation can be adopted both for the correction of the effect of the porosity and of the second phase. In this last case, the terms λ_p and v_p are replaced respectively with λ_2 and v_2, where the number 2 refers to a second solid phase.

Equ. 1-21 was re-expressed as:

$$\lambda_1 = \frac{2\lambda_s^2 - \lambda_s\lambda_2(3v_2 - 1)}{\lambda_2 + \lambda_s(2 - 3v_2)} \qquad \textit{Equ. 3-8}$$

where 1 refers to the spinel phase and 2 to the alumina phase. For λ_2, the thermal conductivity values of the single-crystal were used (λ = 37 $W \cdot m^{-1} \cdot K^{-1}$ at room temperature). The equation estimated a thermal conductivity of the spinel phase in the AR78 sample of 11.4 $W \cdot m^{-1} \cdot K^{-1}$ at room temperature (**Figure 3-7**).

The same procedure was then adopted for the Alumina Spinel Bricks. Making the assumption that the refractory material is a mixture of only two phases, **Equ. 3-8** was used to evaluate the thermal conductivity of the alumina grains by removing the effect of the spinel phase (λ_1 = 11.4 $W \cdot m^{-1} \cdot K^{-1}$ at room temperature). The results are shown in **Figure 3-8**.

It is possible to observe that the two curves are still apart, but an improvement was made. At room temperature, the refractory material exhibits a thermal conductivity value of 33 $W \cdot m^{-1} \cdot K^{-1}$ and thus, the difference between the sapphire sample is within 12%. This difference might be linked to the approximation that the refractory material is only a mixture of alumina and spinel phases, which is not 100% correct. The presence of small fractions of impurities can also affect the thermal properties. Popov et al. [88] demonstrated that small quantities of Cr and Ti, which substitute into the Al_2O_3 lattice, reduces the conductivity value by a small amount.

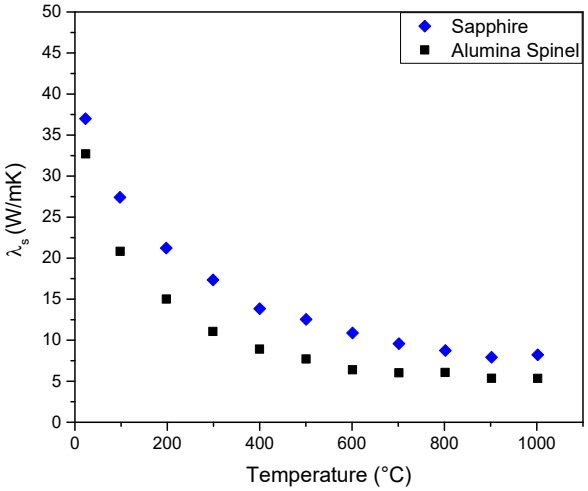

Figure 3-8: *Thermal conductivity as a function of the temperature after removing the microstructural effects (porosity and grain boundaries) and the effect of the second phase.*

3.2.5. Addition of a cement phase

Nowadays, the use of Alumina Spinel Castables in steel ladle applications has significantly increased due to their superior corrosion and penetration resistance against basic molten slag [90]. These refractory materials are composed of different grain size fractions of alumina (as matrix and aggregates) and spinel. In the case of the spinel phase, it must be added in the fine fraction to attain the best penetration resistance in an amount of no more than 20 - 25% wt. to obtain a good slag resistance parameter [90]. In the preparation of the castables, the cement is used as binder and thus, it was decided to study the influence of the cement on alumina-based model materials.

Super ground reactive alumina with very low silica and soda content (P172 LSB) was mixed with three different percentages of calcium aluminate cement (SECAR 71): 5% wt., 7% wt. and 10% wt. The alumina is characterized by a particle size D50 of 0.40 µm [91], which was achieved by dry ball-milling. These very small particles are so reactive that they can start to sinter at 1000 °C.

The SECAR 71 is a hydraulic binder designed to be used at temperatures higher than 1400 °C, which makes it suitable for refractory materials [92]. It is characterized by approximatively 70% wt. of alumina and a good balance between CA and CA_2 phases (C = CaO and A = Al_2O_3) which leads to excellent stability, optimum workability and high temperature performance of the products.

The alumina mixed with the cement represents the “solid” part, while the acetic acid and the distilled water the “liquid” part. The advantage of using distilled water is linked to the purity of H_2O. In fact, the distillation process removes the presence of impurities. The $C_2H_4O_2$ was chosen as a dispersant in order to have a good distribution of the cement inside the samples. A dispersant ratio of 2% wt. of the “solid” part was used. This value was chosen experimentally: several tests were made in order to obtain a solution of alumina + cement with enough fluid to be casted inside the moulds. The acid was firstly dissolved in distilled water and then added to

the alumina + cement powders. This step is important in order to avoid agglomeration of the cement. The amount of water was calculated using a H_2O / solid ratio of 0.35.

Table 3-2 summarizes the used formulations.

Table 3-2: *Alumina + cement sample formulations.*

Name	*Al_2O_3 (P172 LSB)*	*Cement (SECAR 71)*	*$C_2H_4O_2$ (90%)*	*H_2O*
5% wt. cement	47.5 g	2.5 g	1 g	17.5 g
7% wt. cement	46.5 g	3.5 g	1 g	17.5 g
10% wt. cement	45 g	5 g	1 g	17.5 g

For the sample preparation, the following procedure was used: i) the "solid" and the "liquid" parts were poured inside a plastic mould and mixed with the help of an electric mixer for 40 sec; ii) with the help of a spatula, the powder stacked at the walls of the mould was moved toward the centre of the container and the solution was mixed for another 60 sec; iii) the obtained liquid was poured inside a plastic mould and left to harden at room temperature for one day; iv) the mould was then left one day in an oven at 100 °C to remove the water content slowly to avoid the formation of cracks in the sample; v) finally the sample was removed from the mould and heat treated. The following thermal cycle was used: i) from room temperature up to 100 °C with a heating rate of 2 K/min and a dwell time of 1 h for a further reduction of the water content; ii) from 100 °C to 1600 °C with a heating rate of 5 K/min and a dwell time of 2 h for sintering; iii) from 1600 °C to room temperature with a cooling rate of 5 K/min.

The obtained samples were then machined for making specimens suitable for the laser flash method: 10 mm in diameter and 2 mm thick. The laser flash measurements were carried out up to 1200 °C in an argon atmosphere (**Figure 3-9**).

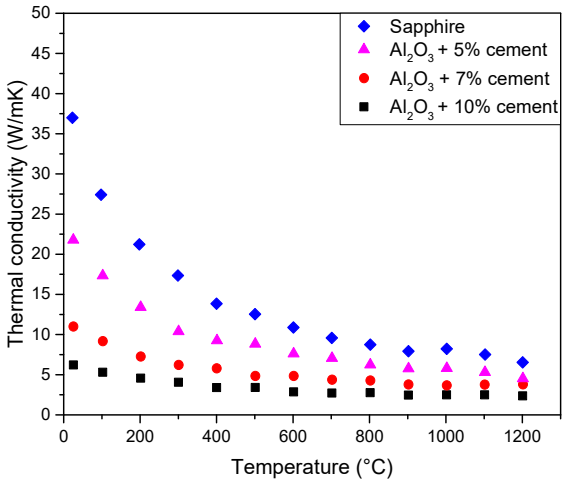

Figure 3-9: *Thermal conductivity as a function of the temperature of the alumina - cement samples. Three percentages of SECAR 71 were chosen: 5% wt., 7% wt. and 10% wt. The curves are compared with sapphire (blue points).*

The graph shows for all the four materials a decrease of the thermal conductivity values

with the increase of the temperature, which is the typical behaviour related to the increase of phonon-phonon scattering. Furthermore, the thermal conductivity values of the formulations decrease with the increase of the cement content. At room temperature, the values change from 21.8 $W \cdot m^{-1} \cdot K^{-1}$ for the sample with 5% wt. of cement to 6.2 $W \cdot m^{-1} \cdot K^{-1}$ for the sample with 10% wt. of cement. Let us now apply the same analysis as used previously to estimate the alumina grain conductivity from the experimental results taking into account the effects of the microstructure.

3.2.5.1. Effect of the porosity

Equ. 3-1 was used for evaluating the amount of porosity in the model materials. The results are presented in **Table 3-3**.

Table 3-3: *Summary of the percentage of porosity for the alumina + cement samples.*

Materials	*Porosity (%)*
5% wt. cement	13
7% wt. cement	18
10% wt. cement	15

Even if the three samples exhibit similar pore volume fractions (v_p), the thermal conductivity values evaluated experimentally are quite different. This suggests that the specimens have different thermal conductivity values for the solid phase. **Equ. 3-3** was used to estimate the solid phase conductivities from the experimental results (**Figure 3-10**).

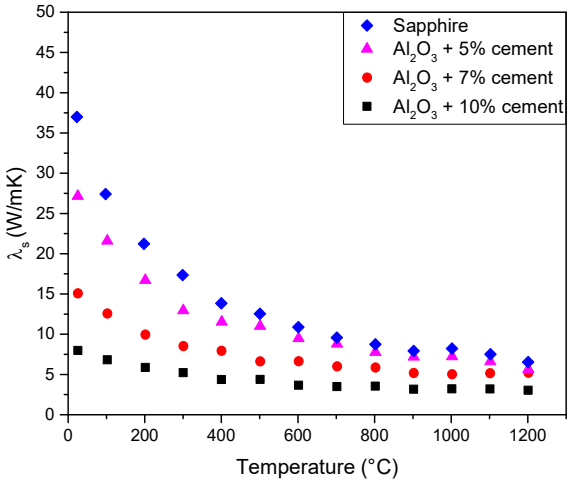

Figure 3-10: *Thermal conductivity of the solid phase as a function of the temperature.*

The graph supports the hypothesis of different values of λ_s. At room temperature, the thermal conductivity values are: 27 $W \cdot m^{-1} \cdot K^{-1}$ for the sample with 5% wt. of cement, 15 $W \cdot m^{-1} \cdot K^{-1}$ for the sample with 7% wt. of cement and 8 $W \cdot m^{-1} \cdot K^{-1}$ for the sample with 10% wt. Furthermore, the curves obtained for the specimen with 5% wt. cement and the sapphire are quite close. In contrast, those obtained for the samples with 7% wt. and the 10% wt. are significantly attenuated.

3.2.5.2. Effect of the grain boundaries

Using the Kapitza approach with **Equ. 3-4**, the results are expressed in terms of thermal resistivity (λ_s^{-1}) versus temperature (**Figure 3-11**).

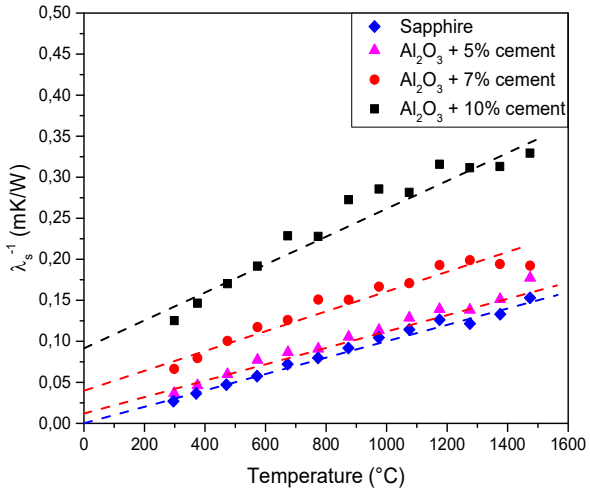

Figure 3-11: *Thermal resistivity values as a function of the temperature after removing the effect of the porosity.*

The graph shows that for each material a linear fit can be made. Furthermore, the curves for the alumina + cement samples lie above the curve of the sapphire. In the case of the sample with 5% wt. of cement, the linear fit is parallel to the single-crystal. In the case of the specimens with 7% wt. and 10% wt. of cement, the slope of the resistivity with temperature takes a higher value as in the case of the alumina AKP-1300 (**Figure 3-5a**) and the alumina-spinel (**Figure 3-5b**). It can be pointed out that the slope of the linear fit increases with the cement content. The more insulating cement phase attenuates heat conduction through the alumina grains. It is also possible that this phase has its own temperature dependence, contributing to the increased thermal resistivity at high temperatures. Despite these difficulties, **Equ. 3-7** is then used to calculate the grain contribution (**Figure 3-12**).

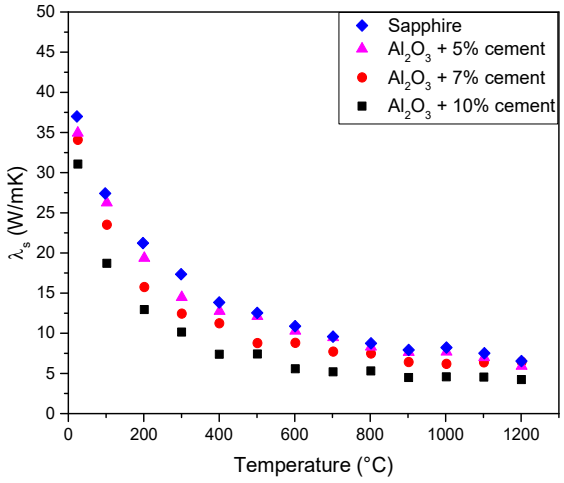

Figure 3-12: *Thermal conductivity as a function of the temperature after removing the microstructural effects (porosity and grain boundaries).*

Figure 3-12 shows that the curves are rather close but they do not perfectly match the sapphire behaviour. At room temperature, the thermal conductivity values change from 35 $W \cdot m^{-1} \cdot K^{-1}$ for the sample with 5% wt. of cement to 31 $W \cdot m^{-1} \cdot K^{-1}$ for the sample with 10% wt. of cement.

Another aspect to consider is the effect of the presence of the second phase, which is represented by the cement itself.

3.2.5.3. *Effect of the second phase*

The thermal conductivity of the cement phase was taken from studies in the literature [93]. Several temperature behaviours were tested, but all gave the same results. At room temperature, a value of 1.05 $W \cdot m^{-1} \cdot K^{-1}$ was used with a temperature dependence given by [93]:

$$\lambda = 1.035 + 7 \cdot 10^{-4} T \qquad \textit{Equ. 3-9}$$

where T is the investigated temperature expressed in °C. **Equ. 3-8** was then used to calculate the conductivity of the alumina phase by removing the effect of the presence of a second phase. The results are presented in **Figure 3-13**.

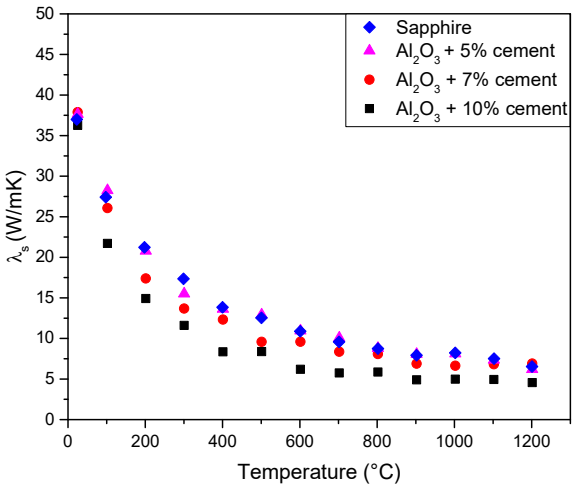

Figure 3-13: *Thermal conductivity as a function of the temperature after removing the microstructural effects (porosity and grain boundaries) and the effect of the second phase.*

The graph shows a good agreement between the sapphire and the sample with 5% wt. of cement. In the case of the specimens with 7% wt. and 10% wt. of cement, only at room temperature the values match to the thermal conductivity of the sapphire. At high temperatures, the curves are closer but there are still differences. This discrepancy may in part be linked to an imperfect knowledge of the microstructure. Therefore, further investigation, such as SEM and EDS analysis, might help to better understand these differences. However, the broad details have been taken into account in a realistic way.

3.3. Conclusion

The thermal, mechanical and other physical properties of a material are strongly

modulated by the microstructure. Therefore, to better understand the relationship between the thermal properties and the microstructure of refractory materials, experimental investigations were made on Alumina Spinel Bricks. The obtained results were compared with the behaviour of four alumina-based model materials. The purpose was to identify the contribution of each microstructural effect, such as porosity, grain boundaries, presence of a second phase and of the cement, individually. The analysis of simpler model materials can help to explain better the behaviour of more complex systems, such as refractories.

Once each effect is identified, it is possible to model the experimental results in terms of the microstructural parameters and to deduce the thermal conductivity of the solid phase. In the specific case investigated of alumina-based refractories, this value should be the same as that of sapphire (single-crystal).

First of all, the porosity was taken into account using Landauer's relation to calculate the thermal conductivity of the solid phase. The second step took into account the presence of grain boundaries, which were considered as Kapitza resistances at the interfaces. These two contributions were enough in the case of the model materials to confirm that the thermal conductivity of the grain approaches the behaviour of sapphire. A bit different was the case of the refractory material. In fact, another aspect was taken into account, which is the presence of a second phase (spinel). This was described using the percolation model of Landauer. A difference within 12% was found between the refractory material and the single-crystal. This could be attributed to the assumption that the alumina spinel is a mixture of only two phases: alumina and spinel. However, the presence of impurities can also have some effect.

The effect of the cement was studied preparing samples with three percentages of cement: 5% wt., 7% wt. and 10% wt. This phase is important in the case of Alumina Spinel Castables. A decrease of the thermal conductivity values with the increase of the cement content was observed. Furthermore, the same procedure adopted for the alumina-based model materials and the refractory material was used on the specimens containing cement in order to deduce the thermal conductivity of the grains. At the end of the analysis, the calculated curves matched the behaviour of the sapphire only at room temperature, while at high temperatures they were still apart. This was attributed to an imperfect knowledge of the microstructure.

Chapter 4 :

Industrial refractory materials in the working environment

The present chapter will examine three real cases of industrial problems and their effects on the thermal properties of insulating refractory materials: i) the interface thermal resistance (contact zone between the bricks); ii) the influence of compression load (due to the pressure exerted by the hot liquid steel on the linings) and iii) the influence of carbon pick-up.

4.1. Interface thermal resistance

The ladle lining is a masonry construction, which means that it is made of units (the bricks) laid together with or without mortar. Therefore, the presence of joints plays an important role in thermo-mechanical studies. One of the main important parameters to describe joints is the thermal conductance, which is the inverse of the interface thermal resistance (R_{int}). This coefficient describes the aptitude for heat conduction through the interface between two solid bodies in contact. The studies of R_{int} started in 1941 with Kapitza who observed a temperature discontinuity at the boundary between copper and liquid helium while a heat flux was passing through the interface [94].

From the thermal point of view, the joints cause a drop of the temperature at the interfaces. Even if two surfaces seem macroscopically flat, at the microscopic level they present a certain roughness (**Figure 4-1**).

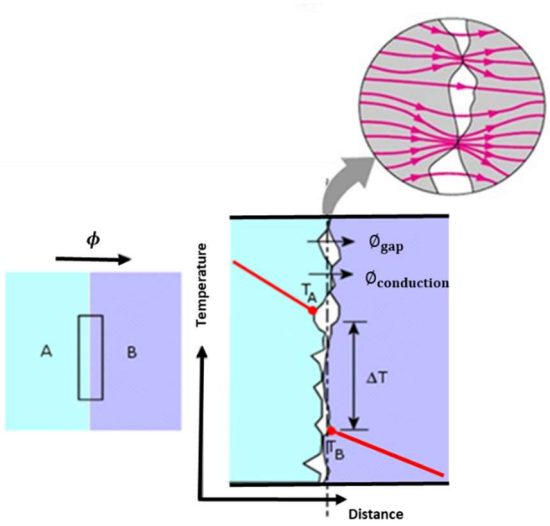

Figure 4-1: *Schematic diagram of the interface thermal resistance* [95].

As a consequence, the real contact area is much smaller than the apparent contact area. This means that the amount of heat transferred from one surface to the other by solid state

conduction is reduced, increasing the thermal resistance at the contact zone [96][97].

The thermal resistance (R_{int}) is given by **Equ. 4-1:**

$$R_{int} = \frac{\Delta T}{\emptyset} \qquad \textit{Equ. 4-1}$$

where ΔT is the observed temperature drop and ϕ is the heat flux density flowing across the interface. At this present day, there is not an official procedure in the refractory field to determine this parameter. Therefore, in the following paragraphs, two methods are compared in order to estimate the interface thermal resistance: one in the steady-state using the heat flow meter (**paragraph 2.2.1**) and one in the transient regime involving the laser flash method (**paragraph 2.2.5**).

4.1.1. Heat flow meter

Firstly, the measurements were made on square slabs with typical dimensions of 30x30 mm^2 and different thicknesses between 2 mm and 15 mm in order to estimate the thermal conductivity of the material (**Figure 4-2**). A weight of 315 g (compression load: $3.43 \cdot 10^{-3}$ MPa) was placed on top of the upper plate to improve the thermal contact between the sample and the two plates. The measured values were corrected taking into account the effect of heat losses (**paragraph 2.2.1** and **2.3.2**).

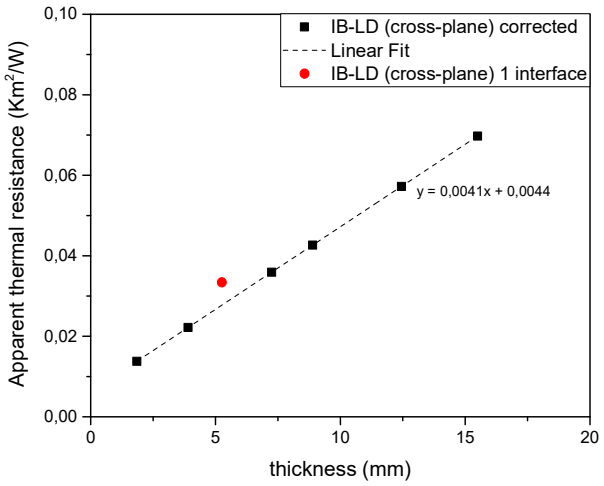

Figure 4-2: *Experimental results plotted as a function of the thickness both for the individual samples (black points) and the two samples in contact (red point).*

Secondly, two samples in contact were measured at room temperature following the same procedure of the individual specimens. The same compression load ($3.43 \cdot 10^{-3}$ MPa) was applied in order to improve the contact between the samples and the two plates, as well as between the two specimens in contact. The apparent thermal resistance (R_{app}) was calculated using **Equ. 2-1**, while the interface thermal resistance was calculated using **Equ. 4-2**:

$$R_{int} = R_{app} - \frac{d}{\lambda} - R_c \qquad \textit{Equ. 4-2}$$

where d is the total thickness of the two samples in contact, λ the thermal conductivity of the material, obtained after heat loss correction, and R_c the contact resistance between the two samples and the two copper plates. The apparent thermal resistance of a specimen with the same thickness of the two samples in contact is assumed to be on the linear fit of the experimental data plotted as a function of d. If the obtained value is above the line, the difference is due to the presence of an extra interface which increases the total thermal resistance of the system. **Figure 4-2** confirms this interpretation: the red point is the R_{app} of the two specimens in contact and is above the broken line.

Table 4-1 summarizes the interface thermal resistance of all the investigated insulating materials calculated using **Equ. 4-2**.

Table 4-1: *Summary of the interface thermal resistance of all the investigated materials using the heat flow meter (IB = Insulating Boards; IFB = Insulating Fireclay Bricks)*

Materials	R_{int} $(m^2 \cdot K \cdot W^{-1})$
IB-LD	$1.7 \cdot 10^{-4}$
IB-MD	$2.1 \cdot 10^{-3}$
IB-HD	$1.6 \cdot 10^{-3}$
IFB	$3.0 \cdot 10^{-3}$

In all the cases, the values are of the order of 10^{-4} - 10^{-3} $m^2 \cdot K \cdot W^{-1}$, in agreement with the literature values estimated for dry joints [98]. However, in modelling studies, usually the adopted value is of the order of 10^{-9} $m^2 \cdot K \cdot W^{-1}$, which takes into account two parameters: i) the presence of the mortar, and ii) the effect of the compression loads. To reduce the interface thermal resistance, the contact area should be increased.

One way is to increase the compression load, but unlike metals, ceramics do not deform easily. To verify this statement, measurements with higher compression load were made ($5.29 \cdot 10^{-3}$ MPa). The obtained values were still of the order of 10^{-4} - 10^{-3} $m^2 \cdot K \cdot W^{-1}$ with a small difference in the number. For instance, in the case of Medium Density Insulating Boards (IB-MD), R_{int} decreased from 2.1 to $1.1 \cdot 10^{-3}$ $m^2 \cdot K \cdot W^{-1}$.

A second way is to add a mortar and this has a huge impact. The mortar covers the roughness of the sample's surface increasing the contact area.

4.1.2. Laser flash method

Room temperature measurements in an air atmosphere were also made with the laser flash method. The procedure adopted was: firstly two samples of the same material were measured separately and then together. In both cases, the same parameters were used. Unlike the heat flow meter, it was not possible to improve the contact area between the two specimens by adding a compression load. However, the InSb detector was able to pick-up enough signal (T-t curve) for the analysis of the interface thermal resistance.

A steady-state series resistor model was applied, despite the transient situation, to

estimate the interface thermal resistance (**Equ. 4-3**):

$$\frac{d_T}{\lambda_{tot}} = \frac{d_1}{\lambda} + \frac{d_2}{\lambda} + R_{int} \qquad \textit{Equ. 4-3}$$

where "tot" refers to the two samples in contact, while 1 and 2 to the individual specimens. This simplified model was already tested using a computer model, which showed that **Equ. 4-3** gives satisfactory results for interface thermal resistance [99]. The results are presented in **Table 4-2** and are comparable with those obtained with the heat flow meter.

Table 4-2: *Summary of the interface thermal resistance of all the investigated materials using the laser flash method (IB = Insulating Boards; IFB = Insulating Fireclay Bricks).*

Materials	R_{int} $(m^2 \cdot K \cdot W^{-1})$
IB-LD	$4.2 \cdot 10^{-4}$
IB-MD	$4.7 \cdot 10^{-3}$
IB-HD	$2.5 \cdot 10^{-3}$
IFB	$3.8 \cdot 10^{-3}$

For both methods, the interface thermal resistances are of the order of 10^{-4} - 10^{-3} $m^2 \cdot K \cdot W^{-1}$. In the case of the laser flash (**Table 4-2**), the values are bigger than those obtained with the heat flow meter (**Table 4-1**). One reason can be linked to the fact that in the heat flow meter, the contact area was improved by adding a weight on the top plate. This was not possible in the laser flash method. On the other hand, the approach using **Equ. 4-3** could be replaced with a more sophisticated two layer model in order to take into account the transient situation.

In conclusion, the procedure used in the case of the heat flow meter was considered to be more reliable than that of the laser flash method. In either case, the interface thermal resistance is estimated to be of the order of 10^{-4} - 10^{-3} $m^2 \cdot K \cdot W^{-1}$. This parameter can then be expressed in terms of thermal conductance and used as first approximation in modelling studies for the thermal behaviour of joints in steel ladle linings.

4.2. Influence of compression loads

One of the purposes of the insulation layer is to keep the linings in a stable compressed situation to prevent joints opening and breakout of hot liquid steel. When the hot liquid steel is poured inside the ladle, the wall of the vessel is subjected to a hydrostatic pressure and a temperature increase. This increase causes a volume expansion of the inner layers of the ladle that induces a significant compression load on the insulation layer. Normally, the maximum compression load imposed on the insulating lining is around 5 - 10 MPa [100]. If the layer is not strong enough to resist against the compression, the insulating lining will become thinner and denser losing effectiveness [11]. In the worst-case scenario, considering that there is generally no mortar between the bricks of the working lining and if the ladle is free to deform, the joints on the hot face will open allowing the liquid steel to penetrate into the lining. Ultimately it represents a safety risk with the destruction of the integrity of the lining. Therefore,

requirements of such insulating refractory materials are: i) low thermal conductivity values, and ii) sufficient compressive strength. Though, they exhibit a quite low tensile strength, fortunately the compressive failure stress is typically 3 to 10 times stronger for a ceramic material. Indeed, brittle ceramic materials are unable to yield and relieve the stress when a tensile load is applied. Unlike metals, they break without plastic deformation [101].

To estimate the maximum load withstood by the investigated samples, of Insulating Boards (IB) and Insulating Fireclay Bricks (IFB), uniaxial compression tests were made on square samples (70x70 mm^2 of area and 25 - 32 mm in thickness) with a loading rate of 0.025 kN/s [102]. The measurements were performed at the Department of Civil Engineering in Coimbra (FCTUC). **Table 4-3** shows the cold crushing strength (CCS) for each material. This parameter represents the maximum compression load that the refractory specimen can withstand before failure at room temperature.

Table 4-3: *Summary of the cold crushing strength of each insulating refractory materials.*

Materials	***CCS (MPa)***
IB-LD	5.8 ± 1.2%
IB-MD	12.2 ± 1.2%
IB-HD	32.5 ± 1.2%
IFB	5.3 ± 1.2%

From **Table 4-3**, it is evident that normally Low Density Insulating Boards (IB-LD) and Insulating Fireclay Bricks (IFB) are not used for large ladles or severe operation conditions. This table underlines the importance of modelling studies. Nowadays, due to the possibility of predicting the thermo-mechanical behavior of the steel ladle lining, it is possible to establish in advance if a material can be recommended for a specific application and guarantee operational safety.

On the other hand, Medium Density (IB-MD) and High Density (IB-HD) Insulating Boards are totally suitable for the purposes of the insulating lining. Their maximum compressive strengths are higher than 5 - 10 MPa. Furthermore, since the maximum load supported by the insulating lining is less than the cold crushing strength of the material, this means that in service conditions the material exhibits an elastic behaviour (**appendix B**), which indicates, in a first approach, that once the force is removed, the board comes back to the original state without damage. This aspect is important considering the cycling effects caused by the operations of filling/emptying of the ladles. However, measuring the dimensions of the samples before and after compression load, it was possible to observe a small increase in the density (approximately 2% wt.).

4.2.1. Thermal expansion

For studying the influence of compression loads on the thermal expansion, a thermomechanical analysis (TMA) was used. The equipment measures the unidirectional

change in length (**Equ. 1-25**) as a function of the temperature when a load is applied with a push rod of 1.72 mm in diameter. Three compression loads were studied: 0.02 MPa, 0.21 MPa and 0.42 MPa. For each of them, two samples were measured. In the case of the Insulating Boards (IB), two directions were studied: "cross-plane" and "in-plane" directions. In contrast, for the Insulating Fireclay Bricks (IFB) only the "cross-plane" direction was tested. The measurements were carried out in an air atmosphere up to 700 °C for IB and 1300 °C for IFB with a heating/cooling rate of 5 K/min and 30 min of dwell time. The samples were cut in a rectangular shape of 5x5 mm^2 in area and approximately 13 mm in length. Before the measurements, the specimens were left 24 h in an oven at 100 °C. The results were corrected with a reference material (alumina).

4.2.1.1. Insulating Boards

Let us start with the "cross-plane" direction and the lowest compression load (**Figure 4-3**).

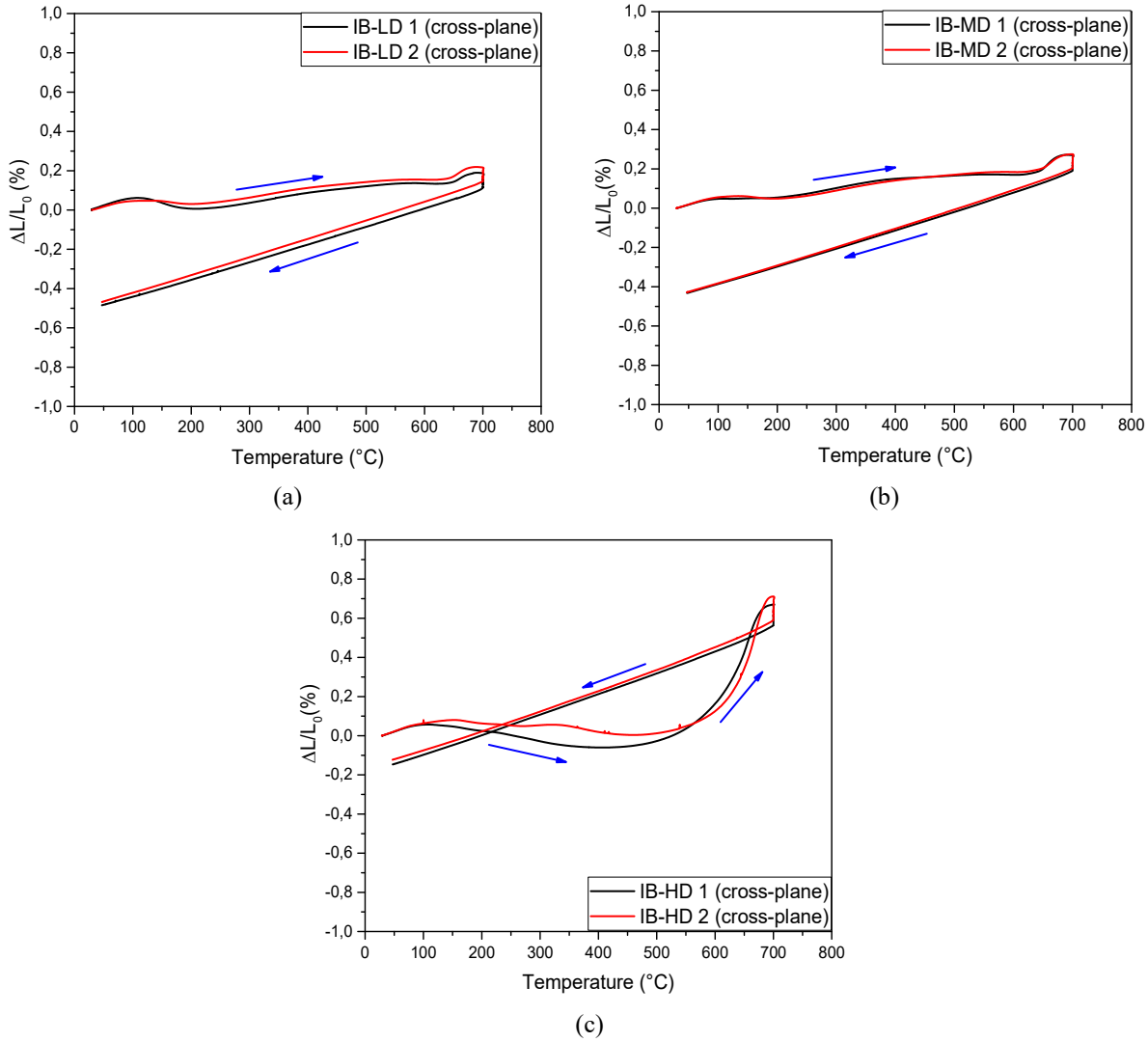

Figure 4-3: *Dilatometry measurements on a) Low Density Insulating Boards, b) Medium Density Insulating Boards and c) High Density Insulating Boards. All the materials are analysed in the "cross-plane" direction with a compression load of 0.02 MPa.*

In each case, the graphs show a good reproducibility between the dilatometric curves of the two samples. However, for the three kinds of Insulating Boards, the lowest compression load presented the greatest variations. The two samples measured exhibited the same shape but any differences between the curves were larger (for the lowest compression load, the measurements were made on 2 sets of 2 specimens). With the increase of the load, these variations in reproducibility were reduced to almost zero. Given the irreversible character of these dilatometric cycles, the force exerted by the push road was insufficient to affect the microstructural evolution of the refractory.

To better understand the effect of the microstructure on the dilatometric variations, DTA (differential thermal analysis) and TGA (thermal gravimetric analysis) measurements were performed (**Figure 4-4**). In the graph, it is possible to observe an endothermic peak between 20 °C and 250 °C, which is linked to the loss of the physically adsorbed water and the water molecules residing in the particle spaces of the vermiculite. According to literature studies [82][83], this intercalated water forms layers not in immediate contact with the cation (Mg^{2+}). Furthermore, the loss of water causes a loss of mass of approximately 4% wt. due to the change in the unit cell of the vermiculite, for the three Insulating Bords.

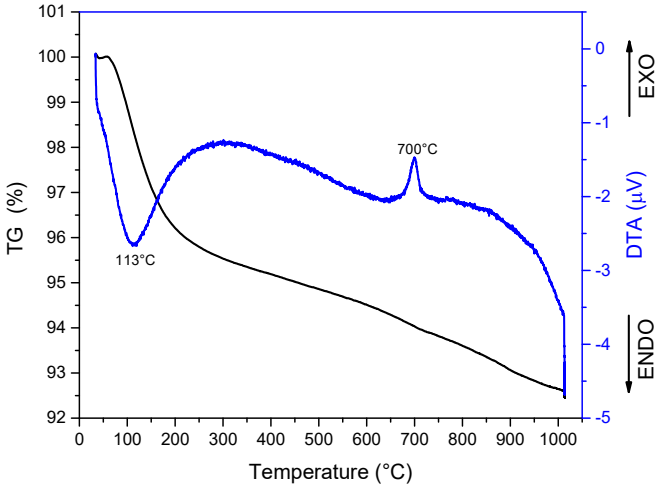

Figure 4-4: *DTA (differential thermal analysis) and TGA (thermal gravimetric analysis) measurement of an Insulating Board.*

This behaviour explains why in **Figure 4-3**, it is possible to observe an initial expansion (from room temperature to 100 °C) followed by a slight shrinkage (- 0.02%) between 100 - 200 °C in the cases of Low Density (IB-LD) and Medium Density (IB-MD) Insulating Boards, and between 100 - 450 °C in the case of High Density Insulating Boards (IB-HD). Even if the samples were dried before the tests, the chosen temperature (100 °C) was not enough to completely remove the intercalated water. Furthermore, **Figure 4-3c** shows a particular trend of the dilatometric curve, which might be linked to the way of processing. The difference between the three kinds of Insulating Boards is related to the imposed shaping compaction pressure, which is higher in the case of IB-HD. The increase in the shaping compression load causes a decrease of the porosity and of the interlayer distance (d_{int}). Lower d_{int} implies a more compact structure of the vermiculite and in particular, it tends to prevent water from exudation from the sample. Therefore, to completely remove the water molecules residing in the particle

spaces of the vermiculite, it might be necessary for the board to attain higher temperatures.

Figure 4-4 also shows an exothermic peak in the region 600 - 700 °C, which is probably caused by the formation of a new amorphous phase. Since the HT- XRD (high temperature XRD) measurements did not reveal any new peak at the corresponding temperature and considering the nature of the refractory, it was deduced that this phase was amorphous (**appendix C**). This phase formation seems also to be highlighted in **Figure 4-3a, b**, where it is possible to observe a slight expansion around 600 - 650 °C, which is even more pronounced in **Figure 4-3c**. Furthermore, during the dwell time at 700 °C, the materials exhibit densification which could be related to the appearance of this phase. Another aspect revealed in **Figure 4-3** is a final shrinkage for all the investigated materials: - 0.48% IB-LD, - 0.43% IB-MD and - 0.14% IB-HD, compared to the initial sample dimension. Therefore, the principal features of the dilatometric curves can be related to the microstructural evolution of the Insulating Boards.

Let us now make the same investigation for the "in-plane" direction, starting with the lowest compression load (**Figure 4-5**). The same operating conditions as the "cross-plane" direction were used. Therefore, the only difference between **Figure 4-3** and **Figure 4-5** is the investigated direction.

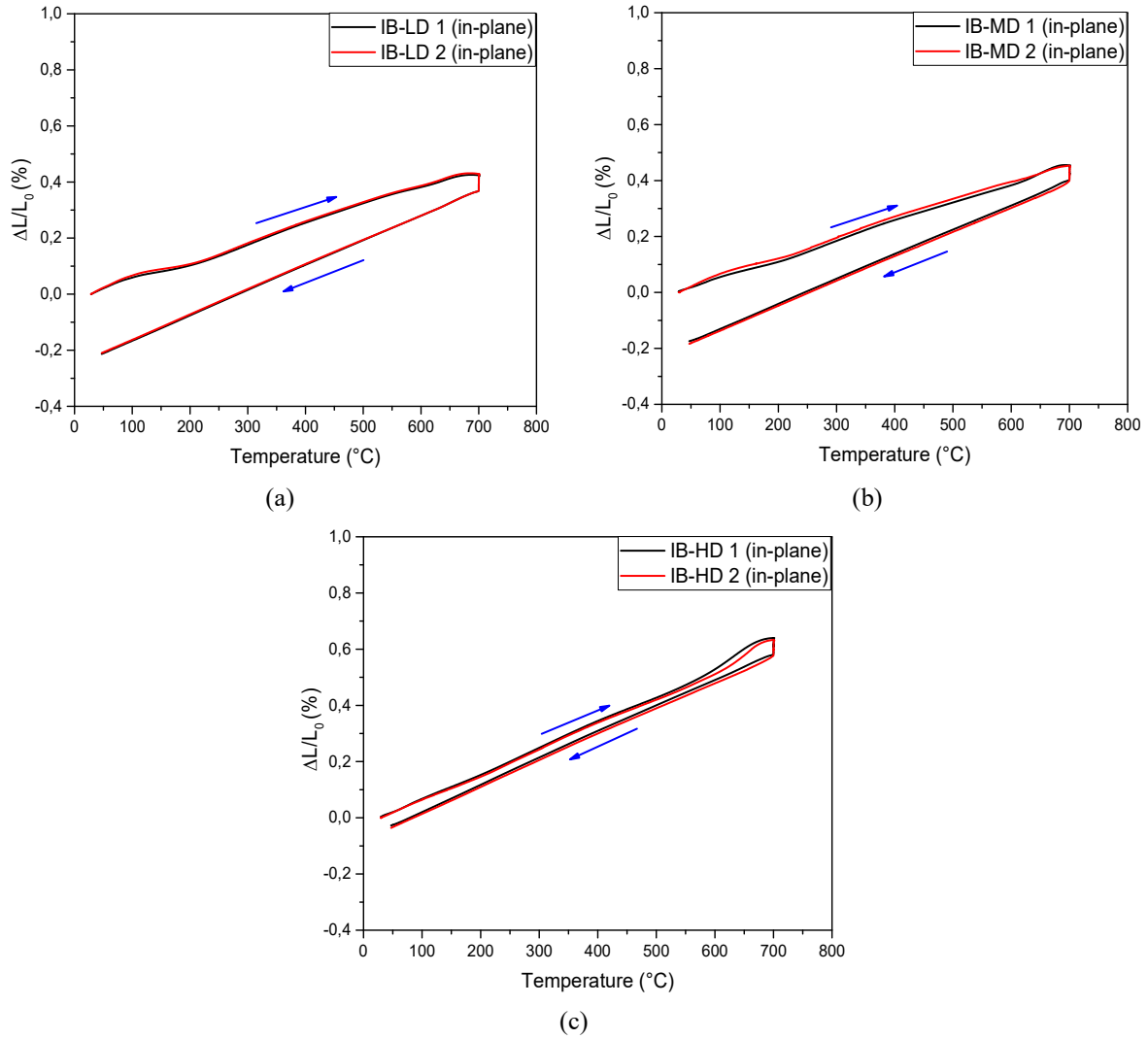

Figure 4-5: *Dilatometry measurements on a) Low Density Insulating Boards, b) Medium Density Insulating Boards and c) High Density Insulating Boards. The analysis is made in the "in-plane" direction (0.02 MPa).*

First of all, it is important to underline that in this case any variations between samples are almost zero even for the lowest compression load. Secondly, the microstructural changes between 100 - 200 °C and 600 - 650 °C are less evident. Furthermore, in the case of High Density Insulating Boards (IB-HD), the dilatometric curve is completely different from the "cross-plane" direction. Finally, the final shrinkage is smaller: - 0.21% IB-LD, - 0.18% IB-MD and - 0.03% IB-HD. All these points suggest a preferential orientation of the vermiculite structure.

The next step of the analysis was the investigation of the effect of an applied external compression load on the thermal expansion. Only the "cross-plane" direction is shown in **Figure 4-6**. However, the same trends were observed for the "in-plane" direction. For each compression load, the same experimental program was used: thermal cycle up to 700 °C with a heating/cooling rate of 5 K/min and 30 min of dwell time in an air atmosphere. Three compression loads were studied by simply increasing the weight on top of the push rod: 0.02 MPa (5 g), 0.21 MPa (50 g) and 0.42 MPa (100 g). For each compression load, two samples were investigated.

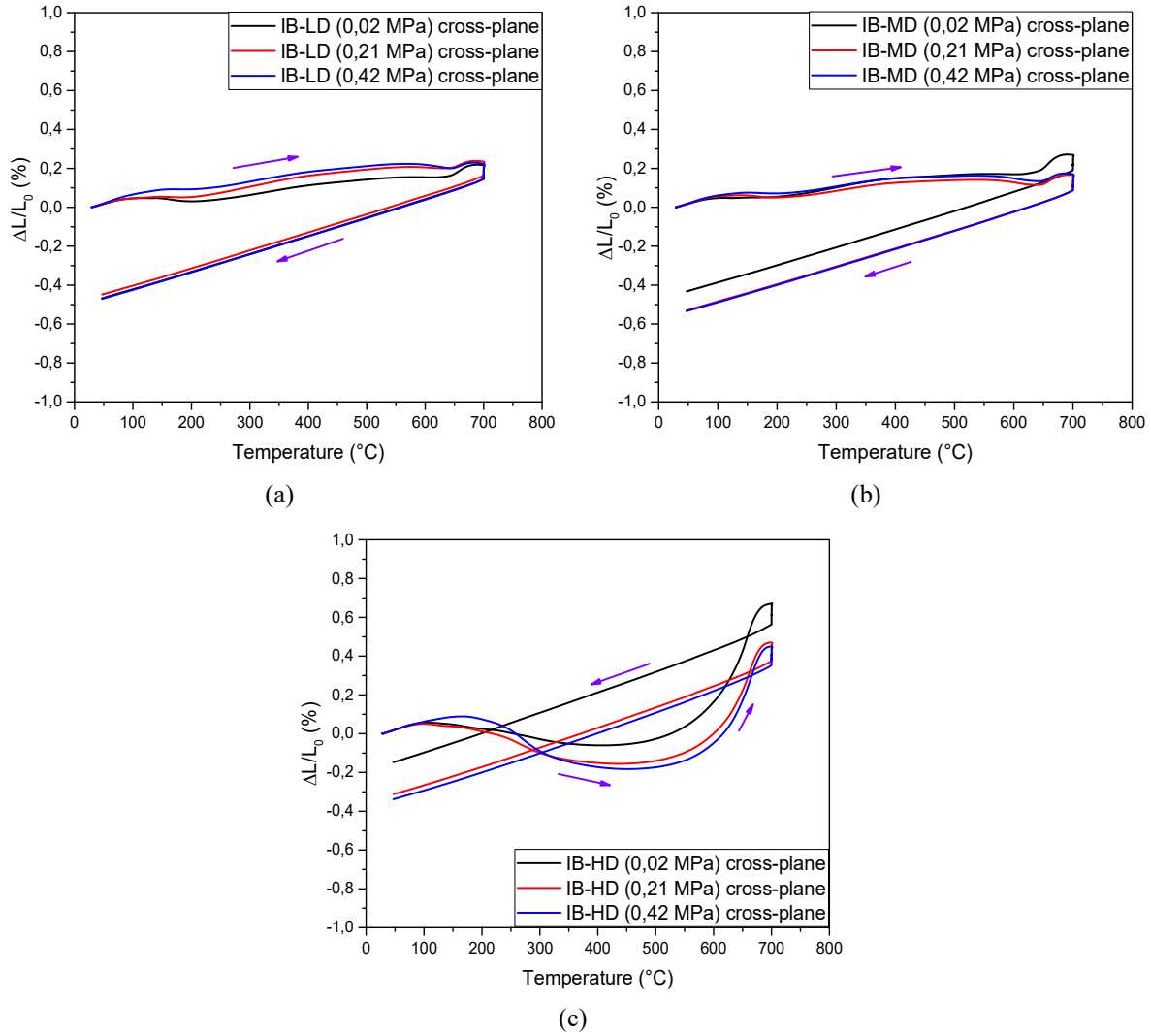

Figure 4-6 : *Effect of compression load on a) Low Density Insulating Boards, b) Medium Density Insulating Boards and c) High Density Insulating Boards. All the materials are analysed in the "cross-plane" direction.*

With the increase of the compression load, variation of the measurements between individual samples was close to zero, which supports the interpretation that the lowest compression load is not able to remove dimension effects due to the microstructural history of the particular refractory sample. Furthermore, the two higher loads (0.21 MPa and 0.42 MPa) also causes an increase of the final shrinkage (except for the IB-LD "cross-plane", which is almost constant). This is related to two aspects: on one hand, to the removal of the intercalated water which causes a first reduction of the interlayer distance (d_{int}); on the other hand, to the presence of the load itself, which further reduces d_{int}.

An aspect to highlight is related to the steel ladle process. Before starting the production of steel, the vessel is pre-heated for reducing: i) thermal shocks, ii) damage of the refractory linings, and iii) temperature drop in the ladle [103]. As a consequence, all the microstructural changes within the insulating layer material occur during this step. For this reason, in the case of the Insulating Boards, a second cycle was studied for all the investigated compression loads. This second cycle follows the same experimental program of the first: thermal cycle up to 700 °C with a heating/cooling rate of 5 K/min and 30 min of dwell time in an air atmosphere, and 1 h of dwell time between the two cycles.

Figure 4-7 shows the comparison between the three investigated compression loads during a second thermal cycle in the case of Low Density Insulating Boards (IB-LD) in the "cross-plane" direction. This is used as reference for all the three grades of boards with different pore volume fractions since all the Insulating Boards exhibit dilatometric curves with similar coefficients of thermal expansion (**Table 4-4**).

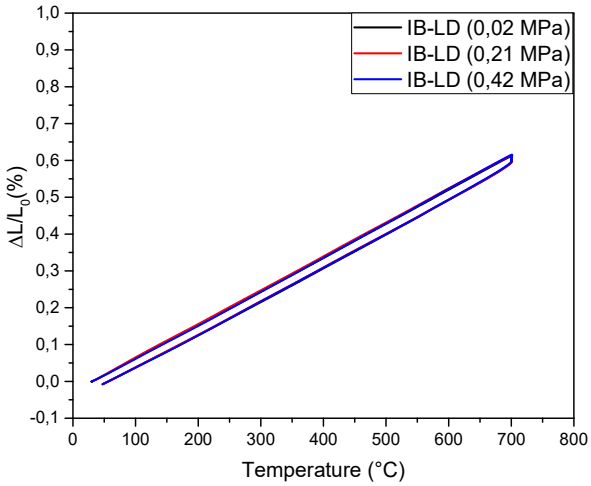

Figure 4-7: *Dilatometry measurements of Low Density Insulating Board in the "cross-plane" direction, during a second thermal cycle under three investigated compression loads.*

In service conditions, the Insulating Boards are stable. The graph shows a reversible cycle without any microstructural changes. Furthermore, the increase of compression load has no influence on events imputed to this behaviour. The dilatometric curves obtained for the three investigated loads overlap perfectly.

The coefficient of linear expansion (α_L) is then calculated using **Equ. 1-25**. **Table 4-4** summarizes the obtained values in the two directions: "cross-plane" (CP) and "in-plane" (IP).

It is possible to observe that the values in the "cross-plane" direction are slightly higher than those in the "in-plane" direction with a difference of: + 2.0% in the case of IB-LD, + 2.6% in the case of IB-MD and + 8.9% in the case of IB-HD. However, the differences are quite small and this is a positive aspect. Normally, when a material is used in high temperature processes, the desired thermal expansion should be as low as possible in order to avoid unexpected damage. Furthermore, if this value is similar in different directions, it may increase the lifetime of the material because it expands isotropically at the macroscopic scale.

Table 4-4: *Coefficients of linear expansion for the Insulating Boards during the second thermal cycle in the "cross-plane" (CP) and "in-plane" (IP) directions. The values are the same for the three investigated compression loads.*

Materials	***α_L (1/°C) 20 - 700 °C heating/cooling***	***α_L (1/°C) 20 - 700 °C heating/cooling***
	CP	IP
IB-LD	$9.1 \cdot 10^{-6}$	$8.9 \cdot 10^{-6}$
IB-MD	$9.3 \cdot 10^{-6}$	$9.1 \cdot 10^{-6}$
IB-HD	$10 \cdot 10^{-6}$	$9.4 \cdot 10^{-6}$

Table 4-4 also shows that in both directions the values increase slightly with the increase of density (**paragraph 2.3.4**). The High Density Insulating Boards (IB-HD) shows the highest value of coefficient of thermal expansion. Finally, the difference between the results obtained in the two directions is still related to the orientation of the vermiculite structure. When the material is subjected to compression load, this will promote the removal of the intercalated water. As a consequence, the layers of the vermiculite are less structured and thus, when subjected to a thermal cycle, they are freer to expand. As demonstrated in **Figure 4-3** and **Figure 4-5**, the boards show a preferential orientation in the "cross-plane" direction. Therefore, this direction shows a slightly higher value of thermal expansion for the three nuances.

4.2.1.2. Insulating Fireclay Bricks

Insulating Fireclay Bricks (IFB) are isotropic materials and thus, only the "cross-plane" direction was investigated. Two samples per each compression loads were tested with typical dimensions: 5x5 mm^2 of area and approximately 13 mm in length. The following experimental program was used: thermal cycle up to 1300 °C with a heating/cooling rate of 5 K/min and 30 min of dwell time in air atmosphere. The specimens were left 24 h in an oven at 100 °C before the measurements.

Let us start to study the lowest compression load (**Figure 4-8**). For this kind of refractory material, the variation between different samples is close to zero even for the lowest compression load. This can be explained considering that Insulating Fireclay Bricks are stable up to around 1000 °C, which is confirmed by DTA/TGA measurements. Above this temperature, the meta-kaolin partially melts and then recrystallizes into an Al/Si phase [14][85]. However, this reaction does not seem to have any influence on the thermal expansion. Furthermore, the graph shows a rather small final shrinkage (- 0.02%), which supports the

hypothesis that the microstructure does not have a significant effect.

The two main phases present in the refractory material are corundum and mullite (**Figure 2-3**), and thus in **Figure 4-8**, the thermal expansion curves of both of these phases are shown for heating/cooling (reversible cycle). It is evident that the dilatometric curve of Insulating Fireclay Bricks is much closer to that of the mullite, which might suggest a higher amount of this phase.

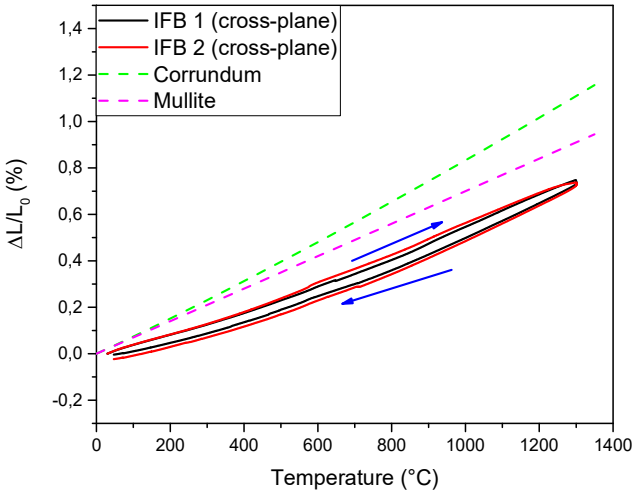

Figure 4-8: *Dilatometry measurements on Insulating Fireclay Bricks. The material is analysed in the "cross-plane" direction with a compression load of 0.02 MPa. The graph also shows the thermal expansion of alumina (green line) and mullite (magenta line).*

Equ. 1-25 was used to calculate the coefficient of linear expansion in two different temperature ranges, during the cooling cycle. Between 1300 °C and 1100 °C, a value of $8.2 \cdot 10^{-6}$ 1/°C was obtained, while between 400 °C and 20 °C the value decreased to almost the half ($3.9 \cdot 10^{-6}$ 1/°C). Thus at higher temperatures, the coefficient of thermal expansion is greater than that at lower temperatures. This difference can be attributed both to intrinsic linear expansion behaviour and to micro-cracking within the microstructure. In fact, it is amplified in the case of a thermally damaged material [104].

As temperature increases on heating, the amorphous phase begins to expand (and later to soften) closing micro-cracks, ultimately healing the material. So at the beginning of the cooling, the material is assumed to be free of damage. Between 1300 °C and 1100 °C, the amorphous phase becomes rigid and the mismatch in thermal expansion between α-alumina and mullite induces local thermal stresses around the phases. When the magnitude of these stresses is too high, they are progressively released through diffuse micro-cracking within the microstructure. As a consequence, the dilatometric curve moves gradually away from the starting cooling linearity with an associated reduction in the coefficient of thermal expansion. Young's modulus measurements performed by V. Tadaion (RWTH - Aachen) show the characteristic hysteresis curve of thermally damaged materials, which supports this interpretation (**appendix D**).

The influence of the compression load on the thermal expansion was then studied using the same values tested in the case of Insulating Boards (0.21 MPa and 0.42 MPa). The results

are shown in **Figure 4-9**. In the graph, it is possible to observe an increase of the final shrinkage (from - 0.02% to - 0.16%) with the increase of the compression load.

The graph also shows that the dilatometric curves for 0.21 MPa and 0.42 MPa are still similar to that of the mullite but only up to 1200 °C. Above this temperature, the material exhibits a shrinkage due to creep. This is a permanent deformation that can occur at high temperatures in the presence of load. The rate of deformation is a function of the material's properties, time, temperature and the applied load. The lowest compression load (0.02 MPa) might not be high enough to cause the deformation.

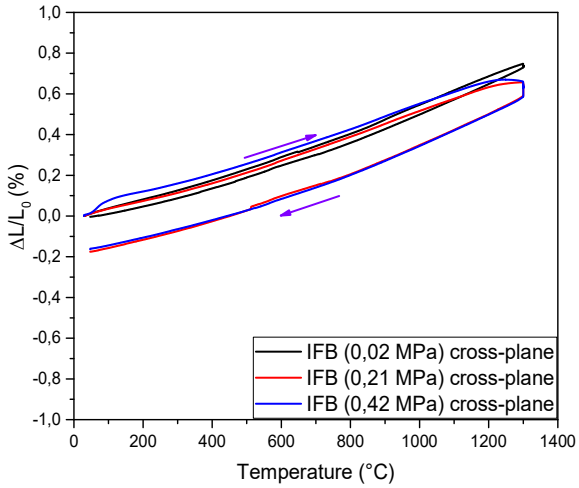

Figure 4-9 : *Effect of compression loads on Insulating Fireclay Bricks. The material is analysed in the "cross-plane" direction.*

4.2.2. Thermal conductivity

To study the influence of the compression load on the thermal conductivity, the hot disk method was chosen (**paragraph 2.2.4**). The measurements were made at room temperature in an air atmosphere. For each pair of samples, four measurements were made. The set-up consists in adding a weight on top of the two halves of the sample. Two compression loads were investigated: 0.02 MPa and 0.04 MPa. These two values were chosen for three main reasons: i) they are small enough to not damage the TPS probe; ii) they are small enough to be achievable by simply placing a weight of respectively 5 kg and 10 kg on top of the samples; iii) the pile made up of samples and weights is not too tall to be dangerous (safety reasons). The measurements were made on square samples with typical dimensions: 50x50 mm^2 of area, 12 - 15 mm of thickness for the Insulating Boards, and 32 mm of thickness for Insulating Fireclay Bricks.

Two analysis software modules were used: isotropic and anisotropic modules. The isotropic module was also used in the case of Insulating Boards, in order to have an overview of the effect of the compression load. In the case of the anisotropic module, the same specific heat per unit volume ($\rho \cdot C_p$) was used both for the samples with and without load. This might be not 100% accurate because the density of the materials can change with the compression load. However, following **paragraph 4.2**, any changes in this parameter should be less than

2% and the compressive loads are small.

Table 4-5 shows the results obtained using the isotropic software module. The values are expressed as percentage differences between the thermal conductivity values with and without compression load. It is possible to observe two different behaviours for the isotropic and anisotropic materials. In the case of Insulating Fireclay Bricks (IFB), the increase of the compression load leads to a constant decrease of the thermal conductivity, which is in within the standard deviation of measurements (**Table 2-4**). In the case of Insulating Boards (IB), **Table 4-5** shows a greater decrease of λ in the case of the lower compression load. Furthermore, the values are higher than the measurement uncertainty (**Table 2-4**).

Table 4-5: *Hot disk measurements under compression load at room temperature. The results are evaluated using an isotropic software module for all the investigated materials.*

Materials	***0.02 MPa (%)***	***0.04 MPa (%)***
IB-LD	- 7.8%	- 2.6%
IB-MD	- 8.3%	- 2.0%
IB-HD	- 6.8%	- 0.2%
IFB	- 1.9%	- 1.9%

The decrease of the thermal conductivity with the increase of the compression load is quite unusual. For a loosely packed material like IB, when a load is applied, the density of the material may increase because the porosity decreases. This causes an increase of the thermal conductivity (**paragraph 1.2.2.2**). More likely, the increase of the load improves the grain - grain contacts reducing the grain boundaries thermal resistance and consequently, λ increases (**paragraph 1.2.2.1**) [105].

Thus to explain these decreased values, let us examine the results obtained using the anisotropic software module in the case of the Insulating Boards (**Table 4-6**).

Table 4-6: *Hot disk measurements under compression load at room temperature. The results are evaluated using an anisotropic software module to take into account the anisotropic behaviour of the Insulating Boards.*

Materials	***0.02 MPa (%)***		***0.04 MPa (%)***	
	CP	IP	CP	IP
IB-LD	+ 1.6%	- 12.5%	+ 1.2%	- 7.0%
IB-MD	+ 2.4%	- 11.2%	+ 1.8%	- 8.3%
IB-HD	+ 3.5%	- 8.4%	+ 3.5%	- 5.8%

The table shows an increase of the thermal conductivity values in the “cross-plane” (CP) direction and a decrease of the thermal conductivity values in the “in-plane” (IP) direction for both compression loads. Thus, the overall thermal conductivity decreases as shown in **Table 4-5**. Furthermore, as for the results obtained with the isotropic software module, the effect seems to be higher for the lower compression load (0.02 MPa).

Table 4-6 also shows that the difference in the thermal conductivity values in the "in-plane" direction is greater than the "cross-plane" direction. In the first case, λ changes between 5.8% and 12.5%, while in the second case between 1.2% and 3.5%. The presence of a compression load can force the removal of the intercalated water. Considering that the thermal conductivity values decrease with the decrease of the water content (**paragraph 2.3.3**), this interpretation explains why the values are significantly lower. Therefore, if the samples are firstly dried, the difference should be smaller. This hypothesis can be verified by further experimental studies.

It is also interesting to underline that the ratio between the thermal conductivity values in the two directions depends on the specific heat per unit volume ($\rho \cdot C_p$). For the calculation, the same value was used also after compression. However, the density can slightly increase with the increase of the compression load. Therefore by taking into account the theory of the hot disk method described in **paragraph 2.2.4**, this means that the thermal conductivity values in the "in-plane" direction may be higher than those calculated (**Equ. 2-14**) and consequently, the thermal conductivity values in the "cross-plane" direction are lower (**Equ. 2-15**). However, this variation should not be too much significant since the Insulating Boards are quite "rigid" materials.

To conclude, since in service conditions, the materials are dried (they are typically used at temperatures above 300 °C), the compression load seems not to have a significant impact on the thermal conductivity. This is also related to the ability of the refractory materials tested in this work to resist compression loads.

4.3. Influence of carbon pick-up on thermal conductivity

The last aspect considered is the aging of the materials in service conditions. This behaviour is affected by the working environment and will cause a change of the material's properties, leading to the need for replacement of the material itself in order to guarantee the same safety and operation conditions for the complete industrial campaign. This process is a very important problem for the steelmaking and glassmaking industries. Engineers work constantly to find a refractory material with the longest service life in order to reduce the impact on the production costs.

To go further in the discussion, let us examine the characteristics of a post-mortem sample of Medium Density Insulating Board (**Figure 4-10**).

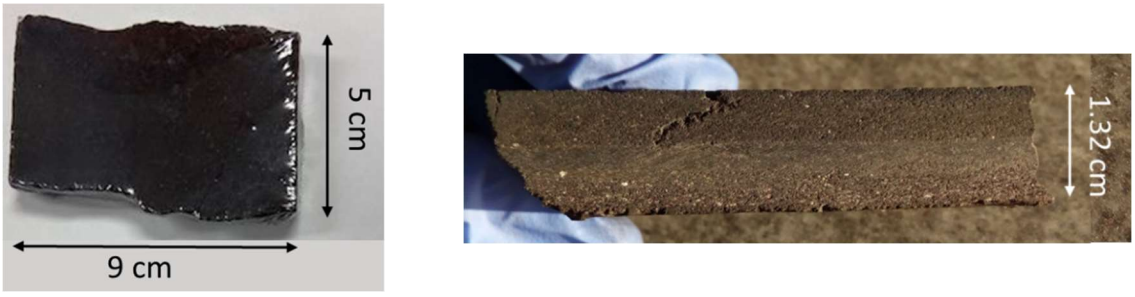

(a) (b)

Figure 4-10: *Post-mortem sample of Medium Density Insulating Board (IB-MD). The pictures show that the refractory material is completely covered by carbon, both outside (a) and inside (b).*

The piece supplied by the company was extracted from the top part of the ladle at the level of the slag line, after being in service for around 14 - 16 months. **Figure 4-10** shows that the specimen is completely black, both outside and inside. Considering that this type of refractory normally exhibits a brown colour, very significant carbon contamination seems to have occurred.

The following sections will discuss the influence of the carbon pick-up on the thermal properties, as well as the origin of the contamination.

4.3.1. Identification of the amount of carbon

To estimate the amount of carbon present in the investigated sample, two methods were compared: i) the first takes into account the variation of density, and ii) the second measures the amount of carbon in % wt.

In the first case, two samples were considered. The first specimen was extracted from a board of Medium Density Insulating Boards without carbon contamination, with density ρ_i. The second was the entire available sample of the post-mortem Medium Density Insulating Board, with density ρ_f. To estimate the variation of the density ($\Delta\rho$) from the original unaged material, the following equation was used:

$$\Delta\rho\ (\%) = \left(\frac{\rho_f - \rho_i}{\rho_i}\right) \cdot 100 \qquad \textit{Equ. 4-4}$$

The calculation gives an estimation of around 22% wt. It is also important to remember that in service conditions, the boards are subjected to a compression load due to the hydrostatic pressure exerted by the hot liquid steel on the wall of the vessel and to the volume expansion of the inner layers. Therefore, this effect should be considered in the variation of the density.

Normally, the maximum compression load applied to the insulating lining in the steel ladles is ~ 7 MPa [100]. So uniaxial compression tests were made on square samples (70x70 mm^2 of area and 25 mm in thickness) with a loading rate of 0.025 kN/s. The measurements evaluated a cold crushing strength (CCS) of 12.2 MPa in the case of Medium Density Insulating Boards (**Table 4-3**). Furthermore, the load-displacement curve (**appendix B**) showed that in service conditions, the material exhibits an elastic behaviour (applied compressive stress equal to 7 MPa) which indicates in a first approach that once the force is removed, the board comes back to the original state without damage. However, measuring the dimensions of the samples before and after compression, it was possible to observe a small reduction in the density of around 2% wt. After removing this contribution from **Equ. 4-4**, the calculation gives a variation of the density of 20% wt.

In the second case, the measurements were made both at RHI-Magnesita Company (Leoben, Austria) and at IRCER lab. About 100 mg of powdered sample were weighed in an alumina crucible and burned in a high-frequency combustion furnace (T_{max}: 2000 °C) with iron and tungsten chips. The complete combustion was achieved in an integrated oxygen lance, which floods the crucible with high-purity oxygen. The resulting gas was then analysed by two IR detectors, calibrated with a characteristic wavelength for detecting low and high CO_2 and

CO concentrations [106]. This method measured around 3 - 4% wt. of carbon. Considering that the density of the carbon can vary between 1.8 g/cm^3 and 2.3 g/cm^3 depending on the nature, this proportion causes a maximum increase of the density of the original unaged material of around 5% wt. This means that between the two methods, there is a difference of 15% wt.

To explain this discrepancy, X-ray fluorescence (XRF) measurements were made on the samples with and without carbon. The results show that in the post-mortem material the carbon is not the only additional phase. The analysis detected: i) 5.81% wt. of chlorine in the form of NaCl (ρ = 2.16 g/cm^3) and KCl (ρ = 1.98 g/cm^3), which were also confirmed by SEM analysis, ii) 0.30% wt. of PbO (ρ = 9.53 g/cm^3) and iii) 0.33% wt. of bromide in the form of $CaBr_2$ (ρ = 3.35 g/cm^3), which was validated by the increase of the amount of calcium in the system. The sum of all these compounds leads to a further increase of the density of 15% wt. and thus, the two methods are comparable.

Traces of lead oxide may be related to the scrap introduced in the ladle [107]. The presence of NaCl and KCl might be linked to the slag [108]. When the slag makes contact with the refractory lining, whose temperature is lower than the melting point of the slag, it is cooled below its solidus temperatures promoting the occurrence of a layer that adheres to the lining. This layer is the cause of certain problems (i.e. it reduces the overall efficiency of the metal handling system), and thus to avoid its formation, additives called fluxes are added to decrease the melting point of the slag. These additives can be: sodium carbonate, calcium carbide, borates, fluorspar, potassium chloride, sodium chloride, calcium aluminates etc. [108]. $CaBr_2$ may be linked to the pre-heating process of the steel ladle. The ladle is heated up to 900 - 1000 °C by pre-heated air [103]. The air is often heated using waste gas, for instance coming from the burning of the coal and the coke in the blast furnace. Calcium bromide is usually added to help control mercury emissions during the burning [109].

To summarize, the post-mortem material exhibits ~ 10% wt. of extra phases compared to the original refractory. Furthermore, since the density of the post-mortem material is higher than that of the original material, the hypothesis is that these phases penetrate inside the open porosity. To verify this assumption, **Equ. 3-1** was used. The results are shown in **Table 4-7**.

Table 4-7: *Summary of the physical properties of the original unaged material (IB-MD) and of the post-mortem material (IB-MD + C).*

Materials	***True density (g/cm^3)***	***Bulk density (g/cm^3)***	***Overall porosity (%)***
IB-MD	2.73	1.2 ± 7%	45 - 55
IB-MD + C	2.73	1.5 ± 7%	35 - 45

The table shows a reduction of the overall porosity range of around 10%, in agreement with the amount of extra phases detected. Furthermore, reported data show no difference in the true density values. The explanation comes from the balance between the density values of the heavier phases ($CaBr_2$ and PbO) and the lighter phases (C, KCl and NaCl), which finally leads to an average value close to 2.73 g/cm^3.

4.3.2. Effect of carbon on thermal properties

4.3.2.1. Specific heat

The evaluation of the specific heat was carried out using two approaches performed on Medium Density Insulating Board samples containing or not the carbon contamination: an experimental method (Differential Scanning Calorimetry) and a calculation method based on the rule of mixtures [71].

The DSC is a thermo-analytical technique in which the difference in the amount of heat required to increase the temperature of a sample and a reference is measured as a function of temperature [16]. Both the sample and the reference are maintained at nearly the same temperature throughout the experiment. The reference sample should have a well-defined heat capacity over the range of temperatures to be scanned [110]. The basic principle underlying this technique is that when the sample undergoes a physical transformation, such as a phase transition, a given heat will need to flow into it compared to the reference to maintain both at the same temperature. Whether more or less heat must flow to the sample depends on whether the process is exothermic or endothermic.

For this method, the samples were ground and left 24 h in an oven at 100 °C before the measurements. The experiments were carried out from 15 °C up to 35 °C with a heating rate of 5 K/min in a static air atmosphere and with sapphire as the reference. The measurements were made using a SETARAM μDSC7. The method at room temperature gave a specific heat value of 800 $J \cdot kg^{-1} \cdot K^{-1}$ for the original unaged material (IB-MD) and 690 $J \cdot kg^{-1} \cdot K^{-1}$ for the post-mortem material (IB-MD + C). The experimental results were then compared with the values obtained using **Equ. 2-17**. The rule of mixtures at room temperature also predicts a decrease of the specific heat value in the case of IB-MD + C.

4.3.2.2. Thermal conductivity

The evaluation of the thermal conductivity was made using two techniques: the laser flash method and the hot disk method. In the case of the laser flash method, the measurements were made only in the “cross-plane” direction, due to the small amount of available material, up to 800 °C in an argon atmosphere. In the case of the hot disk method, the measurements were made at room temperature in an air atmosphere.

A first measurement with the hot disk method was made using the isotropic analysis software module (**Table 4-8**). The purpose of this test was to evaluate the overall thermal conductivity behaviour of the post-mortem material. The advantage of using this module is that it is not necessary to know the specific heat per unit volume. The measurements were carried out on the original unaged material (IB-MD) and the post-mortem material (IB-MD + C) with the same conditions. For each sample, four tests were made.

The table shows an increase of the thermal conductivity for the post-mortem sample infiltrated by carbon of around 26%. The post-mortem sample has been subjected to several thermal cycles in service conditions. Thus, this increase is in part linked to the microstructural

evolution, which occurs during the first cycle (**Figure 4-4**) and to the effect of the compression loads. These two effects cause an increase of the density and consequently, an increase of the thermal conductivity values (**paragraph 4.2.2**).

Table 4-8: *Thermal conductivity values obtained with the hot disk method (TPS) at room temperature using an isotropic analysis software module.*

Materials	***TPS*** λ ***(W·m^{-1}·K^{-1})***
IB-MD	0.35 ± 1.5%
IB-MD + C	0.43 ± 1.5%

Let us now consider the results obtained using the anisotropic software module (**Table 4-9**).

Table 4-9: *Thermal conductivity values obtained with the hot disk method (TPS) at room temperature using an anisotropic software module. The table shows only the "cross-plane" (CP) direction.*

Materials	***TPS*** λ ***(W·m^{-1}·K^{-1})***
	CP
IB-MD	0.28 ± 1.5%
IB-MD + C	0.35 ± 1.5%

As for the isotropic module (**Table 4-8**), the table shows an increase of around 26% for the post-mortem sample infiltrated by carbon (IB-MD + C). Therefore, the analysis confirms that the presence of the carbon (3 - 4% wt.) and other species (6 - 7% wt.), combined with the effects of compression loads and microstructural evolution, causes an increase of the thermal conductivity values of the refractory material.

Let us now examine the laser flash results. In this case, samples were cut in different zones or depths with respect to the thickness of the board. **Table 4-10** summarizes the main physical properties.

Table 4-10: *Summary of the main physical properties for each investigated zone. The mass is evaluated on the samples before and after laser flash measurements.*

Zone	***Density*** ***(g/cm^3)***	***Mass*** ***(g)***	
		Before	After
Top	1.8 ± 7%	0.63	0.58
Central	1.5 ± 7%	0.43	0.41
Bottom	1.2 ± 7%	0.29	0.29

The first difference, that it is possible to observe, is a gradient of density between the three zones. The bottom zone has the same density of the original unaged material, while the

top zone has a density higher than that of the entire post-mortem sample (**Table 4-7**), and closer to the density of the carbon (1.8 - 2.3 g/cm^3). Furthermore, there is an increase of the mass loss from the bottom to the top zones after the laser flash measurements. Additionally, the samples cut in the top zone were still black at the end of the tests, even after a second thermal cycle.

Figure 4-11 shows the laser flash results for the samples cut: a) in the top zone, b) in the central zone and c) in the bottom zone. For each zone, two samples were analysed and three measurements for each temperature were made. The results are compared with those obtained for the material without carbon (black dots).

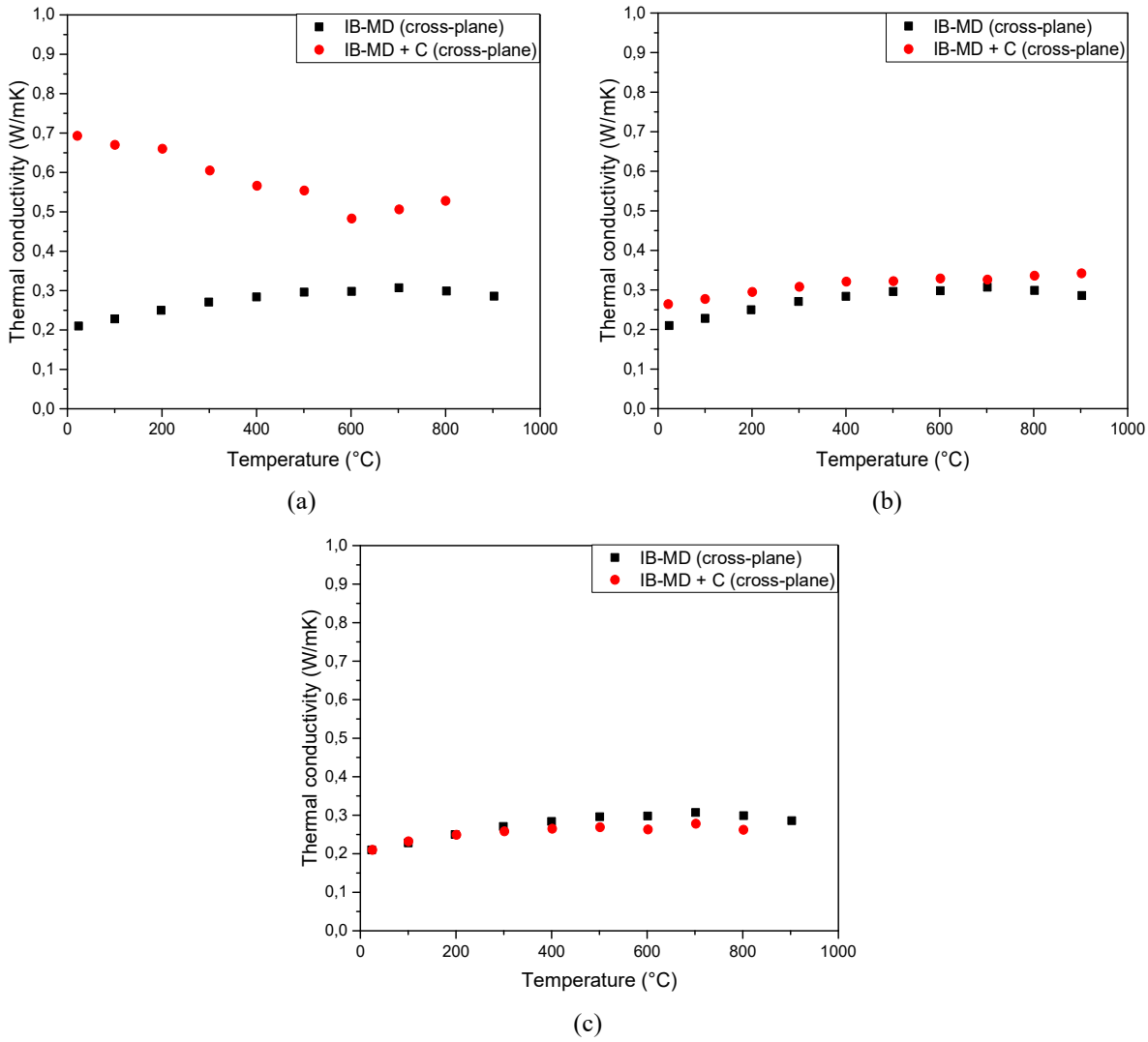

Figure 4-11: *Thermal conductivity vs temperature of post-mortem Medium Density Insulating Board samples. The samples were cut in the different zone: top zone (a), central zone (b) and bottom zone (c).*

Figure 4-11b and **Figure 4-11c** show that the presence of carbon has a small effect on thermal conductivity. In the sample cut in the middle depth of the board, there is a slight increase of λ. Furthermore, at the end of each measurement, the samples became brown (the typical colour of the Insulating Boards), which implies that the carbon content was essentially removed. A different situation is presented in **Figure 4-11a**. In this top zone of the post-mortem specimen, the effect on thermal conductivity is quite consistent. At room temperature, λ changes from 0.22

$W \cdot m^{-1} \cdot K^{-1}$ for the original unaged material to 0.67 $W \cdot m^{-1} \cdot K^{-1}$ for the post-mortem material.

To explain these three behaviours, EDS (Energy-dispersive X-ray spectroscopy) measurements were made on specimens cut in the three zones of the post-mortem sample (**Figure 4-12**). This type of measurement is not accurate for low atomic number, as in the case of the carbon, but gives a qualitative information on the distribution of elements. Furthermore, an error bar of ± 5% is estimated due to the un-flat nature of the analysed surfaces. The advantage of this technique is that **Figure 4-12** shows a concentration gradient in the carbon content. In the top zone of the sample, (**Figure 4-12a**), the amount of carbon is higher than the rest.

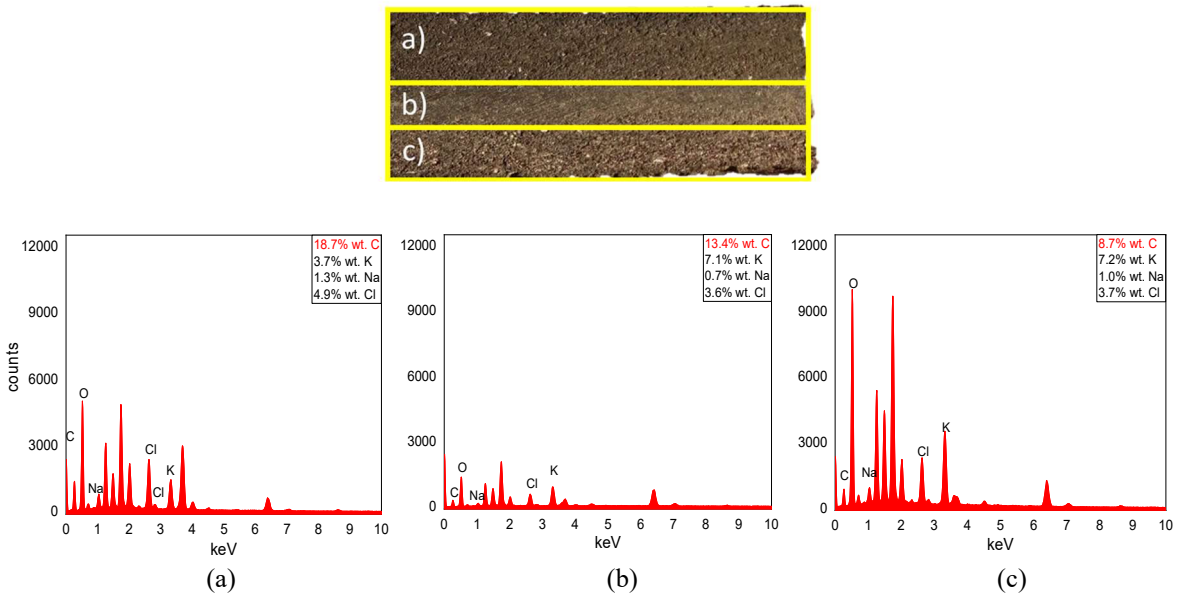

Figure 4-12: *EDS measurements on a post-mortem sample of Medium Density Insulating Board. Three zones can be identified: a) high carbon content, b) medium carbon content; c) low carbon content.*

This can explain why the laser flash measurements made on samples cut out of this zone reveal a higher thermal conductivity (**Figure 4-11a**). Generally carbon based refractories exhibit higher values of conductivity [7][14]. Furthermore, the EDS chemical analysis in this zone shows a higher quantity of NaCl and KCl (4.9% wt. Cl) than the other zones (3.7% wt. Cl). This was also confirmed by SEM analysis. The image took in the top zone presented a higher quantity of cubic crystals. Therefore, the combination of a higher quantity of additional compounds leads to a significant increase of the thermal conductivity values of the refractory materials. Therefore, the EDS analysis confirms the interpretation of increased thermal conductivity values correlate with the variation of the carbon content (and of the other phases) for each zone.

Furthermore, the thermal diffusivity results, which are not affected by the C_p values, confirm the presence of a greater effect in the top zone. In this zone, α decreases from 0.48 mm^2/s at room temperature to 0.29 mm^2/s at 700 °C for the post-mortem material, while the original unaged material has a quite constant behaviour close to 0.27 mm^2/s. In contrast, for the samples cut in the central and bottom zones, the diffusivity values of the post-mortem material are also constant and closer to the original unaged material (respectively 0.22 mm^2/s and 0.24

mm^2/s).

To summarize, the analysis on the post-mortem sample leads to the following conclusion: the presence of 3 - 4% wt. of carbon and 6 - 7% wt. of additional phases (mostly in the form of NaCl and KCl), combining with the effects of microstructural evolution and compression loads, causes an increase of the overall thermal conductivity of around 26%. Furthermore, the laser flash method shows the presence of a 4 mm more conducting layer, while the remaining part (~ 70% of the board) does not show a significant change of the thermal conductivity values. Thus, it might be deduced that the Insulating Board is still operational despite the infiltration of carbon.

Let us now try to go deeper into the origin of the carbon deposition and, how its non-homogenous distribution can develop.

4.3.3. Origin of the carbon

For this purpose, it is important to consider the location of the board in the steel ladle. As explained in the previous chapters, these refractory materials are used in the insulating lining of the vessel (**Figure 3**). In the specific case of the investigated sample, the specimen was extracted from the top part of the ladle at the level of the slag line. To resist the aggressive and corrosive environment caused by the presence of the slag and of the high operating temperatures, the slag line is normally made of Magnesia-Carbon Bricks (MgO-C). The advantages of including carbon in the refractory material are: i) high thermal shock resistance, which is linked to the low thermal expansion and the high thermal conductivity of the graphite; ii) high corrosion resistance due to the low wettability of the carbon to the slag [7][14]. On the other hand, the disadvantage consists of the easy oxidation of the carbon which might lead to the degradation of the brick.

Carbon can be oxidized by two main mechanisms: direct and indirect oxidation [111][112]. In the first case, C reacts with the gaseous oxygen:

$$2C_{(s)} + O_{2\,(g)} \longrightarrow 2CO_{(g)} \qquad \textit{Equ. 4-5}$$

In the second case, C reacts with the solid oxide in MgO or other oxides, which are present in the refractory or in the slag:

$$MgO_{(s)} + C_{(s)} \longrightarrow Mg_{(g)} + CO_{(g)} \qquad \textit{Equ. 4-6}$$

Considering **Figure 4-13**, **Equ. 4-5** becomes important at temperatures below 1400 °C and **Equ. 4-6** at temperatures above 1400 °C. In the ladle, the temperature of the slag is around 1600 - 1650 °C. Therefore, **Equ. 4-6** seems to be the main mechanism of oxidation of the carbon. However, the more critical step is represented by the pre-heating process [103], during which the ladle is heated at temperatures below 1200 °C by pre-heated air. The oxygen present in the gas reacts with the carbon by direct oxidation (**Equ. 4-5**). This effect is much more critical at the beginning of the ladle campaign when there is not a slag layer on the working lining to reduce the corrosion mechanism [113].

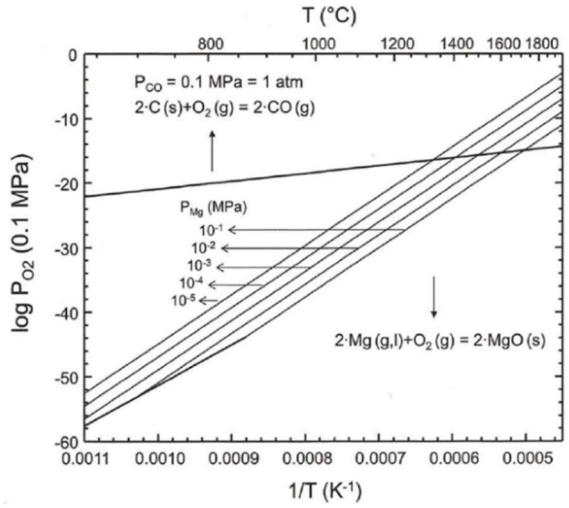

Figure 4-13: *Thermodynamic stability of MgO with carbon content* [113].

The hypothesis is now that CO diffuses through the linings from the slag zone to reach the insulation layer. Then, in this part of the refractory wall, there is another reaction to consider:

$$2CO_{(g)} \Longleftrightarrow CO_{2\,(g)} + C_{(s)} \qquad \textit{Equ. 4-7}$$

which is called the Boudouard reaction [114]. As shown in **Figure 4-14** at temperatures less than 627 °C, the reaction is shifted to the right with the increase of the amount of $CO_{2(g)}$ and $C_{(s)}$. Taking into account that the typical temperature range of the insulating lining is between 300 - 400 °C for the face in contact with the steel shell (cold face), and 800 - 900 °C for the face in contact with the safety lining (hot face), **Equ. 4-7** ought to explain the presence of carbon in these aged refractory materials.

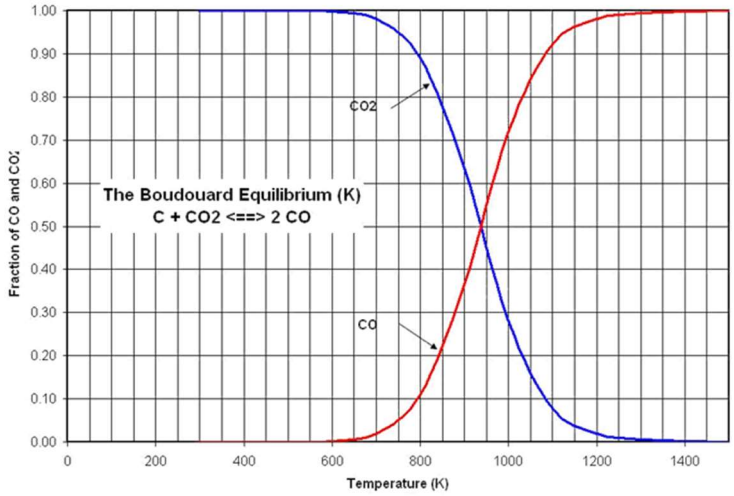

Figure 4-14: *Boudouard equilibrium diagram* [114].

Figure 4-14 also shows that the maximum amount of carbon is obtained at temperatures < 327 °C, which means in the colder part of the board (i.e. near the steel shell). Furthermore, the zone with the highest amount of C also shows a higher amount of potassium and sodium chloride. Considering the NaCl-KCl phase equilibrium diagram (**Figure 4-15**), the presence of solid sodium and potassium chloride is obtained at temperatures below 650 °C. This supports

the interpretation that the zone with the higher amount of additional phases is that in contact with the external steel shell (cold face). Higher quantity of extra phases leads to a significant increase of the density (**Table 4-10**). Thus, this might suggest that the face of the lining which exhibits the higher conductivity values (**Figure 4-11a**) is the cold face of the board. For validating this deduction, an easy test would be to take another piece from the steel ladle, to mark which side is in contact with the steel shell and to repeat all the tests described up to now.

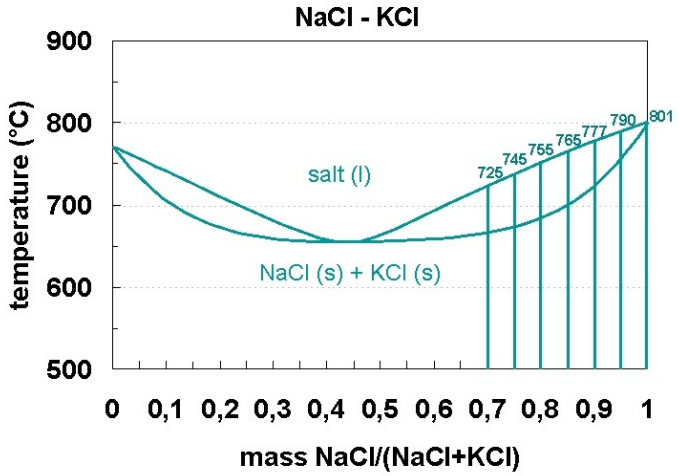

Figure 4-15: *NaCl-KCl phase equilibrium diagram* [115].

4.4. Conclusion

Three real cases of industrial problems were studied:

- Effect of joints (interface thermal resistance)
- Effect of compression loads
- Effect of carbon pick-up

The steel ladle is the vessel to hold and transport the hot liquid steel, where all the secondary metallurgy operations take place. It is made of different linings of refractory materials in order to achieve the required thermo-mechanical characteristics. Therefore, joints play an important role in modelling studies. One parameter to describe them is the thermal conductance, the ability to conduct heat through the interface of two solid bodies in contact. Nowadays, there is not an official procedure in the refractory field to determine this parameter. In this chapter, two techniques were compared for evaluating the interface thermal resistance, which is the inverse of the thermal conductance: one in the steady-state using the heat flow meter and one in transient regime involving the laser flash method. Both gave values of the order of 10^{-4} - 10^{-3} $m^2 \cdot K \cdot W^{-1}$. However, the more reliable procedure was that of the heat flow meter. Furthermore, the interface thermal resistance can be reduced by improving the contact area, which can be made in two ways: i) higher compression load (slight effect), ii) presence of a mortar.

The compression loads can have an influence of the thermal properties. The insulating

layer has two main functions: i) reducing the heat losses through the lining and ii) keeping the ladle in a compressed state. Therefore, the refractory materials used in this zone have low thermal conductivity values and sufficient compressive strength. The hot disk method was used to investigate the influence of two compression loads (0.02 MPa and 0.04 MPa) on the thermal conductivity. The results show not a significant effect for both refractory materials: Insulating Boards (IB) and Insulating Fireclay Bricks (IFB). In the case of the thermal expansion, IB are stable in service conditions and thus, the compression load has no influence on the behaviour. In contrast, in the case of the IFB, it slightly reduces the thickness of the brick.

Another problem to consider is the effect of aging. This mechanism was studied on Medium Density Insulating Boards. It was observed that with 3 - 4% wt. of carbon and 6 - 7% wt. of other additional phases, combining with the effects of microstructural evolution and compression loads, the overall thermal conductivity increases of around 26%.

Chapter 5 :
Conclusions and perspectives

Refractories are ceramic materials that have played a fundamental role in the development of industrial processes for the production of iron, steel, concrete and glass. These kinds of materials can withstand high temperatures, pressure, and chemical attacks, without degrading or softening. For instance, alumina-spinel bricks and magnesia-carbon bricks are used in the working lining of steel ladles. This zone is subjected to: i) high temperatures (around 1600 °C), ii) thermal shocks (due to the operations of filling/emptying), and iii) corrosive environment (presence of slag and hot liquid steel). Therefore, the study of the thermal properties becomes of important priority. In fact, when a material is subjected to a change of temperature, the energy exchanged is controlled by thermal conductivity and heat capacity. Furthermore such thermal properties depend on the temperature itself and can evolve with the state of the microstructure [11]. Knowledge of these properties as a function of the temperature and their evolution can improve the performance of the refractory materials and, at the same time, help to avoid serious working accidents.

The aim of this work (**Figure 5-1**) was to study the thermal properties of insulating refractory materials used in the insulating lining of steel ladles, which is the interlayer located between the external steel shell and the safety lining. The work was part of a European project called ATHOR (Advanced THermomechanical multiscale mOdelling of Refractory linings), created with the purpose of training 15 early stage researchers in multi-disciplinary engineering fields for a better understanding of thermomechanical behaviour of refractory linings used in the iron and steel industries [1].

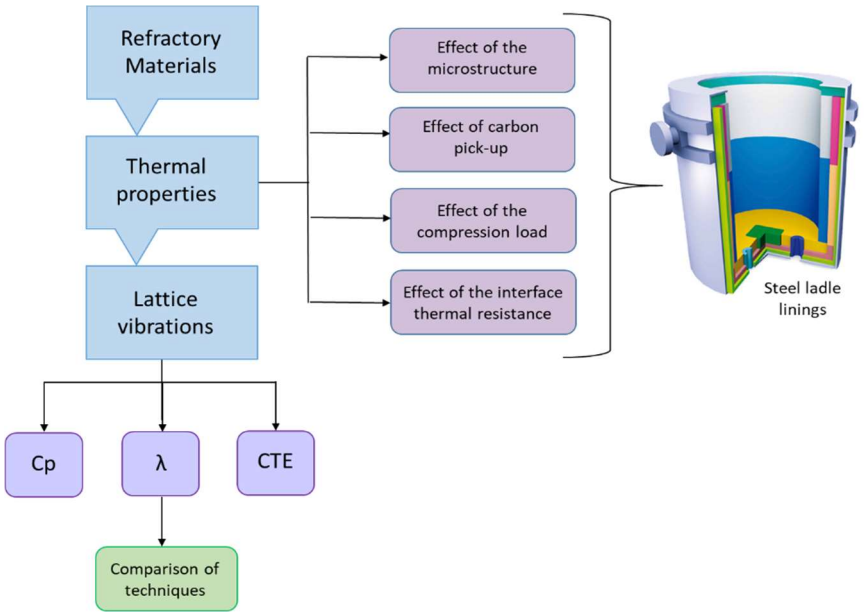

Figure 5-1: *Schematic of the topics studied in the current work.*

Three main thermal properties were studied: specific heat capacity, thermal conductivity and thermal expansion. To describe them, it was crucial to introduce firstly the concept of lattice vibrations and phonon scattering mechanisms.

The specific heat represents the amount of energy necessary to increase the temperature of a substance by one degree Celsius. It is related to the internal energy, whose major contribution for ceramic materials is given by lattice vibrations (harmonic approximation). This property was evaluated with two techniques: i) Differential Scanning Calorimetry (experimental test) [16] and ii) the rule of mixtures (empirical formula) [71] based on simpler components with data from literature.

On the other hand, the thermal conductivity and the thermal expansion can be described only taking into account anharmonic effects of the lattice vibrations. The thermal conductivity represents the ability of the material to propagate the heat, both in the solid and pore phases. For a polycrystalline material, the thermal conductivity of the solid phase is the sum of two contributions: a) heat conduction due to lattice vibration, b) radiation due to the presence of a transparent medium, which is usually negligible. This property was studied by comparing five measurement techniques: heat flow meter [50], Dr. Klasse technique [55], hot wire method [116], hot disk method [61] and laser flash method [65].

Finally, the thermal expansion is the ability of the material to change its dimensions due to a change of temperature. This is related to the atomic vibrations and asymmetry in the interatomic pair potential: with the increase of the temperature, the atoms vibrate with higher amplitude and as a consequence the interatomic distance between two atoms increases. The property was studied by dilatometry measurements [16].

The second chapter of the work was dedicated to the comparison of different techniques for thermal conductivity measurements. These were tested on three kinds of refractory materials: Insulating Boards, Insulating Fireclay Bricks and Alumina Spinel Bricks. The alumina-spinel is usually used in the working lining, so it showed a different behaviour compared to that of the insulating materials. For measurements of the Insulating Boards at room temperature, a maximum discrepancy of around 40% was found. This was attributed to:

- 5 - 10% to the role of lateral heat losses
- 15 - 25% to the effect of the humidity
- 10 - 15% to the anisotropic and heterogeneous behaviour of the material

Taking into account these affects, the discrepancy could be reduced within 10% when the same heat flow direction through the material is considered.

Furthermore, for each technique, advantages and disadvantages were underlined. At the end of the analysis, the hot disk method was chosen as the best technique for the investigated materials. **Table 5-1** summarizes the main factors investigated for: the laser flash method (LFA), the hot disk method (TPS), the hot wire method (HWM), the heat flow meter (HFM) and the Dr. Klasse technique (DKT).

Table 5-1: *Summary of the main parameters investigated for each technique.*

Method	*Measured parameter*	*Range*	*Uncertainty*	*Anisotropy*	*Heat losses*	*Heterogeneity*
LFA	α	0.1-1000 $mm^2\ s^{-1}$	± 5%	2 values - 2 samples	Model correction	-
TPS	λ α	0.005-500 $W\ m^{-1}\ K^{-1}$	2-5% 5-10%	2 values - 1 measurement	-	More precise average value
HWM	λ	< 15 $W\ m^{-1}\ K^{-1}$	1-6%	Average value	-	More precise average value
HFM	λ	< 1 $W\ m^{-1}\ K^{-1}$	± 3%	2 values - 2 samples	Model correction	-
DKT	λ	> 1 $W\ m^{-1}\ K^{-1}$	± 5%	2 values - 2 samples	Insulating material around the sample	More precise average value

The third chapter of the work was focused on the effect of the microstructure on the thermal conductivity. For this purpose, the measurements were made on Alumina Spinel Bricks comparing the results with four alumina-based model materials. Great attention was paid to the role of the porosity, grain boundaries, grain size, phase mixture and presence of cement. **Figure 5-2** summarizes the analysis adopted.

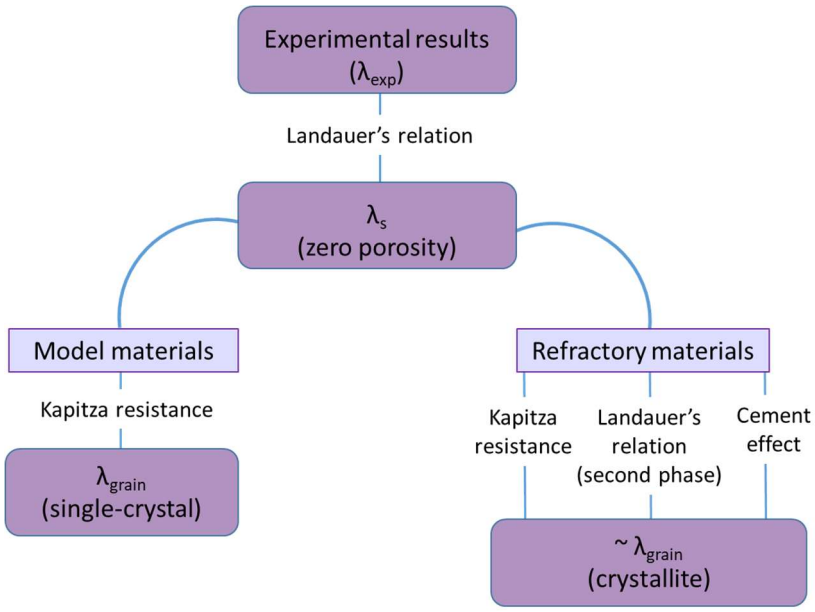

Figure 5-2: *Schematic of the approach adopted to assess the microstructural aspects of the thermal conductivity.*

The approach consists of estimating the thermal conductivity of alumina grains in the complex heterogeneous refractory material by taking into account the microstructural factors. These values were compared to single-crystal alumina (sapphire). The experimental values were firstly corrected for the effect of the porosity. For this purpose, Laundauer's relation [40] was used since all the investigated materials have pore volume fractions (v_p) less than 40%. During this step, the v_p was assumed to be constant for all the temperatures and the thermal

conductivity of the gas was approximated to zero. The second step was to take into account the presence of grain boundaries. They were considered as Kapitza resistances at the interface [30]. In the case of the model materials, these two contributions were enough for evaluating the thermal conductivity of the grains, which was the same as that of the sapphire (single-crystal) since they were all alumina-based materials. In the case of the refractory material, taking into account pore volume fraction and grain boundary thermal resistance yielded an estimate of the grain thermal conductivity within 25% of the value of sapphire. This can be explained by: i) presence of a second phase and ii) presence of impurities.

For these reasons, the effect of the presence of a second phase was studied using Landauer's relation, with the assumption that the refractory material is made of only two phases: alumina (grains) and spinel (matrix). As an alternative approach, the study focused on the role of cement to modulate the thermal conductivity of an alumina-based ceramic material. Three model materials were created with three percentages of calcium aluminate cement: 5% wt., 7% wt. and 10% wt. It was observed a decrease of the thermal conductivity values with the increase of the cement content.

Despite all these steps and approximations, the evaluated thermal conductivity of the grains in the case of the refractory material was within 12% of sapphire implying that the microstructure has been described satisfactory.

The last part of this work was dedicated to study some real cases of industrial interest. One of the investigated aspects was the presence of joints and their influence on the thermal conductivity. The ladle is made of different linings of refractory materials in order to achieve the required thermo-mechanical characteristics. Therefore, joints play an important role in modelling studies. One parameter to describe them is the thermal conductance, the ability to conduct heat through two solid bodies in contact. Nowadays, there is not an official procedure to determine this parameter. Therefore, two techniques were used for evaluating the interface thermal resistance, which is the inverse of the thermal conductance: the heat flow meter and the laser flash method. In both cases, a value of the order of 10^{-4} - 10^{-3} $m^2 \cdot K \cdot W^{-1}$ was found and can be used as first approximation in computer modelling of the steel ladle behaviour at the macroscopic level. It was also demonstrated that this parameter can be decreased by improving the contact area, which can be made in two ways: i) higher compression load (slight effect), ii) presence of a mortar.

Another aspect considered was the effect of the compression load. The insulating lining has two main functions: i) reducing the heat losses through the lining and ii) keeping the ladle in a compressed state. Therefore, the refractory materials used in this zone have low thermal conductivity values and sufficient compressive strength. In service conditions, this zone is normally subjected to a compression load of around 5 - 10 MPa. The hot disk method was used to investigate the influence of two compression loads (0.02 MPa and 0.04 MPa) on the thermal conductivity. The results show no significant effect for both refractory materials, Insulating Boards (IB) and Insulating Fireclay Bricks (IFB). In terms of the thermal expansion, IB are stable in service conditions and thus, the compression load has no influence on the behaviour. In contrast, in the case of the IFB, it slightly reduces the thickness of the brick.

Finally, one of the main problems for the steelmaking and glassmaking industries is represented by the aging of the refractory materials. This behaviour is affected by the working environment and will cause a change of the material's properties, leading to the need for replacement of the material itself in order to guarantee the same safety and operation conditions for the complete industrial campaign. Engineers work constantly to find a refractory material with the longest service life in order to reduce the impact on the production costs. To understand the effect of the aging on thermal properties, analysis was made on a post-mortem sample of Medium Density Insulating Board. The investigated piece was removed from the insulating lining in the top part of the ladle, after 14 -16 month of service life. The material showed a contamination of 3 - 4% wt. of carbon and 6 -7% wt. of additional phases. Two techniques were used: the hot disk and the laser flash methods. The analysis reached the conclusion that the overall thermal conductivity of the material increases of around 26% due to the combination of three effects: i) presence of ~ 10% wt. of additional phases, ii) compression load due the hydrostatic pressure of the hot liquid steel and of the volume expansion of the inner layers, and iii) microstructure evolution due to the high temperatures. Furthermore, the laser flash method shows the presence of a 4 mm more conducting layer in the cold phase of the board (near the steel shell), while the remaining part (~ 70% of the board) does not show a significant change on the thermal conductivity values. Thus, it might be deduced that the Insulating Board is still operational.

To conclude this work, the last question still open is: what to do next? From the ATHOR point of view, the aspects that can be further improved are: i) the anisotropic behaviour with the hot disk method; ii) the effect of heat losses and the presence of an interface thermal resistance on the results obtained with the Dr. Klasse technique; iii) the evaluation of the interface thermal resistance between bricks of different refractory materials, simulating the steel ladle lining; iv) the effect of the aging on other kinds of refractory materials to have a better overview of the steel ladle lining; and v) the effect of thermal shocks and thermal cycling due to the operations of filling/emptying of the ladle. Furthermore, a further investigation of the relationship between the microstructure and the thermal properties can help refractory producers to improve industrial processes, to predict the behaviour of the material in service conditions and to develop new products. In particular, the other aspects that can be considered are: i) the presence of more than two solid phases; ii) the presence of impurities; iii) the presence of micro-cracks; and iv) the effect of radiation contribution at high temperatures.

References

[1] "Project Overview," *EU H2020 MSCA ITN-ETN ATHOR Project*, 2017 [Online]. Available: https://www.etn-athor.eu/project-overview/ (accessed Nov. 17, 2020).

[2] "Refractories Market by Form (Shaped Refractories, Unshaped Refractories), Alkalinity (Acidic & Neutral. Basic), End-Use Industry (Iron & Steel, Power Generation, Non-Ferrous Metals, Cement, Glass), and Region - Global Forecast to 2025," *Refractory Market*, 2020. [Online]. Available: https://www.marketsandmarkets.com/Market-Reports/refractories-market-222632393.html (accessed Nov. 16, 2020).

[3] A. Ghosh, Ahindra; Chatterjee, *Ironmaking and Steelmaking: theory and practise*. PHI Learning Private Limited, 2008.

[4] "A Brief History of Refractories," *TFL Incorporated*, 2020. [Online]. Available: https://tflhouston.com/2018/09/28/a-brief-history-of-refractories/ (accessed Nov. 16, 2020).

[5] V. Nieto, "Steel production: from iron ore to functional industrial products.," *Vepica*, 2019. [Online]. Available: https://www.vepica.com/blog/steel-production-from-iron-ore-to-functional-industrial-products (accessed Nov. 16, 2020).

[6] M. F. Santos *et al.*, "Enhanced numerical tool to evaluate steel ladle thermal losses," *Ceram. Int.*, vol. 44, no. 11, pp. 12831–12840, 2018.

[7] C. Reynaert, E. Sniezek, T. Tonnesen, and J. Szczerba, "Impact of composition changes of alumina-rich slags on the corrosion of refractories found in steel ladles," in *UNITECR 2019*, 2019, pp. 409–412.

[8] R. Kaczmarek *et al.*, "Thermomechanical behaviour of an alumina spinel refractory for steel ladle applications," in *UNITECR 2019*, 2019, pp. 421–424.

[9] W. A. Calvo, P. Ortega, M. J. Velasco, V. Muñoz, P. Pena, and A. G. Tomba Martinez, "Characterization of alumina-magnesia-carbon refractory bricks containing aluminium and silicon," *Ceram. Int.*, vol. 44, no. 8, pp. 8842–8855, 2018.

[10] N. Schmitt, Y. Berthaud, J. F. Hernandez, P. Meunier, and J. Poirier, "Damage of monolithic refractory linings in steel ladles during drying," *Br. Ceram. Trans.*, vol. 103, no. 3, pp. 121–133, 2004.

[11] D. Vitiello *et al.*, "Thermal properties characterization of refractory materials used in the insulation layer of steel ladles," in *UNITECR 2019*, 2019, pp. 454–457.

[12] ISO Standard, "Terminology for refractories," *ISO 836-2001*, pp. 1–30, 2001.

[13] ASTM International, "Standard Terminology Relating to Refractories," *ASTM C71 - 12*, vol. 15.01, pp. 1–6, 2006.

[14] C. A. Schacht, *Refractories Handbook*. Marcel Dekker, Inc, 2004.

[15] G. Inden, *Introduction to thermodynamics*. 1995.

[16] H. Czichos, T. Saito, and L. Smith, Eds., *Springer Handbook of Metrology and Testing*, 2nd editio. Springer, 2011.

[17] H. Ibach and H. Luth, *Solid-state physics*, Second Edi. Springer US, 2012.

[18] D. Cahill, "Lattice Vibrations And Heat Transport In Crystals And Glasses," *Annu. Rev. Phys. Chem.*, vol. 39, no. 1, pp. 93–121, Jan. 1988.

[19] A. Einstein, "On a heuristic viewpoint concerning the production and transformation of light," *Ann. Phys.*, vol. 17, pp. 132–148, 1905.

[20] M. Razeghi, *Fundamentals of solid state engineering*. Kluwer Academic, 2002.

[21] X. Oudet, "Le corps noir et la loi de Dulong et Petit," *Ann. la Fond. Louis Broglie*, vol. 29, no. 4, pp. 733–745, 2004.

[22] F. R. Charvat and W. D. Kingery, "Thermal Conductivity: XIII, Effect of Microstructure on Conductivity of Single-Phase Ceramics," *J. Am. Ceram. Soc.*, vol. 40, no. 9, pp. 306–315, 1957.

[23] W. D. Kingery, "Thermal Conductivity: XII, Temperature Dependence of conductivity for single-phase ceramics," *J. Am. Ceram. Soc.*, vol. 38, no. 7, pp. 251–255, 1955.

[24] D. Schwen, "Normal and Umklapp scattering for phonons," *Wikipedia*, 2005. [Online]. Available: https://en.wikipedia.org/wiki/Umklapp_scattering (accessed Mar. 12, 2020).

[25] D. S. Smith, S. Fayette, S. Grandjean, C. Martin, R. Telle, and T. Tonnessen, "Thermal resistance of grain boundaries in alumina ceramics and refractories," *J. Am. Ceram. Soc.*, vol. 86, no. 1, pp. 105–111, 2003.

[26] P. G. Klemens, "Theory of lattice thermal conductivity: Role of low-frequency phonons," *Int. J. Thermophys.*, vol. 2, no. 1, pp. 55–62, 1981.

[27] F. C. Schwerer, J. W. Conroy, and S. Arajs, "Matthiessen's rule and the electrical resistivity of iron-silicon solid solutions," *J. Phys. Chem. Solids*, vol. 30, no. 6, pp. 1513–1525, 1969.

[28] W. D. Kingery, "Thermal Conductivity: XIV, Conductivity of Multicomponent Systems," *J. Am. Ceram. Soc.*, vol. 42, no. 12, pp. 617–627, 1959.

[29] J. D. N. Cheeke, "The Kapitza resistance and heat transfer at low temperature," *Le J. Phys. Colloq.*, vol. 31, no. C3, pp. C3-129-C3-136, Oct. 1970.

[30] D. S. Smith, F. Puech, B. Nait-Ali, A. Alzina, and S. Honda, "Grain boundary thermal resistance and finite grain size effects for heat conduction through porous polycrystalline alumina," *Int. J. Heat Mass Transf.*, vol. 121, pp. 1273–1280, 2018.

[31] S. Grandjean, "Réponse thermique à l'échelle locale dans les matériaux céramiques, effets des pores et des joints de grains," Thesis, University of Limoges, 2002.

[32] A. L. Loeb, "Thermal Conductivity: VIII, A Theory of Thermal Conductivity of Porous Materials," *J. Th.e Am. Ceram. Soc.*, vol. 37, no. 2, pp. 96–99, 1954.

[33] J. R. Dorfman and H. Van Beijeren, "The Kinetic Theory of Gases," in *Statistical mechanics*, B. J. Berne, Ed. Plenum Press, 1977, pp. 65–175.

[34] S. H. Chen and S. C. Saxena, "Thermal conductivity of argon in the temperature range 350 to 2500 k," *Mol. Phys.*, vol. 29, no. 2, pp. 455–466, 1975.

[35] E. Litovsky, M. Shapiro, and A. Shavit, "Gas pressure and temperature dependences of thermal conductivity of porous ceramic materials: part 2, refractories and ceramics with

porosity exceeding 30%," *J. Am. Ceram. Soc.*, vol. 79, no. 5, pp. 1366–1376, 1996.

[36] J. Bourret, "Elaboration de céramiques alvéolaires à base de kaolin: propriétés thermiques et mécaniques," Thesis, University of Limoges, 2012.

[37] V. R. Tarnawski and W. H. Leong, "A series-parallel model for estimating the thermal conductivity of unsaturated soils," *Int. J. Thermophys.*, vol. 33, no. 7, pp. 1191–1218, 2012.

[38] J. Z. Xu, B. Z. Gao, and F. Y. Kang, "A reconstruction of Maxwell model for effective thermal conductivity of composite materials," *Appl. Therm. Eng.*, vol. 102, pp. 972–979, 2016.

[39] J. K. Carson, S. J. Lovatt, D. J. Tanner, and A. C. Cleland, "Thermal conductivity bounds for isotropic, porous materials," *Int. J. Heat Mass Transf.*, vol. 48, no. 11, pp. 2150–2158, 2005.

[40] D. S. Smith *et al.*, "Thermal conductivity of porous materials," *J. Mater. Res.*, vol. 28, no. 17, pp. 2260–2272, 2013.

[41] R. Landauer, "The electrical resistance of binary metallic mixtures," *J. Appl. Phys.*, vol. 23, no. 7, pp. 779–784, 1952.

[42] H. W. Russell, "Principles of heat flow in porous insulators," *J. Am. Ceram. Soc.*, vol. 18, pp. 1–5, 1935.

[43] D. W. Lee and W. D. Kingery, "Radiation Energy Transfer and Thermal Conductivity of Ceramic Oxides," *J. Am. Ceram. Soc.*, vol. 43, no. 11, pp. 594–607, 1960.

[44] A. Schauer, "Thermal Expansion of Solids and the Temperature Dependence of Lattice Vibration Frequencies," *Can. J. Phys.*, vol. 42, pp. 1857–1864, 1964.

[45] Z. Xun, S. U. N. Sheng, X. U. Tao, and Z. Tongyi, "Temperature dependent Grüneisen parameter," *Sci China Tech Sci*, vol. 62, pp. 1565–1576, 2019.

[46] S. A. Suvorov and V. V. Skurikhin, "Vermiculite - A promising material for high-temperature heat insulators," *Refract. Ind. Ceram.*, vol. 44, no. 3, pp. 186–193, 2003.

[47] A. Bhargavi Rani, A. R. Raja Annamalai, M. R. Majhi, and A. Harish Kumar, "Synthesis and characterization of forsterite refractory by doping with kaolin," *Int. J. ChemTech Res.*, vol. 6, no. 2, pp. 1390–1397, 2014.

[48] D. Chen, H. Gu, A. Huang, M. Zhang, F. Zhou, and C. Wang, "Mechanical Strength and Thermal Conductivity of Modified Expanded Vermiculite/Forsterite Composite Materials," *J. Mater. Eng. Perform.*, vol. 25, no. 1, pp. 15–19, 2016.

[49] S. Samadi, S. Jin, D. Gruber, H. Harmuth, and S. Schachner, "Statistical study of compressive creep parameters of an alumina spinel refractory," *Ceram. Int.*, vol. 46, no. 10, pp. 14662–14668, 2020.

[50] ASTM International, "Standard Test Method for Steady-State Thermal Transmission Properties by Means of the Heat Flow Meter Apparatus," *ASTM C518 - 15*, pp. 1–15, 2015.

[51] J. Bourret, E. Prud'Homme, S. Rossignol, and D. S. Smith, "Thermal conductivity of geomaterial foams based on silica fume," *J. Mater. Sci.*, vol. 47, no. 1, pp. 391–396, 2012.

[52] ISO Standard, “Thermal insulation — Determination of steady-state thermal resistance and related properties — Heat flow meter apparatus,” *ISO 8301-1991*, 2010.

[53] M. Trojan, “O: One-dimensional analytical models of frictional heating during braking,” in *Encyclopedia of Thermal Stresses*, 2014.

[54] S. Schriebl, A. Spanring, R. Krischanitz, and J. Brueck, “RHI Bulletin,” *The journal of refractory Innovations - Industrial Edition*, vol. 2, 2015.

[55] R. Wulf, “Wärmeleitfähigkeit von hitzebeständigen und feuerfesten Dämmstoffen - Untersuchungen zu Ursachen für unterschiedliche Messergebnisse bei Verwendung verschiedener Messverfahren,” Thesis, Technical University Bergakademie Freiberg, 2009.

[56] W. N. Dos Santos, “Advances on the hot wire technique,” *J. Eur. Ceram. Soc.*, vol. 28, pp. 15–20, 2008.

[57] T. Tonnesen, R. Telle, D. S. Smith, and S. Fayette, “A modified equipment for determination of thermal conductivity of refractories by the hot-wire method-a critical review and comparison with the laser-flash-method,” in *UNITECR 1999*, 1999, pp. 416–420.

[58] W. N. Dos Santos and R. Gregorio, “Hot-wire parallel technique: A new method for simultaneous determination of thermal properties of polymers,” *J. Appl. Polym. Sci.*, vol. 85, no. 8, pp. 1779–1786, 2002.

[59] J. Boer, J. Butter, B. Grosskopf, and P. Jeschke, “Hot wire technique for determining high thermal conductivities,” *Refract. J.*, pp. 22–28, 1980.

[60] U. Hammerschmidt and W. Sabuga, “Transient hot wire (THW) method: Uncertainty assessment,” *Int. J. Thermophys.*, vol. 21, no. 6, pp. 1255–1278, 2000.

[61] S. E. Gustafsson, “Transient plane source techniques for thermal conductivity and thermal diffusivity measurements of solid materials,” *Rev. Sci. Instrum.*, vol. 62, no. 3, pp. 797–804, 1991.

[62] Y. He, “Rapid thermal conductivity measurement with a hot disk sensor: Part 1. Theoretical considerations,” *Thermochim. Acta*, vol. 436, no. 1–2, pp. 122–129, 2005.

[63] “Hot Disk Thermal Constants Analyser: Instruction Manual.” Hot Disk AB, pp. 1–128, 2015.

[64] ISO Standard, “Plastic - Determination of thermal conductivity and thermal diffusivity - Part 2: Transient plane source method,” *ISO 22007-22008*, pp. 1–24, 2008.

[65] ASTM International, “Standard Test Method for Thermal Diffusivity by the Flash Method 1,” *ASTM E1461 - 13*, pp. 1–11, 2013.

[66] W. J. Parker, R. J. Jenkins, C. P. Butler, and G. L. Abbott, “Flash method of determining thermal diffusivity, heat capacity, and thermal conductivity,” *J. Appl. Phys.*, vol. 32, no. 9, pp. 1679–1684, 1961.

[67] K. D. Maglic, A. Cezairliyan, and V. E. Peletsky, *Compendium of thermophysical property measurement methods 2: Recommended measurement techniques and practices*. Springer Science + Business Media, 1992.

[68] J. A. Cape and G. W. Lehman, “Temperature and finite pulse-time effects in the flash

method for measuring thermal diffusivity," *J. Appl. Phys.*, vol. 34, no. 7, pp. 1909–1913, 1963.

[69] A. Degiovanni and M. Laurent, "Une nouvelle technique d'identification de la diffusivité thermique pour la méthode « flash »," *Rev. Phys. Appliquée*, vol. 21, no. 3, pp. 229–237, 1986.

[70] H. Mehling, G. Hautzinger, O. Nilsson, J. Fricke, R. Hofmann, and O. Hahn, "Thermal diffusivity of semitransparent materials determined by flash laser method applying a new analytical model," *Int. J. Thermophys.*, vol. 19, no. 3, pp. 941–949, 1998.

[71] D. Günther and F. Steimle, "Mixing rules for the specific heat capacities of several HFC-mixtures," *Int. J. Refrig.*, vol. 20, no. 4, pp. 235–243, 1997.

[72] O. Knacke, O. Kubaschewski, and K. Hesselmann, *Thermal Chemical Properties of Inorganic Substances*, 2nd Ed. Springer Verlag, 1977.

[73] A. P. F. Albers, T. A. G. Restivo, L. Pagano, and J. B. Baldo, "Effect of testing conditions on the laser flash thermal diffusivity measurements of ceramics," *Thermochim. Acta*, vol. 370, no. 1–2, pp. 111–118, 2001.

[74] O. Hahn, R. Hofmann, H. Mehling, F. Raether, and J. Fricke, "Transiet heat transfer in coated diathermic media: a theoretical study," in *High Temperatures-High Pressures*, 1997, vol. 29, pp. 693–701.

[75] S. Fayette, "Conduction thermique dans les matériaux hétérogènes, influence des joints de grain," Thesis, University of Limoges, 2001.

[76] A. Lindemann and F. Neidhardt, "Thermal conductivity of inhomogeneous materials," 2015.

[77] B. Nait-Ali, C. Danglade, D. S. Smith, and K. Haberko, "Effect of humidity on the thermal conductivity of porous zirconia ceramics," *J. Eur. Ceram. Soc.*, vol. 33, no. 13–14, pp. 2565–2571, 2013.

[78] S. Oummadi, "Drying behaviour of ceramic green bodies : experimental characterization and numerical modeling," Thesis, University of Limoges, 2019.

[79] S. Oummadi, B. Nait-Ali, A. Alzina, M.-C. Paya, J.-M. Gaillard, and D. S. Smith, "Optical method for evaluation of shrinkage in two dimensions during drying of ceramic green bodies," *Open Ceram.*, vol. 2, no. 100016, 2020.

[80] H. Wu, S. Grabarnik, A. Emadi, G. De Graaf, and R. F. Wolffenbuttel, "Characterization of thermal cross-talk in a MEMS-based thermopile detector array," *J. Micromechanics Microengineering*, vol. 19, no. 7, 2009.

[81] M. L. V. Ramires, C. A. Nieto Castro, Y. Nagasaka, A. Nagashima, M. J. Assael, and W. A. Wakeham, "Standard Reference Data for the Thermal Conductivity of Water," *J. Phys. Chem. Ref. Data*, vol. 24, no. 3, pp. 1377–1381, 1995.

[82] L. A. Pérez-Maqueda *et al.*, "Study of natural and ion exchanged vermiculite by emanation thermal analysis, TG, DTA and XRD," *J. Therm. Anal. Calorim.*, vol. 71, no. 3, pp. 715–726, 2003.

[83] P. Kresten and G. Berggren, "The thermal decomposition of vermiculite," *Thermochim. Acta*, vol. 23, pp. 171–182, 1978.

[84] J. Chen, M. Zhang, H. Wang, and L. Li, "Evaluation of thermal conductivity of asphalt concrete with heterogeneous microstructure," *Appl. Therm. Eng.*, vol. 84, pp. 368–374, 2015.

[85] P. M. Nigay, T. Cutard, and A. Nzihou, "The Impact of the particle size distribution of organic additives on the microstructure of a clay ceramic and its thermal and mechanical properties," *Ceram. Int. Elsevier*, vol. 43, no. 2, pp. 1747–1754, 2017.

[86] I. Kieliba, T. Tonnesen, R. Telle, M. Huger, E. Guéguen, and C. Parr, "Alumina-Spinel Castables under Thermal Cycling Conditions - in Situ Characterisation," in *UNITECR 2019*, 2019, pp. 912–915.

[87] Z. A. Munir, D. V. Quach, and M. Ohyanagi, "Electric current activation of sintering: A review of the pulsed electric current sintering process," *J. Am. Ceram. Soc.*, vol. 94, no. 1, pp. 1–19, 2011.

[88] P. A. Popov, V. D. Solomennik, P. V. Belyaev, L. A. Lytvynov, and V. M. Puzikov, "Thermal conductivity of pure and Cr3+ and Ti3+ doped Al2O3 crystals in 50-300 K temperature range," *Funct. Mater.*, vol. 18, no. 4, pp. 476–480, 2011.

[89] H. M. Rietveld, "A profile refinement method for nuclear and magnetic structures," *J. Appl. Crystallogr.*, vol. 2, no. 2, pp. 65–71, 1969.

[90] M. A. L. Braulio, M. Rigaud, A. Buhr, C. Parr, and V. C. Pandolfelli, "Spinel-containing alumina-based refractory castables," *Ceram. Int.*, vol. 37, no. 6, pp. 1705–1724, 2011.

[91] "Specialty Aluminas for Techical ceramics - brochure," *ALTEO, A new world of alumina*. 2018.

[92] "Secar 71 - product data sheet," *Kerneos, aluminate-technologies*. 2016.

[93] N. Ukrainczyk and T. Matusinović, "Thermal properties of hydrating calcium aluminate cement pastes," *Cem. Concr. Res.*, vol. 40, no. 1, pp. 128–136, 2010.

[94] P. L. Kapitza, "Heat transfer and superfluidity of helium II," *Phys. Rev.*, vol. 60, no. 4, pp. 354–355, 1941.

[95] Dassault Systèmes, "Résistance thermique de contact," *Aide de Solidworks*, 2012. [Online]. Available: http://help.solidworks.com/2012/french/solidworks/cworks/Thermal_Contact_Resistance.htm (accessed Oct. 27, 2020).

[96] K. Narendra Babu, "Thermal Contact Resistance: Experiments and Simulation," Master's Thesis, CHALMERS University of Technology, 2015.

[97] Y. Xian, P. Zhang, S. Zhai, P. Yuan, and D. Yang, "Experimental characterization methods for thermal contact resistance: A review," *Appl. Therm. Eng.*, vol. 130, no. 1, pp. 1530–1548, 2018.

[98] J. P. Holman, *Heat Transfer*, Tenth edit. Mc Graw Hill - Higher Education, 2010.

[99] J. Absi, D. S. Smith, B. Nait-Ali, S. Grandjean, and J. Berjonnaux, "Thermal response of two-layer systems: Numerical simulation and experimental validation," *J. Eur. Ceram. Soc.*, vol. 25, no. 4, pp. 367–373, 2005.

[100] Y. M. Lee, S. Kumar, J. Bradley, L. Rebouillat, and N. Roy, "Improvement of thermal efficiency in steel ladles," in *UNITECR 2013*, 2013, pp. 323–328.

[101] C. B. Carter and M. G. Norton, *Ceramic materials: science and engineering*. Springer, 2007.

[102] ASTM International, "Standard test methods for cold crushing strength and modulus of rupture of refractories," *ASTM C133-97*, pp. 1–6, 2015.

[103] B. Glaser, M. Görnerup, and D. Sichen, "Thermal modelling of the ladle preheating process," *Steel Res. Int.*, vol. 82, no. 12, pp. 1425–1434, 2011.

[104] N. Tessier-Doyen, "Etude experimentale et numerique du comportment thermomecanque des materiaux refractaires modeles," Thesis, University of Limoges, 2003.

[105] C. Poulier, D. S. Smith, and J. Absi, "Thermal conductivity of pressed powder compacts: tin oxide and alumina," *J. Eur. Ceram. Soc.*, vol. 27, no. 2–3, pp. 475–478, 2007.

[106] "LECO Analysis," *Element Materials Technology*. [Online]. Available: https://www.element.com/materials-testing-services/chemical-analysis-labs/leco-analysis (accessed Sep. 29, 2020).

[107] United States Environmental Protection Agency, "Assessing the Management of Lead in Scrap Metal and Electric Arc Furnace Dust," 2009.

[108] R. L. Naro, D. Williams, and P. Satre, "Control of Slag and Insoluble Buildup in Ladles, Melting and Pressure Pour Furnaces," *ASI Int.*, 2015.

[109] E. Gates, B. Padgett, B. Harper, B. Tossey, and J. Shingledecker, "Corrosion resistance of alloys in calcium bromide and calcium chloride solutions," in *NACE - International Corrosion Conference Series*, 2017, vol. 3, pp. 1823–1836.

[110] D. Vitiello, I. Kieliba, G. Derrick, and M. Huger, "Deliverable D1.3: Devices for Thermo-Physical Properties Characterisation," 2019. [Online]. Available: https://www.etn-athor.eu/public-documentation/.

[111] M. A. Faghihi-Sani and A. Yamaguchi, "Oxidation kinetics of MgO-C refractory bricks," *Ceram. Int.*, vol. 28, no. 8, pp. 835–839, 2002.

[112] S. Jansson, V. Brabie, and P. Jönsson, "Corrosion mechanism of commercial MgO-C refractories in contact with different gas atmospheres," *ISIJ Int.*, vol. 48, no. 6, pp. 760–767, 2008.

[113] J. Poirier *et al.*, *Corrosion of Refractories: The Impacts of Corrosion*, vol. 2C. FIRE Compendium Series, 2018.

[114] T. Miles, "The Boudouard Equation," *Biomass Energy Foundation*, 2016. [Online]. Available: http://gasifiers.bioenergylists.org/reedboudouard (accessed Sep. 24, 2020).

[115] R. Bolivar and B. Friedrich, "The influence of increased NaCI: KCI ratios on metal yield in salt bath smelting processes for aluminium recycling," *World Metall. - ERZMETALL*, vol. 62, no. 6, pp. 366–371, 2009.

[116] J. J. Healy and J. J. De Groot, "The theory of the transient hot-wire method for measuring thermal conductivity," *Physica*, vol. 82C, pp. 392–408, 1976.

Appendix A1

Experimental results with the heat flow meter (**paragraph 2.2.1**) at ambient conditions in the case of Low Density Insulating Boards (IB-LD), Medium Density Insulating Boards (IB-MD), High Density Insulating Boards (IB-HD) and Insulating Fireclay Bricks (IFB). The values are taken in the "cross-plane" direction.

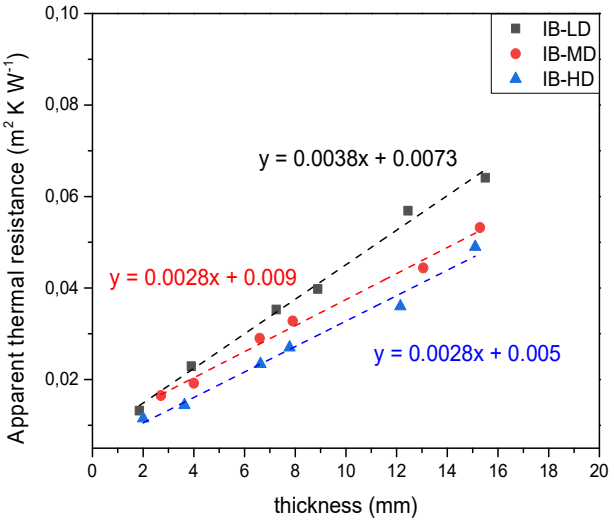

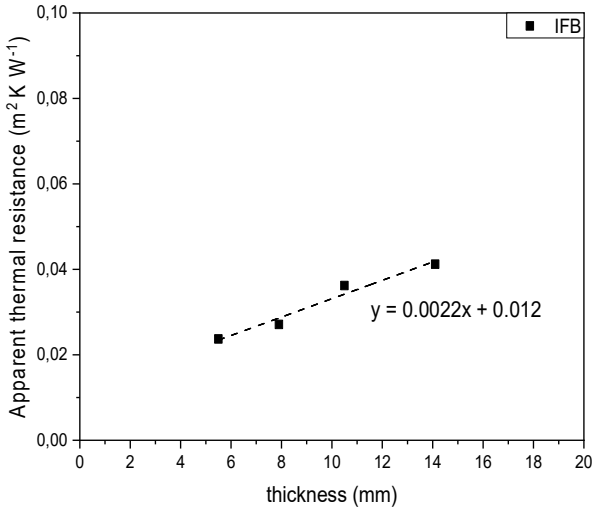

Appendix A2

Experimental results with the hot disk method (**paragraph 2.2.4**) at ambient conditions in the case of Low Density Insulating Boards (IB-LD), Medium Density Insulating Boards (IB-MD), High Density Insulating Boards (IB-HD), Insulating Fireclay Bricks (IFB) and Alumina Spinel Bricks (ASB). The values are taken in the "cross-plane" direction.

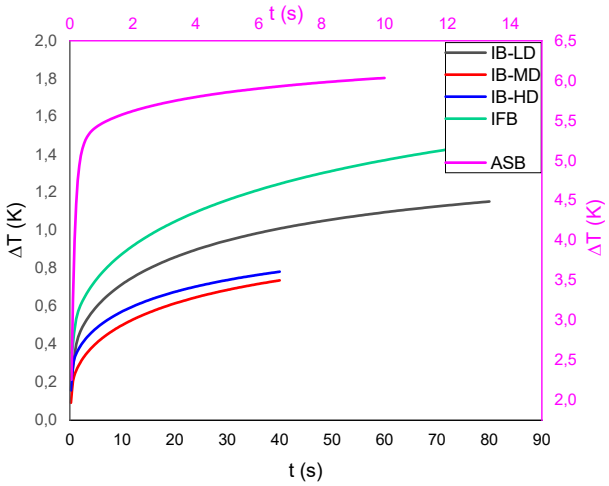

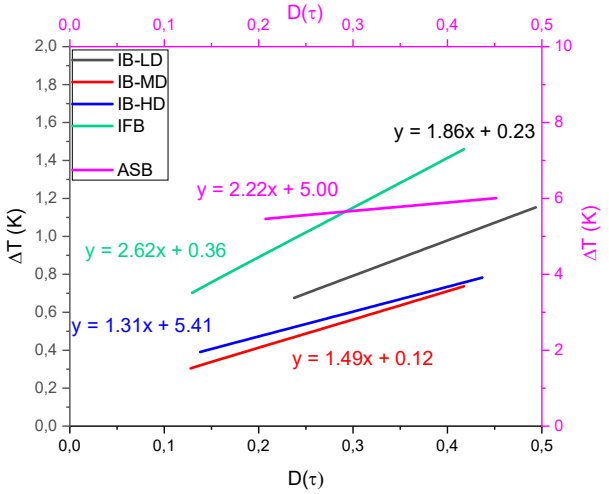

Appendix A3

Experimental results with the laser flash method (**paragraph 2.2.5**) at ambient conditions (black line) and at high temperatures (red line) in the case of Low Density Insulating Boards (IB-LD), Medium Density Insulating Boards (IB-MD), High Density Insulating Boards (IB-HD), Insulating Fireclay Bricks (IFB) and Alumina Spinel Bricks (ASB). The values are taken in the "cross-plane" direction.

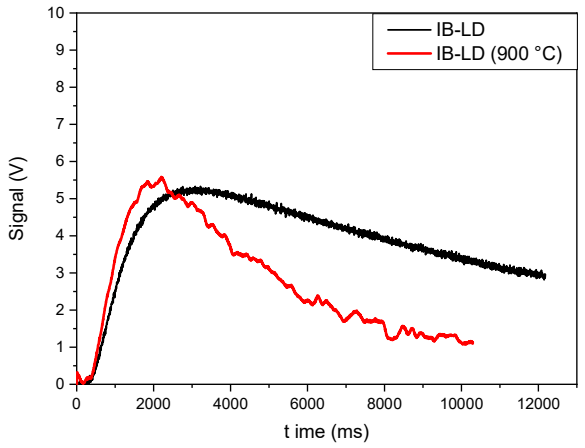

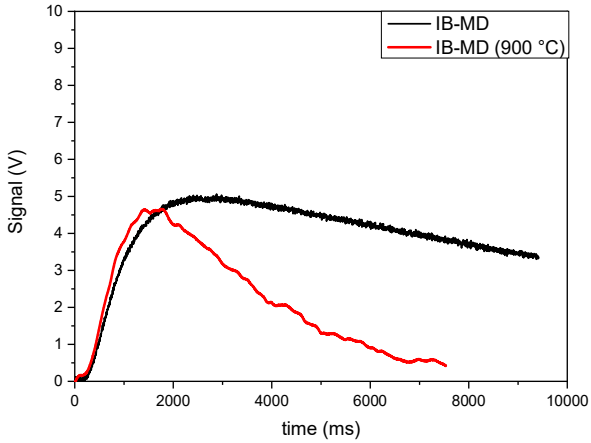

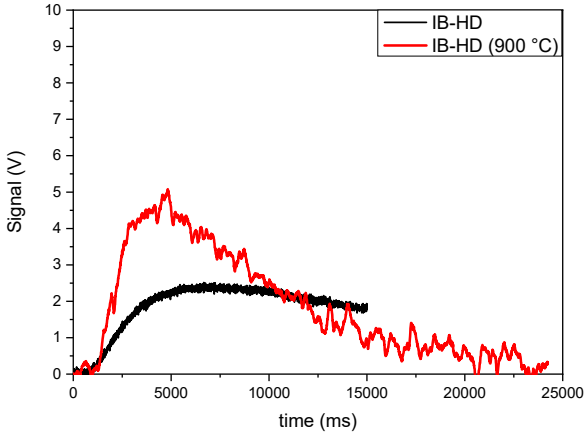

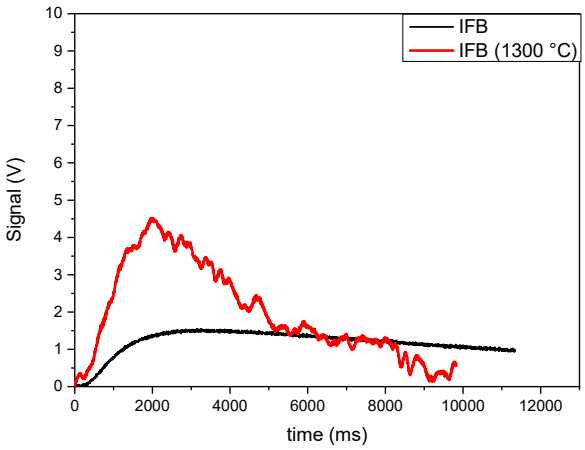

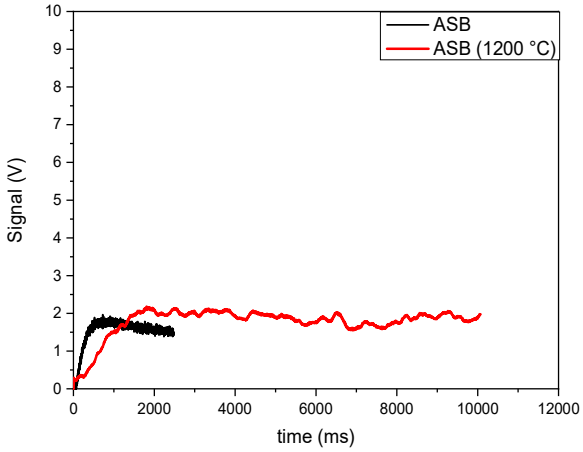

Appendix B

To estimate the maximum load withstood by the investigated samples, Insulating Boards and Insulating Fireclay Bricks, uniaxial compression tests were made on square samples (70x70 mm^2 of area and 25 - 32 mm in thickness) with a loading rate of 0.025 kN/s. The measurements were performed at the Department of Civil Engineering in Coimbra (FCTUC). The load-displacement curves in the case of Medium Density Insulating Boards (IB-MD) and High Density Insulating Boards (IB-HD) in the "cross-plane" direction are presented.

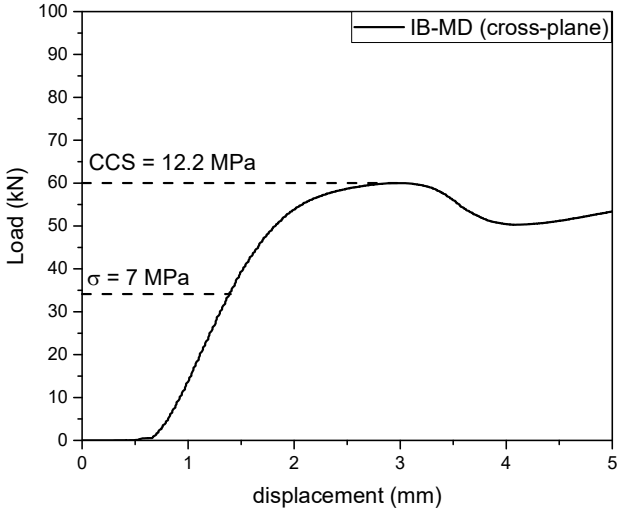

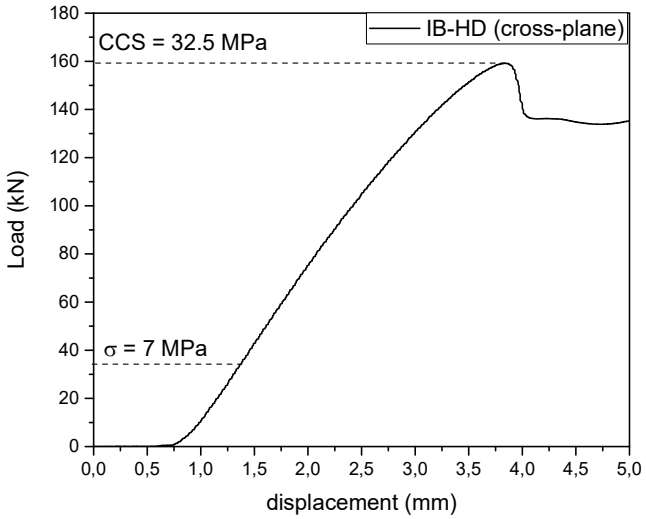

Appendix C

High temperature X-ray diffraction (HT-XRD) analysis was made in the case of Low Density Insulating Boards (IB-LD). It was considered as a reference for the three kinds of porosity. The measurements were made from room temperature up to 700 °C with a heating rate of 40 K/min. Six measurements were taken at 700 °C every 20 min.

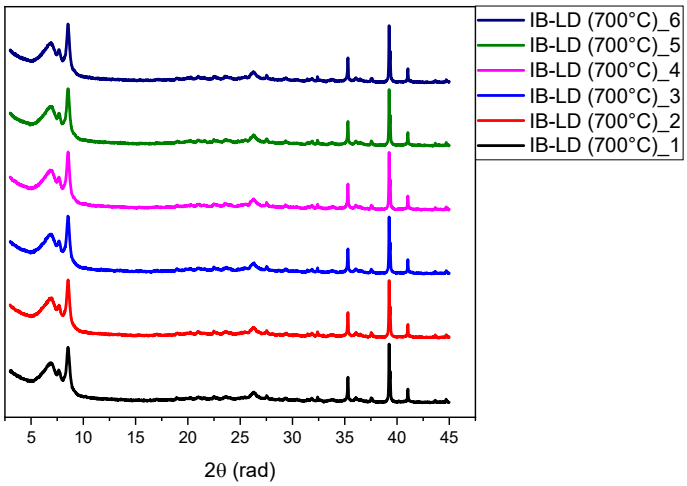

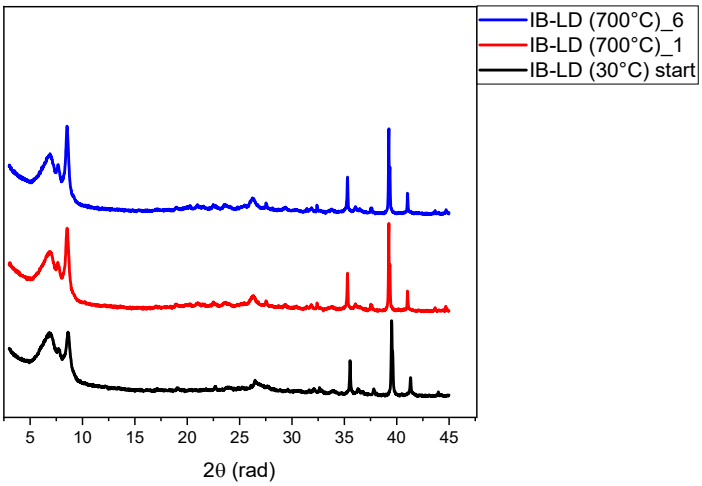

Appendix D

Young's modulus measurements were made by V. Tadaion at RWTH Aachen University (Germany) on Insulating Fireclay Bricks. The measurements were made by Impulse Excitation method using a resonant frequency and damping analyzer (RFDA) equipment from IMCE Company.

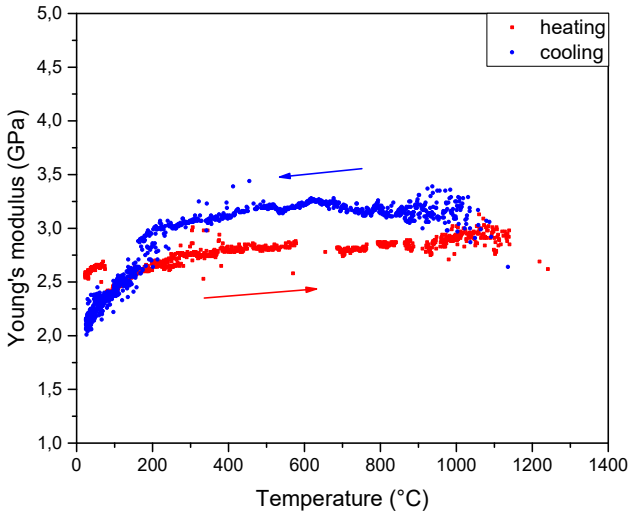

Propriétés thermo-physiques de matériaux réfractaires isolants

Les performances des matériaux réfractaires isolants sont fortement dépendantes de leurs propriétés thermo-physiques. La première partie de cette thèse est consacrée à l'évaluation de la conductivité thermique, qui est un paramètre important dans la modélisation du transfert de chaleur à travers le revêtement d'une poche d'acier. Les méthodes expérimentales utilisées ont révélé des différences entre les valeurs mesurées, qui peuvent être réduit d'environ 10% pour une direction du flux de chaleur considérée, dès lors que les pertes de chaleur, l'humidité, l'anisotropie et l'hétérogénéité sont prises en compte. La conductivité thermique est donc significativement influencée par la microstructure. Étant donné que les réfractaires industriels sont des matériaux multi-phasés complexes, une approche permettant de mieux appréhender leur comportement consiste à étudier des matériaux modèles de microstructure voisine mais simplifiée, afin d'identifier la contribution de paramètres tels que la porosité, les joints de grains, la taille des grains et la présence de secondes phases. Puis trois cas d'intérêt industriel en lien avec les réfractaires précédents ont été examinés. Comme une poche d'acier est constituée de différentes briques, les joints jouent un rôle majeur. Leur résistance thermique interfaciale a été estimée entre 10^{-4} et 10^{-3} $m^2 \cdot K \cdot W^{-1}$, ce qui constitue une valeur expérimentale de haute importance pour améliorer la fiabilité de la modélisation. De plus, le revêtement est soumis à des contraintes de compression induites par la pression hydrostatique de l'acier en fusion, ce qui implique que les matériaux requièrent une résistance mécanique suffisante. Pour des valeurs de contrainte appliquée de 0.4 MPa et de 0.04 MPa, aucun effet significatif n'a été observé respectivement sur la dilatation et la conductivité thermique des matériaux isolants étudies. Enfin, l'un des principaux problèmes rencontré dans l'industrie sidérurgique concerne la corrosion, qui conduit souvent au remplacement prématuré des matériaux afin de garantir des conditions de service optimales. Le rôle de la contamination par le carbone sur la conductivité thermique du revêtement isolant a ainsi été évalué.

Mots-clés : propriétés thermiques, matériaux réfractaires isolants, microstructure, contrainte de compression, joints, corrosion, poche d'acier

Thermo-physical properties of insulating refractory materials

The performance of insulating refractory materials is determined by the thermo-physical properties. The first part of this thesis is dedicated to the evaluation of the thermal conductivity, which is an input parameter in modelling studies of heat transfer through a steel ladle lining. Comparison of different methods for its determination leads to some variation in the experimental results. However, taking into account effects such as heat losses, humidity, anisotropy and heterogeneity, the discrepancy could be reduced to within 10% when the same heat flow direction through the material is considered. Thermal conductivity is significantly modulated by the microstructure. Given that refractories are multi-phase materials, model materials with similar microstructures were studied to identify the role of factors such as porosity, grain boundaries, grain size and presence of second phases. Then three real cases of industrial interest were examined. The ladle is a vessel made by different bricks. Therefore, joints play an important role. The interface thermal resistance was estimated to be in the range 10^{-4} to 10^{-3} $m^2 \cdot K \cdot W^{-1}$ useful as a first approximation in computer modelling. In fact the lining is subjected to hydrostatic pressure when the ladle is filled with hot liquid steel implying the materials require sufficient compressive strength. For compression loads up to 0.4 MPa on the thermal expansion and up to 0.04 MPa on the thermal conductivity of insulating lining materials, no significant effect was observed. Finally, one of the main problems for steelmaking industry is represented by corrosion, which can require replacement of the materials in order to guarantee the same operation condition for all the campaign. The role of carbon contamination for the thermal conductivity of the insulating lining was evaluated.

Keywords: thermal properties, insulating refractory materials, microstructure, compression load, joints, corrosion, steel ladle